Studies in Computational Intelligence 761

Kanad Ray
Millie Pant
Anirban Bandyopadhyay *Editors*

Soft Computing Applications

Springer

Studies in Computational Intelligence

Volume 761

Series editor

Janusz Kacprzyk, Polish Academy of Sciences, Warsaw, Poland
e-mail: kacprzyk@ibspan.waw.pl

The series “Studies in Computational Intelligence” (SCI) publishes new developments and advances in the various areas of computational intelligence—quickly and with a high quality. The intent is to cover the theory, applications, and design methods of computational intelligence, as embedded in the fields of engineering, computer science, physics and life sciences, as well as the methodologies behind them. The series contains monographs, lecture notes and edited volumes in computational intelligence spanning the areas of neural networks, connectionist systems, genetic algorithms, evolutionary computation, artificial intelligence, cellular automata, self-organizing systems, soft computing, fuzzy systems, and hybrid intelligent systems. Of particular value to both the contributors and the readership are the short publication timeframe and the world-wide distribution, which enable both wide and rapid dissemination of research output.

More information about this series at http://www.springer.com/series/7092

Kanad Ray · Millie Pant
Anirban Bandyopadhyay
Editors

Soft Computing Applications

Springer

Editors
Kanad Ray
Amity School of Applied Sciences
Amity University Rajasthan
Jaipur, Rajasthan
India

Anirban Bandyopadhyay
Surface Characterization Group
National Institute for Materials Science
Tsukuba, Ibaraki
Japan

Millie Pant
Department of Applied Science
and Engineering
IIT Roorkee
Saharanpur, Uttar Pradesh
India

ISSN 1860-949X ISSN 1860-9503 (electronic)
Studies in Computational Intelligence
ISBN 978-981-10-8048-7 ISBN 978-981-10-8049-4 (eBook)
https://doi.org/10.1007/978-981-10-8049-4

Library of Congress Control Number: 2017963856

Printed on acid-free paper

This Springer imprint is published by Springer Nature
The registered company is Springer Nature Singapore Pte Ltd.
The registered company address is: 152 Beach Road, #21-01/04 Gateway East, Singapore 189721, Singapore

Preface

Exploring the tolerance for imprecision is the bottom line of soft computing. Partially proven facts, unsurety, tentativeness of achieving tractability, sturdiness, and low solution cost are the traits of soft computing unlike hard computing. The arena of chartering here is the human mind. Fuzzy logic, neural computing, evolutionary computation, machine learning, and probabilistic reasoning spanning across belief networks, chaos theory, and parts of learning theory come under the Web of soft computing. The swift growth and its successful applications hint that the influence of soft computing will be realized hugely in the coming times. Soft computing will expand farther and is likely to claim a very significant share in science and engineering. After the hugely successful accomplishment of the First International Conference 'Soft Computing: Theories and Applications' in 2016 at Amity University Rajasthan, Jaipur, India, where we had 150 accepted papers, we had decided to screen, segregate, expand, extend and selected eight chapters under the aegis of the International publishing giant Springer. And for all these inimitable endeavors, we would like to accord our heartfelt indebtedness to Amity University Rajasthan, IIT Roorkee, and MIR Labs, without whom this overwhelming response would not have been feasible.

Jaipur, Rajasthan
Dr. Kanad Ray
Amity University Rajasthan

Roorkee, India
Dr. Millie Pant
IIT Roorkee

Tsukuba, Japan
Dr. Anirban Bandyopadhyay
NIMS

Contents

About the Editors

Dr. Kanad Ray is a Professor and Head of Physics at the Amity School of Applied Sciences, Amity University Rajasthan (AUR), Jaipur, India. He has obtained MSc and PhD degrees in Physics from Calcutta University and Jadavpur University, West Bengal, India. In an academic career spanning over 22 years, he has published and presented research papers in several national and international journals and conferences in India and abroad. He has authored a book on the Electromagnetic Field Theory. His current research areas of interest include cognition, communication, electromagnetic field theory, antenna and wave propagation, microwave, computational biology, and applied physics. He has served as Editor of Springer Book Series. Presently, he is an Associate Editor of Journal of Integrative Neuroscience published by IOS Press, Netherlands. He has established a MOU between his University and University of Montreal, Canada, for various joint research activities. He has also established collaboration with National Institute for Materials Science (NIMS), Japan, for joint research activities and visits NIMS as a Visiting Scientist. He organizes international conference series such as SoCTA, ICoEVCI as General Chair. He is an Executive Committee Member of IEEE Rajasthan Chapter.

Millie Pant is an Associate Professor in the Department of Paper Technology, Indian Institute of Technology Roorkee (IIT Roorkee), India. A well-known figure in the field of swarm intelligence and evolutionary algorithms, she has published several research papers in respective national and international journals.

Dr. Anirban Bandyopadhyay is a Senior Scientist at the National Institute for Materials Science (NIMS), Tsukuba, Japan. He completed his PhD degree in Supramolecular Electronics at the Indian Association for the Cultivation of Science (IACS), Kolkata, in 2005. From 2005 to 2008, he was an Independent Researcher, as Research Fellow at the International Center for Young Scientists (ICYS), NIMS, Japan, where he worked on the brain-like bio-processor building. In 2008, he joined as a Permanent Scientist at NIMS, working on the cavity resonator model of human brain and design-synthesis of brain-like organic jelly. From 2013 to 2014, he was a Visiting Scientist at the Massachusetts Institute of Technology (MIT), USA. He has

received several honors, such as the Hitachi Science and Technology Award 2010, Inamori Foundation Award 2011–2012, Kurata Foundation Award, Inamori Foundation Fellow (2011–), and Sewa Society International Member, Japan. He has patented ten inventions: (i) a time crystal model for building an artificial human brain, (ii) geometric musical language to operate a fractal tape to replace the Turing tape, (iii) fourth circuit element that is not memristor, (iv) cancer and Alzheimer's drug, (v) nano-submarine as a working factory and nano-surgeon, (vi) fractal condensation-based synthesis, (vii) a thermal noise harvesting chip, (viii) a new generation of molecular rotor, (ix) spontaneous self-programmable synthesis (programmable matter), and (x) fractal grid scanner for dielectric imaging. He has also designed and built multiple machines and technologies: (i) THz-magnetic nano-sensor, (ii) a new class of fusion resonator antenna, etc. Currently, he is building time crystal-based artificial brain using three ways: (i) knots of darkness made of fourth circuit element, (ii) integrated circuit design, and (iii) organic supramolecular structure.

A Brain-like Computer Made of Time Crystal: Could a Metric of Prime Alone Replace a User and Alleviate Programming Forever?

Shruthi Reddy, Dheeraj Sonker, Pushpendra Singh, Komal Saxena, Surabhi Singh, Rutuja Chhajed, Samanyu Tiwari, K. V. Karthik, Subrata Ghosh, Kanad Ray and Anirban Bandyopadhyay

Abstract Big data or data overflow problem is due to century-old wrong information theory practiced even today that believes every single event that has happened, is happening, and will happen in the universe could be recreated as sum of simple events. We say, events are connected by geometric shapes, e.g., eight points of a cube represent eight events; to integrate events, either one places new geometric shapes inside any of the eight points, or consider entire cube as a single point located in a new giant geometric shape. Brain has no algorithm running, how does it make decision? Making a decision by building a scientific theory means predicting future from a given set of events; here, we propose to do that by using a pattern of all possible choices a given set of events could be grouped. This pattern is like space–time metric of astrophysics. When we convert any event into a 3D topological shape changing with time, those shapes are fed into this pattern of event-groups namely, phase prime metric. The output is another changing shape that links all possible unknown patterns that could happen in future; so, without any algorithm we can analyze big data and run a robot. We reject Turing's machine. For

S. Reddy · D. Sonker · P. Singh · K. Saxena · S. Singh · R. Chhajed · S. Tiwari
K. V. Karthik · A. Bandyopadhyay (✉)
Advanced Key Technologies Division, National Institute for Materials Science,
1-2-1 Sengen, Tsukuba, Ibaraki 305-0047, Japan
e-mail: anirban.bandyo@gmail.com

P. Singh · K. Ray
Department of Physics, Amity School of Applied Sciences, Amity University
Rajasthan, NH 8, Kantkalwar, Jaipur 303007, Rajasthan, India

K. Saxena
Microwave Physics Laboratory, Department of Physics
and Computer Science, Faculty of Science, Dayalbagh Educational Institute,
Dayalbagh, Agra, Uttar Pradesh 282005, India

S. Ghosh
Natural Product Chemistry Group, Chemical Science & Technology Division,
CSIR-North East Institute of Science & Technology, Jorhat 785006, Assam, India

K. Ray et al. (eds.), *Soft Computing Applications*, Studies in Computational Intelligence 761, https://doi.org/10.1007/978-981-10-8049-4_1

frequency fractal computing using time crystal, information is not "bit," but a unique time crystal, which is life-like. These crystals holding geometric shape self-assemble to create a clocking topology of phase. To convert information into a 3D geometric structure it follows our phase prime metric. Phase structure changes continuously, sometimes it is manifested as dynamics of mass, spin foam, string, tube etc. Thus, time crystal based brain-like computer of makes a decision using phase prime metric.

Keywords Singularity · Fractal clock · Time crystal · Bloch sphere
Turing machine · Phase prime metric · Geometric phase · Phase shift
Self-assembly · Quantum computing · Topology · Resonance · Biological clock
Geometric musical language · Fractal information theory · Big data
Artificial Brain · Harmonics · Hilbert space · Hypercomputing
Fractal · Fourth circuit element · Artificial intelligence · Morphogenesis

1 Introduction

Historical perspective: Spatial non-linearity is easy to detect, and it is a curved path. However, a temporal non-linearity is tuning the velocity of light and or maximum velocity governing the clocks in a system faster and slower, without physically moving an object from a single point [93]. Measuring and estimating a nonlinear time are crucial, but, historically, the research on the experimental detection of topology of a nonlinear time flow is scarce. Using such nonlinear time, one can speed up computing [23, 51, 63, 106]. Closed time-like loop proposes a nonlinear time that came in the 1930s [25, 111, 114], but lost in history, because a true quantum clock cannot run in a fixed direction and maintain a fixed diameter like a classical clock [1]. In contrast, the smallest time of a fractal clock has a clock inside, so a piece of time remains undefined, and we get singularity everywhere [77, 107]. Singularity is undefined, not useful at all, so does a fractal clock. One idea to use a fractal clock (clock inside a clock inside a clock…) was to run many self-similar (fractal) tapes side by side like a tree [60, 96]. Recently, we proposed a complement to this concept, placing Turing tapes in every single cell of a Turing tape [6, 52]. Until recently, fractal clock devices did not exist in reality, because, even, how to physically plot discrete "time" slices into a single structure was not known. Here we propose that Winfree's concept of "time crystal" [116] could be used [108] to build a structure of phase, where discrete "time" slices could exist. We have discovered such a 3D phase structure in the resonant vibrations of proteins [103–105] and also mimicked that in the fractal superstructures of a synthesized organic "time crystal" material [12]. The singularity that Feynman eschewed in his renormalization (Feynman 1948) [33] is an essential part of this 3D phase structure. We started from Bloch sphere and modified it to construct our experimentally derived 3D phase structure since it would clearly show the difference between classical, quantum and fractal information theories. In quantum, Bloch spheres hold

no geometric shapes. Here in FIT, singularity points are corners of geometric shapes. To self-assemble clocking Bloch spheres that hold new geometric shapes, a corner or singularity point splits (fractal information theory, FIT), [6, 5]. This split enables one dimensionless point to hold another geometric shape inside. This constitutive physical process is analogous to inserting a Turing tape inside every single cell of a Turing tape.

However, simply finding the fundamental information as 3D phase structure is not enough. We need to find how to naturally self-assemble these modified clocking Bloch spheres. By analyzing experimentally derived 3D phase structure of proteins, neurons, brain, organic molecular machine, supramolecule, electronic clocks and circuits, we found a way to morph the natural events using a phase prime metric [42, 62, 100, 117]. ***A phase prime metric is a plot (C-n) of the number of ways (say C) n number of nodes of a standing wave could combine. Every point C in this plot represents all possible ways n random events could have happened together; each point C also represents a single event***. This metric is physically realized by tuning the topology of capacitive elements in an insulator and thus editing its geometric phase [73, 81, 82, 94, 95]. Then, instead of a user, the phase prime metric governs the decision-making without an algorithm. For any given random set of events (event = clocking Bloch sphere holding a geometric shape as described above), phase prime metric integrates topologies of these Bloch spheres; as $n \to \infty$, elementary geometries combine as discrete points to make bigger geometric shapes drawn in a cycle or clock. A geometric musical language (GML) is recently introduced [6] to track the morphing of topology by the phase prime metric. Note that 3D phase structure is a new type of "time crystal" that we propose to integrate all information as topology in a single-phase structure.

What is a time crystal (movement without energy! no)? From any given point in a spatial crystal, by moving toward any direction, one would get different kinds of arrangement of atoms. Figure 1a shows that by rotating 360°, one should find at least two distinct spatial symmetries. One cannot imagine a space in a set of time intervals, as one cannot state a "direction." If the phase oscillates one full swing 360°, it is equivalent to the concept of all directions in a spatial crystal. On the circular 360° path, if at least once, the cycle hosts another small loop that shifts the rate of phase change, then one gets two time symmetries (Fig. 1b). A system point moving along the phase cycle perimeter would experience two different rates of time flow [58, 91]. The large phase cycle which constitutes a "time" is called the host time cycle, and on its path the local phase cycle is called guest time cycle. This guest–host phase assembly is called a time crystal [116]. Phase shift is fundamental to both space and time, and it is abundant in nature [38]. Therefore, information structure, if it is a 3D phase sphere, could represent all existing physical parameters comprehensively.

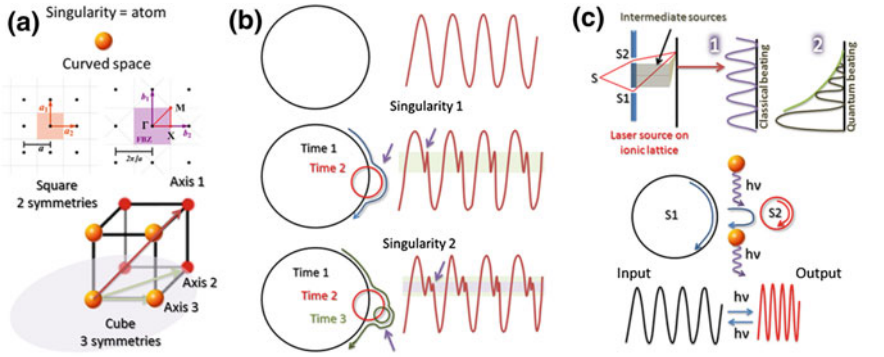

(d)

Winfree time crystal	Wilczeck time crystal
Input white noise, clocking wave is output	Input a clocking signal, output is modified clocking or beating
Clocks are nested one inside another.	Elementary clocks are isolated.
Phase singularity makes time, like curved space makes mass in a material crystal	No singularity, or singularity burst, or phase plane.
Topology of phase singularity has 12 possibilities to make time crystal, it comes from metric of prime.	No restriction on the symmetry of time crystal, like Bravais lattice, group theory, etc.
Clocking never damps. Under noise, crystal is permanent.	Clocking damps out. Crystal is temporary.
Phase cycle self-assembles to make crystal, metric sets rule.	No self-assembly
Resonance, synchrony acts.	Irrelevant.

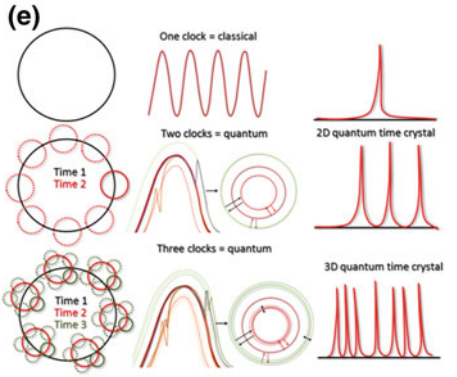

Fig. 1 **a** Spatial crystal. Square has two axes where mass distribution is different. Cube has three such axes. **b** Classical time crystal formation by Winfree. Input is white noise. Top row shows a clock and its output. Sinusoidal output wave deforms, as one new clock adds (middle row). Bottom row shows third clock added. **c** Wilczeck time crystal. S1 and S2 are coherent sources (input is LASER light). quantum beating is tagged as time crystal. **d** Difference between Winfree and Wilczeck time crystals. **e** Quantum version of panel a. Three rows have an additional column of Fourier transform of output (intensity vs. frequency). Nested clock resides all over the perimeter at a time. So, superposed clocks are dotted

Frank Wilczeck's version of time crystal contradicts Winfree's version: Frank Wilczeck revived the lost time crystal of 1977 in 2012 [108]. There is no guest–host phase cycle in Frank's version, i.e., the guest's singularity is absent. The follow-up works have surprisingly rejected the concept of singularity. An external energy input signal oscillates the diameter of a given time cycle by beating as shown in Fig. 1c. After a while, the original cycle returns [44, 119, 121]. This is like the orbital transition of an electron in a molecule. Such evidences neither support classical nor quantum time crystals. Temporal oscillation of diameter of a phase cycle is found in multiple systems. Periodicity in quantum ground state alone is not enough evidence to justify a time crystal. Therein, two different time symmetries do not coexist. If we detect one, citing uncertainty, it violates the basic

definition of a time crystal. Both time symmetries should coexist, with or without entanglement [37]; the uncertainty that we need in quantum would be in the phase path. Now, change in phase path is not much investigated in the history of quantum; it requires understanding of topology when one fuses multiple Hilbert spaces. Frank's version therefore has not two, but one phase cycle; it contradicts the definition of a crystal. Frank Wilczeck's proposal is also tagged "impossible" [26]. See Fig. 1d for comparison between our version of time crystal and Wilczeck's version. Our time crystal is an advanced from that developed in the Winfree era, we bypass the current sensation of time crystal, suspecting that it needs serious corrections on singularity. Figures 1b, e show the possible outputs of a Winfree class time crystal.

What is a singularity? A singularity is a gap in the phase space, where the phase structure of a typical biomaterial is undefined. At these conditions, a system resonantly vibrates, emits or absorbs signal of a particular frequency. Singularity points are corners of geometric shapes in the phase structure. A system point passes through the corners one by one, which we depict as the running of a clock, signals burst.

2 Here Are Twelve Properties of a Time Crystal that Advances the Winfree's Original Concept

(1) Clocks in a neural system self-assemble [7] to modulate time. For this purpose, a need for three clocks is observed in some biosystems [20]. One needs to add at least three interlaced phase cycles to make a time crystal that sustains at least one time symmetry breaking while interacting with its environment. The central clock or phase cycle remains protected by the other two terminal clocks serving as input and output interface with the environment. The slowest clock acts as a host phase cycle. It runs the system point of its guest central phase cycle, which acts as a host to its guest, the fastest clock. The central cycle regulates the two rates of time flows, in its guest–host system (Fig. 1b for classical, 1e for quantum). The central clock interacts with its host and or guest phase cycles without interacting with the environment. (2) In a network of three clocks, if stopping any one of the three guests or host phase cycle stops the other one, then it is a quantum time crystal. If the rest two clocks stop simultaneously, then it is not a time crystal at all; it is like day-to-day watch. Therefore, quantum time crystals claimed thus far would require major revisits. The central clock (phase cycle = clock) [91] survives even if the environment edits the two boundary clocks [97], i.e., slower and the faster ones. In such a three-layered clock, a time crystal turns naturally fault tolerant, i.e., breaking of time symmetry is uninterrupted. If the entanglement breaks, quantum time crystal converts to a classical time crystal (Fig. 1c). (3) We generalize Winfree's concept of singularity. The number of singularity points on the primary phase cycle of a host is the number of guest clocks [8]. It is the number of different time flows experienced by a system point as it moves 360°. Each clock can have its own system point and

can grow its own phase cycle structure or time crystal inside by making a new guest–host system. It can connect with neighboring time crystals or phase cycles as guests of a larger phase cycles. This is self-assembly of time crystals side by side [60, 96] or one inside another [52]. See Fig. 2a. (4) The relative locations of the system points estimate the initial phase differences among different clocks. It significantly changes the output measurement of the time crystal. To re-assemble the disintegrated parts of a time crystal, reviving the initial phase difference between clocks is essential. Such phase reset is abundant in biology [21, 27]; thus, biological systems have a memory to remember the phase gaps of various clocks. (5) When a time crystal has only two clocks, a 2D plane is sufficient to represent. If there are three clocks, then 2D phase cycles orient as a 3D sphere. Since three singularity points ensure holding a triangular geometric shape, this is a clocking Bloch sphere (Fig. 2b). The time crystal becomes information storage and processing device (Fig. 2c). (6) A spatial crystal appears different, from different directions. Its response remains the same as it is determined by the lattice symmetry. For a time crystal, different rotational directions of a system point on the phase cycle measure

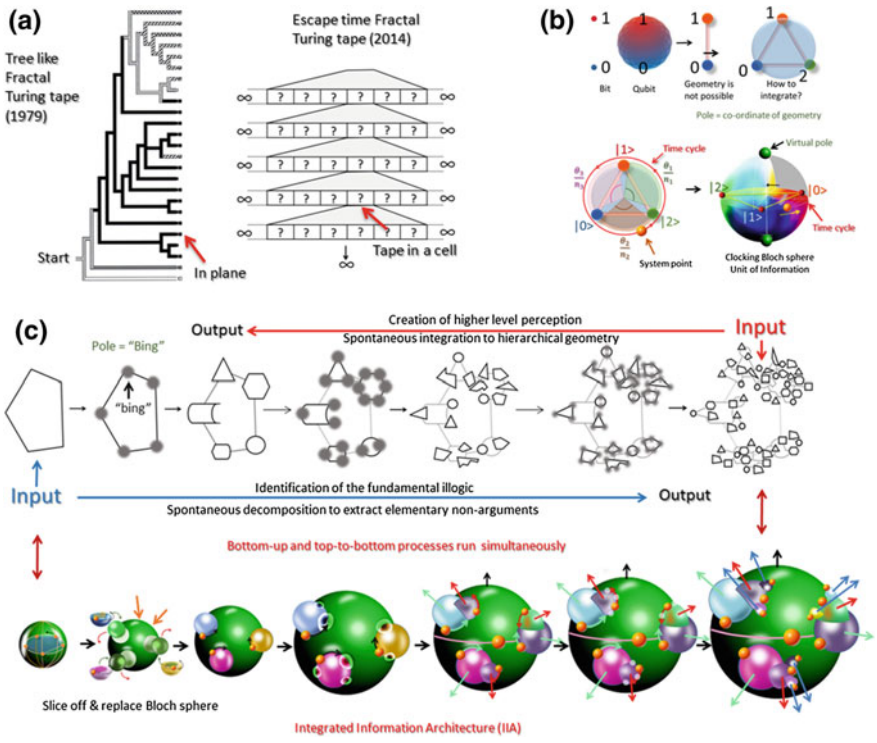

Fig. 2 **a** Two types of fractal wiring of Turing tapes. **b** A transition from bit to qubit (top left) to clocking Bloch sphere holding a geometric shape (bottom right). **c** Top row shows decomposition of a pentagon. Corner points are singularities. Each point holds a geometric shape inside. The bottom row shows the corresponding time crystals

different responses. It depends on three parameters: first, the relative phase difference between the clocks, second, the relative location of the clocks, and third, the relative diameter of the clocks. Follow vectors in Fig. 2c to see three situations. (7) The repetitive patterns of densely connected phase cycles are denoted as a "mass" in a 3D phase structure, when observers' time crystal cannot resolve the distinct clocks in the 3D phase architecture depicted as time crystal. Then, the relative perimeters of the longest phase cycles of the observer and that of the object or event being measured is "space." Thus, a "clock" made of a path whose points are phase values, the path wires discrete events, using an assembly of clocks one gets a circuit representation of mass, space and time [92, 97]. (8) The structure of a time crystal is determined by the topology of oscillators. Instead of breaking symmetry of a spatial lattice structure that generates the resonance frequencies, we need to study the spontaneous breaking of time symmetry. All singularity points may remain intact that is no change would be observed the resonance frequency band, yet, it is possible that time crystal is changing its symmetry. The relative phase path between frequencies is changing. To make a crystal, one has to fit many phase cycles inside a bigger phase cycle; such a nesting of phase is meticulously designed in biology [22]. (9) As described above, the singularity points residing on a phase cycle represent a geometric shape. A small perturbation to a system by applying a noise of selective frequency range reveals the singularity points, just like a noise reveals fermi level [74]. Perturbation creates a ripple of phase shifts [75]. The relative rotations of the phase cycles are restricted by the topological constraints. The topology of phase response curve reveals the variables and the constraints (Kawato and Tsuzuki 1978). The desired 1D, 2D and a 3D time crystal structures form [53, 55, 57]. The formation could be linked to the pattern of primes (Fig. 3a–i). (10) A time crystal is an artwork of singularity points connected by phase; not a single point in it is real. There is no time, space or mass; it is a network of phase [58]. Phase shift is the only event in the information processing, caused either by changing input frequency [39] or by intensity of light pulse [40]. Time crystal represents any information as topology and every topology or geometric shape is a single point or corner point in its higher topology. (11) The appearance of time crystal depends on three parameters: first, the observer's phase detection resolution, second, the relative phase between the observer and the time crystal, and third, the orientation of the observer. (12) The time crystal dynamics strictly depends on the topology of singularity. Neither classical nor quantum mechanics addresses the issue of singularity, so we have proposed a new fractal mechanics that makes a journey into the singularity [6]. Note that a waveform is represented by a system point moving on a circle (Fig. 1a). Using elementary math, we can calculate the number of ways to arrange a given number of waveforms or nodes of a standing wave. Just like there is Bravais lattice, strictly allowed lattice points for spatial symmetry; similarly, for time symmetry breaking, a pattern composition of choices of waveform restricts and regulates the transformation. In a classically static resonance band, one could measure quantum fluctuation of phase paths. In a random fluctuation of phase path of quantum, one could find topology of phase structure following fractal mechanics.

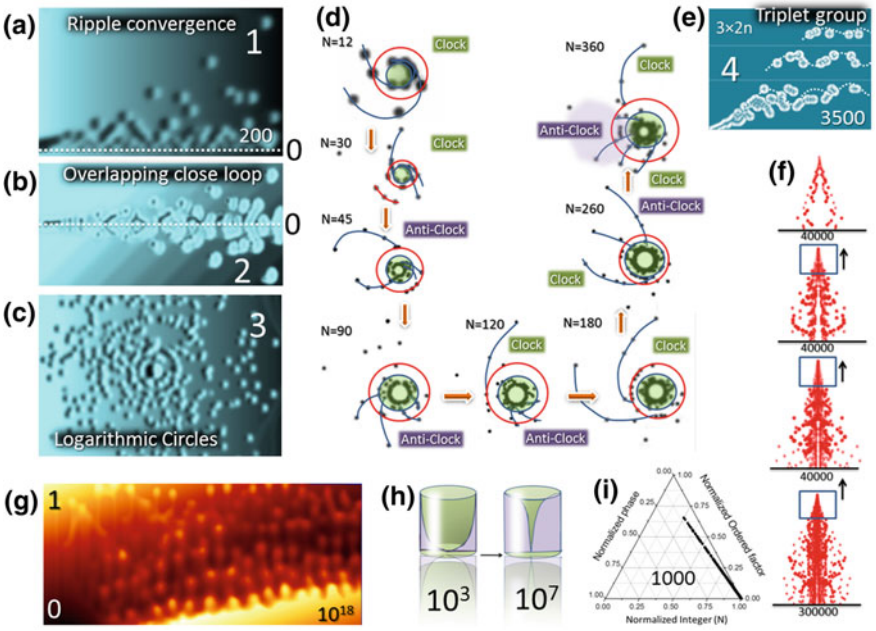

Fig. 3 Twelve phase prime metrics. Vertical axis always represents ordered factor or OF of a number *N*. **a** First metric, $N = 200$, one damping ripple of ordered factor is shown. Several such ripples form and damp as *N* increases. **b** Second metric, OF/2 versus *N* plot shows vertical parallel lines along with connecting shapes. **c** Third metric, polar plot of OF, for $N = 10^9$, period $N = 360$. New cycle begins at 361 and then again at 721, etc. Here, all OF points are connected by line. We get a gap. These gaps make circles. **d** Fourth, fifth and sixth metrics are derived for $N < 360$. For a given *N*, (<360), $1 - N$ numbers are multiplied to reach 360 and thus complete a polar loop. Radius of circle is OF. Then, we see three events to unfold. (1) Alternate creation of 3 clockwise and 3 anticlockwise spirals. (2) At a time only a few spirals are active, the rest sinks inside a circle. (3) A pair of active incomplete circles regulate the formation of spirals. This circle is the activity zone of the metric. **e** Seventh metric. If only those *N* which are products of 3 and 2 are plotted, we find OF-N metric which shows layers of nearly constant distinct oscillating lines. It is the sign of triplet groups governing the metric. **f** Eighth and ninth metrics. If only those *N*, whose OF > *N* are plotted, we find a unique pair of metric. The first one is a central core with a unique pattern. The second one is a triplet. **g** When convergent ripples of primes are plotted similar to panel a, we get a new network of waveform. This is tenth metric. **h** The slopes of OF with *N* increase to 90°, as *N* increases to 10^7. This is two imaginary transformation of discrete OF points into a 3D prolate shape. **i** The triangular plot of *N*, their phase and OF makes a linear line, suggesting that phase is quantized in phase prime metric

Ten biological relevances to a Winfree time crystal obtained via experimental studies of biomaterials: Winfree detected spontaneous emergence of singularity in a biological clock [2, 3]. An automated creation of a guest clock in the phase perimeter of a host clock prompted him to connect the emergence of life with the formation of a time crystal. A time crystal holds two or more distinct rates of time flow in an orderly fashion. It means the system can hold and execute an event.

(1) **The "signal burst or bing" is not important; silence or phase between the "bings" is important**: Detecting a time crystal has a clear route. Find if the resonance frequencies of a material remain the same. Then, check if the phase associated with each resonance peak changes with time. It means the materials dielectric property that regulates the resonance remains unchanged. The geometric parameter of the material edits the phase to run the clocks. For microtubule, it is length [103, 104]. By varying it, one finds a change in the intensity and phase of the peaks, but not the resonance frequency values [56]. ***The ratios of phases for the resonance frequencies determine the geometric shape stored in a microtubule. Similarly, one can determine the geometric information stored in the particular conformations of protein's and their complexes (see Fig. 4a)***. Currently, we are working on inventing a time

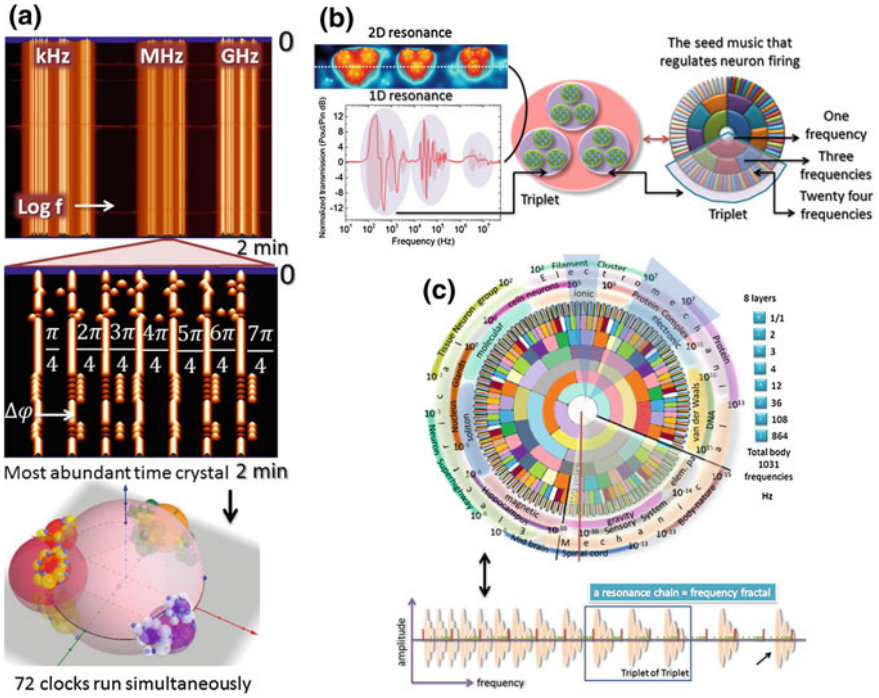

Fig. 4 **a** Top, resonance frequencies of a microtubule plotted in the Log scale continuously recorded for 2 min. Neighboring microtubules are continuously pumped with white noise. No change in resonance frequency is observed. During same time, phase difference between 8 peaks in the MHz domain shows significant shifts with the wireless energy transfer. Using these data, its equivalent time crystal made of 72 clocks is created in the bottom layer. **b** 1D resonance band of a hippocampal rat neuron, measured using coaxial atom probe. 1D resonance means electric field applied in one direction. 2D resonance means electric field applied in two perpendicular directions. Using a line, it is shown that 1D resonance is a single line in the 2D plot. To the right, triplet of triplet of octave made of 72 frequencies is shown using 2D resonance domain and nested frequency data. **c** Triplet of triplet made of 72 frequencies are shown for 12 bands. If one moves one inside another, it finds 12 bands; it is like a resonance chain where only three bands are visible. One has to go 12 times one inside another to access entire resonance chain

crystal pen that will read the 3D information structure as time crystal directly from nature.

(2) **Nesting of clocks was missing in the concept of time crystal**: The existence of time crystals was verified in the elementary life forms, for decades, experimentally. However, the nesting of clocks was never proposed or investigated. Winfree's idea of a singular singularity had to be generalized and we do that. A time crystal of a virus vibrates as a single clock. Inside, each plane of lattice oscillates in period; those are clocks inside clocks. Inside a plane, each group of atoms vibrates like a clock. The crystal acts like a clock inside a clock inside a clock [107]. The network has several layers within as the clocks are also clocked [45]. Such fractal clocking in the biomaterials is a recent discovery [52, 56]. In Fig. 4a, we are showing the resonance band of microtubule. Figure 4b shows that the phase is flipping spontaneously. In Fig. 4c, we demonstrate the corresponding time crystal. However, fractal clocking was reported in the ion channels long back [83].

(3) **Ten geometric resonance properties of biomaterials**: Recently, the resonance frequencies and their associated phases of various biomaterials were measured (Fig. 4a, b) [56, 103–105]. It shows that the emergence of frequencies is not random. They follow unique geometric relationship between them. Here are some features. (a) Various carriers interfere to resonate with the biomaterial cavities. Thus, make their distinct band of resonance frequencies. The experiments show that the distribution of frequencies is grouped as a triplet of triplet as shown in Fig. 4a. It means apparently there are three bands, but if one looks within one band, it finds three more sub-bands (Fig. 4a, top, notice the kHz, MHz and GHz bands). (b) Each region of all nine sub-bands contains one to eight peaks inside; this makes biomaterials E1 to E8 class systems. Biomaterials increases layered sub-bands, but no instance is reported to have more than eight peaks at the lowest level. (c) Figure 4b (bottom) shows the time crystal of a triplet of triplet band; it has 72 clocks embedded in the phase spheres. The diameters of the experimentally measured Bloch spheres remain the same. Only, their relative positions change, and on the 3D spheres, they are visible, distinctly. (d) Resonance frequencies are always associated with the quantized phases. A shift from quantization in a particular peak's phase value is the information (Fig. 4b, middle panel) [5]. (e) As one moves from higher to the lower frequency range, the scale-free power distribution of the frequency band is observed (Fig. 4c) [52, 56]. The intensity of the resonance peaks increases by orders of magnitude. (f) The amount of material is irrelevant. The geometric parameters, length, width, pitch and lattice parameters regulate the self-similarity of arranging the resonance frequencies. (g) Each frequency corresponds to a singularity point [85]. The value of frequency relates to the circle diameter. The frequencies of the resonance peaks would remain static, but not their phase. Using the phase, one can put system points at an accurate location on the host phase cycle's perimeter. This step secures the relative Bloch sphere positions. Thus, biomaterials are mathematically precise devices. (h) The time crystal remains

intact if the fundamental geometric parameters remain constant. Then, it is possible to change the system points and regulate the relative phase or phase shift [76]. The same time crystal would then store different information. This is interesting, because an experimental measurement of detecting resonance frequencies or phase associated with a peak would never show the information. We need to measure specifically the phase shift to see that a biomaterial is processing information. In the eukaryotic cells of the entire kingdom, microtubule rapidly changes its length (dynamic instability), sometimes its diameters (6–19 protofilaments) and then its pitch to morph its shape in incredible ways. Thus, it carries out key tasks of a living life form by editing its topology. (i) Sometimes, it is necessary to add or deduct some clocks or resonance frequencies. Then, the structure would change its typically associated symmetry so that particular singularity points disappear (all phase values get defined) or new singularity point appears. Subtracting or adding a singularity point means destroying the link or creating a link with several layers of geometries hidden within. (j) Number of oscillators or the number of devices has no relation to the number of clocks; it is not even related to the lattice symmetries. The number of lattice symmetries adopted by microtubule is the number of resonance peaks for a microtubule, not the number of clocks. Often, spatial symmetry breaking is associated directly with the time symmetry. ***A composition of lattice symmetries together defines a clock if they all undergo phase transitions as a group***. In the assembly of clocks, only eight dynamic symmetries repeat [103–105]. We have proposed our own fourth circuit element Hinductor for artificially demonstrating biological time crystals and the potential of singularities (Fig. 5a–c; Sahu et al. US patent 9019685B2).

(4) **Magnetic beating of beats**: Electrical beating occurs when two electromagnetic signals of very close frequencies interfere. Biological materials known for producing low magnetic fields (10^{-10} T) could generate beating locally in the lattice. Then, the beat signals could interfere again if the smaller lattice domain is part of a larger structure. Beating of beats could beat again, and such layered structures are rich in biology. Thus, one observes that beating signals cover entire electromagnetic or magnetic frequency domain (Fig. 5d) [5, 69]. Such a hierarchical network of beating requires simultaneous switching off the topological constraints at all level to destroy signaling. Thus, all signals survive together at ambient conditions (Fig. 5e).

(5) **Harvesting thermal, electrical and electromagnetic noise**: Time crystals in biomaterials reveal its unique phase relationship in the presence of a noise (Betz and Chance 1965a); we used noise trick inspired by biology to read the time crystals. Thermal noise compensation is rich in biology [28]; clocks neutralize the thermal noise [30, 50, 65]. Thermal pulses could even activate the biological clocks [46]. The origin of electrical ionic activity is attributed to oscillatory potentials in biology [29]. Even the electromagnetic pulses of light edit the biological clocks [47]. However, ordered signals affect the infrared photon absorption in biosystems. Signal inhibits the noise conversion to resonance-induced interference. It affects the nested beating described above

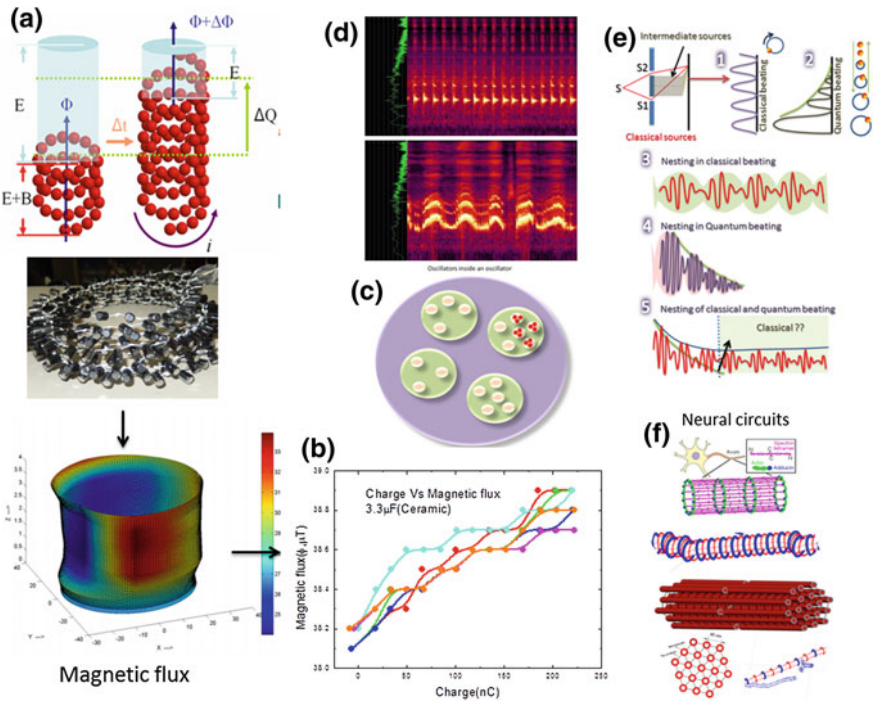

Fig. 5 **a** Fourth circuit element Hinductor not memristor (US patent 9019685B2). Charge stores to generate magnetic flux (top). An analogue made of capacitors (middle). Magnetic field distribution on its surface (bottom). **b** A oscillatory or nearly linear relationship between charge storage and the generation of magnetic flux. **c** Hinductor elements are kept without wiring inside vibrating membranes to create a composition of vibrations. **d** Classical beating (top) and quantum beating (bottom) inside a microtubule (experimental measurement). **e** Quantum and classical beating measurement setup used to detect Wilczeck's time crystal. The concept of fractal beating where classical and quantum beating is nested explained. **f** Ordered architectures inside a neuron, beta-spectrin-actin assembly (STORM data), microtubule bundle are being constructed in NIMS, Japan using Hinductor, the fourth circuit element

(Sahu et al. US patent 9019685B2). Among all frequency domains, biosystems absorb most in the infrared domain.

(6) **Harvesting singularity to self-assemble clocks: Learning, communication, all forms of information processing in neuron occur via time crystals**: Energy transmission is studied following a unique biological route, bottom up. Protein ↔ microfilaments ↔ bundle inside neurons (branches) ↔ bundles of neurons in a cortical column (Fig. 5f). It suggests that a neuron edits the phase of a transmission signal by modifying the neural branches [5, 56, 71]. The effort changes the stored geometric structure of the neurons time crystal, surprisingly, those we claimed it explicitly in 2016, and some old results were very near to it [32]. Neuron may take two steps. If a neuron builds a new branch, it creates a new clock. Else, it locally modifies an existing branch.

That edits the phase of an old clock. Thus, a change in the structure does not mean the creation of a new clock or singularity. Neurons communicate by clocking ionic pulses [61], but the evidence of wavelike communication is also there [68] apart from Ghosh et al's work in 2016. After the creation of a new branch, the system spontaneously investigates two factors: first, whether the phase modification is required in the new clock, and second, whether the new clock is integrated into a suitable location in the existing time crystal.

Similar to neuron, protein, microfilament and neurofilaments, assemblies inside the neural branches and cortical column edit their own time crystals [89]. The modified time crystals continuously edit their physical structure [113]. Greater neural pattern in size often dominates in the higher-level (slower) clocks in the time crystal [118]. Following magnetic beating of beats, all forms of vibrations are topologically connected in the brain. Electromagnetically this would have never been possible, as the electromagnetic signal damps in the cell fluids. Consequently, the proposal that a brain is a single resonance chain (Fig. 4c) [19, 56] is a primitive one, we modify our previous claims a bit and add that brain is a time crystal, and resonance chain is a limited view ignoring the topology of phase.

(7) **A nonlinear correspondence between spatial and temporal assemblies of crystals**: Even a tubulin protein molecule is a time crystal. It self-assembles into another time crystal, microtubule. Then, microtubules self-assemble into a bundle to build the core structure of a neuron, e.g., an axon. Neurons respond as time crystal (Fig. 4b) [32], a bundle of neurons forms a cortical column that is also a time crystal. The bundle of cortical columns also acts as a time crystal. A secondary structure of protein ∼2–5-pm to 1-mm cortical column, spatial journey is about 10^7 orders. However, the temporal scale regulation is from picoseconds to seconds, 10^{12} orders [52]. The parameter that regulates the phase relation of various resonance peaks is geometric. Tubulin's each of the eight conformations holds a particular set of geometry. Similarly, microtubule's different length, lattices hold suitable symmetries. Neuron's branches edit their own symmetries spontaneously. The cortical columns length and symmetries of neuron locations edit their own symmetries. In association with the spatial symmetries, the phase relationship changes together causing a ripple effect in the temporal symmetries. We repeat that the resonance frequencies remain nearly unchanged, yet ***10^7 order time crystal gets changed by 10^{12} spatial scale changes. We cannot isolate particular part of a time crystal and suggest that information is being processed here. To hold memory, various clocks only use the phase space, together; thus information is stored everywhere simultaneously***.

(8) **Interacting with the living cells and proteins in their own language**: The biological structures sense a phase connected time crystal network better than conventional sensors. A sensor absorbs the existence of a signal burst. Biomaterials senses not just phase links between several such bursts, but exactly the pattern following which those links change with time. We did

perform a nice experiment with the neurons. 7–8-day-old neurons were given a specific set of frequencies as time crystal, wirelessly. The suitable neuron responded. No searching is required for searching a suitable time crystal. Electric or electromagnetic signaling faces the effect of a physical boundary of a material. However, magnetic beating of beats do not face boundary; it integrates by a phase map with everything within a magnetic shield. So, communication does not happen like we see it in electrical or electromagnetic case. It was predicted in 2014, as a spontaneous reply [52]. Moreover, it was possible to encode geometric shapes in a neuron. Talking to neurons is possible in its own language (geometric musical language, GML) [6]. Even treating misfolding of proteins is possible by twisting the time crystals [105].

(9) **Clocking integration of resonances: Various kinds of resonances are not isolated events**: A list of published resonance frequencies and our experiments show that the ratios between different frequencies are not integers. Even they are not harmonic. They are anharmonic [56, 87]. The ratio of magnetic resonance frequencies is the golden ratio (phi $\sim$ 1.61). If the fundamental frequency is f_o, then the other sets of frequencies would be $f_o, \varnothing f_o, \varnothing^2 f_o, \varnothing^3 f_o \ldots \varnothing^n f_o$. The electromagnetic resonance frequencies occur at the ratio of pi; $f_o, \pi f_o, \pi^2 f_o, \pi^3 f_o \ldots \pi^n f_o$,. While mechanical resonances occur at ratios of $e, f_o, ef_o, e^2 f_o, e^3 f_o \ldots e^n f_o$. All three resonances are related by a quadratic relationship e^2 + phi^2 = pi^2. By following this equation, the biomaterials ensure an integration of electromagnetic and magnetic resonances delivers a regularized mechanical change in the system. There is a clocking integration even between three different kinds of resonances. It also justifies our fractal information theory, FIT, where we incorporate all topologies in a circle or topology. Nature makes it using the fundamental constants.

(10) **Clocking Bloch sphere holds the geometric locations of singularities**: Our experiments confirmed that the proteins clock like a time crystal, though similar claims were made in the 1970s. At that time, technology was not that advanced to provide a direct evidence. To be a time crystal, any system's resonance frequencies should change their phase as if three clocks are part of one phase cycle. A single system point while completing a full rotation 360° would find that all constituent clocks do not delay it, or let it finish full rotation early. Thus, one has to check if the change of phases of clocking frequencies is quantized. If yes, it is probably a time crystal. Six proteins associated with the neuron firing showed time crystal features: Tubulin, beta-spectrin, actin, ankyrin, clathrin and SNARE complex. Clocking of phase appears to be a universal property of proteins. During clocking, they hold specific geometric shapes (Fig. 6a). We repeat that a clocking Bloch sphere holding the geometric shapes made of singularity points was proposed as the basic information structure of nature in FIT (Fig. 2b, c) [6].

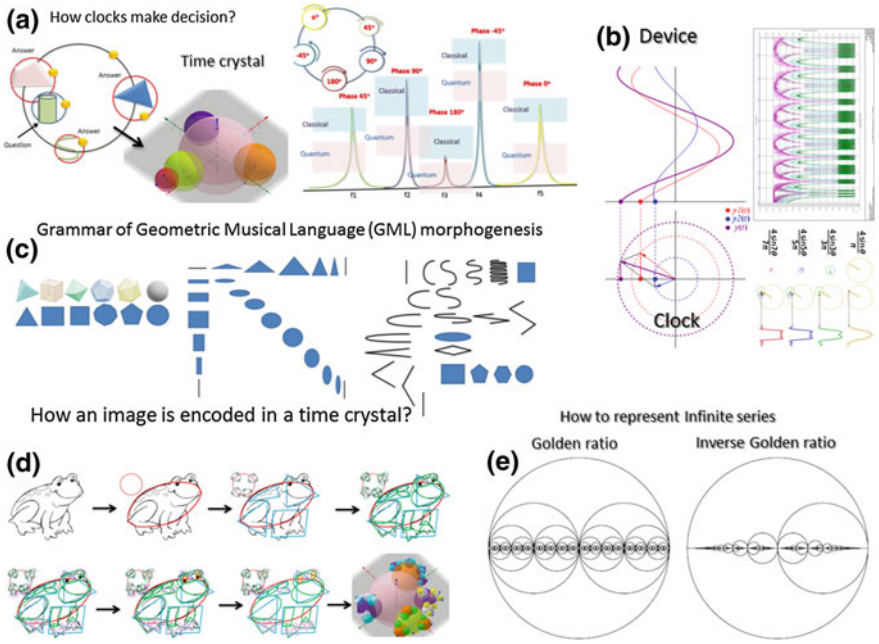

Fig. 6 **a** Geometric decision-making by a clock. This is fundamental operation of a frequency fractal computer. The time crystal representation of this decision-making unit is shown to its right. Reading a resonance band data to construct a time crystal is shown in its right. **b** Clock is a circle, but its output is sinusoidal. If more than three clocks nest, it turns to a binary pulse. **c** Inside a circle, the 1D–2D–3D geometric transformation happened due to the relative rotations of the clocks is listed. **d** In eighth step, a frog is converted into a time crystal. **e** GML and FIT work together by converting all data as part of infinite series: two examples, how to write, golden ratio and its inverse

3 Three Advanced Features of Time Crystal Suitable for Information Processing

1. **Creating a larger singularity or fill in the blanks inside a singularity**: Singularity points of a Bloch spheres bursts in a sequence, clockwise or anti-clockwise to hold the geometric shapes listed in Fig. 6b, c. These singularity points burst signals by harvesting noise in the biomaterials [79]. Singularity bursts of the biomaterials are discussed in detail [4]; however, we think a lot of research needs to be done in the near future on noise. The pattern of noise could play important roles in regulating temporal symmetries. The new fractal information theory (FIT) [6] has also analyzed the information integration. There are two ways to self-assemble multiple time crystals (Fig. 2a): first, inserting multiple time crystals inside a singularity point in a suitable topology, and second, looping time crystals with its neighbors by creating a new clock, i.e., bringing neighbors into a single framework. Figure 2c shows the growth of the

time crystals, how a starting Bloch sphere is sliced and new Bloch spheres are added. Bloch sphere expands/contracts to process information [6].

2. **At least three geometric parameters collectively regulate the phase of nested clocks in the time crystal**: There are four geometric parameters of a dielectric resonator. They are length, width, pitch of helical or other kinds of periodicity and the lattice parameters, which regulates the 12 singularity points in its 3D phase architecture. Two geometric parameters cannot be changed simultaneously. Our study on the fourth circuit elements has shown that if two geometric parameters are varied simultaneously, then singularity points encompass almost entire phase sphere. One has to underpin one of the four parameters that does not terminate major singularity points and causes minimum changes in the clocking time or phase. Say, it is length. Then, by varying the length, one could choose the right geometric shape. One has to write in the material or time crystal a desired phase. This neutral parameter edits structure. Thus, spatial and temporal crystals have to change synchronously to edit 12 singularity points while processing information.
3. **A time crystal is naturally a seed of astronomical number of events**: Creation or deletion of new clocks in the time crystal changes the 3D network of geometric shapes embedded in the phase structure. Simultaneously several clocks run in the crystal to hold the geometric information in multiple layers. The motion of system points in the time crystal links various geometric shapes as shown in Fig. 6d. To an observer, some shapes appear at specific intervals, while the rest of the geometric shapes appear simultaneously. Our time crystal is an advanced form of Winfree's time crystal; it holds clocking geometric shape which is equivalent of an event, not a static data or facts. The time crystals interact with the environment and morph perpetually, like biological systems [36]. The nature never stops changing. Interfacing clocks of time crystals never fully stabilize into a concrete phase structure. Therefore, a standalone time crystal is not a solid, but jelly, wherein, correlated geometric shapes construct an interactive matrix. Its phase flips, resembling a jelly. If nature triggers any of the elements or clock, it ripples the entire matrix. All associated time crystals get coordinated (Fig. 7a–d; Ghosh et al. 2013) [52, 54, 56]. We repeat, when all these processes go on, if one measures resonance frequencies would notice nothing. Time crystals do not need to be programmed to suitably linking with new clocking Bloch spheres. Only feasible compositions allowed mathematically are automatically embedded in the phase prime metric, which guides integration of newcomers. Phase connected 3D network of geometries cannot be linearized into a sequence of tasks. Therefore, it emulates nature as is like a universal sensor. In most cases, the 3D clocking geometry could be accessed in astronomical ways. Even if one twists input in an incredibly large number of ways, yet the structure would sync reliably. In a time crystal of 10 clocks, each clock with 8 possible connecting routes can coexist with 10^8 ways.

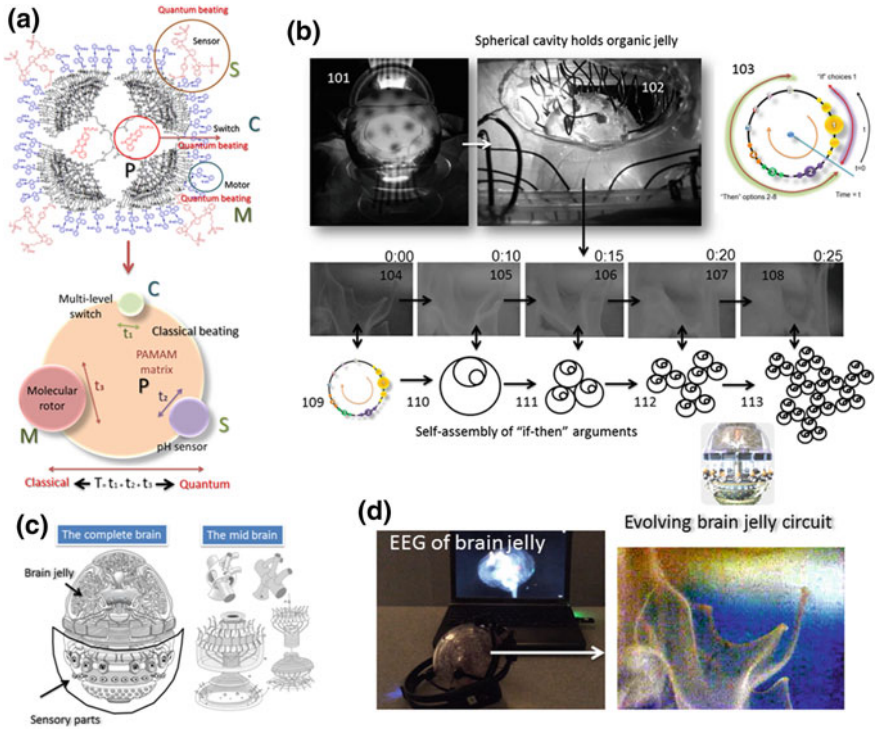

Fig. 7 **a** Elementary organic supramolecular structure used to build the brain jelly. Its time crystal representation is shown below. **b** Experimental images how a set of unit organic time crystals self-assemble to form a neural network like jelly to mimic brain-like activity. **c** An artificial organic brain designed and being developed in NIMS, Japan, for its operation. **d** EEG of organic brain jelly-based time crystal mimics human brain

4 The Necessity of a Universal Metric that Regulates Spontaneous Self-assembly of Time Metric

Nature is rich in time crystals. It has already optimized them by working for several billions of years. We have listed resonance frequency wheel and its corresponding 2D phase cycle network in Table 1a, b. The wheel represents how frequencies assemble together to form nodes in a dielectric resonator. While the 2D phase cycles are part of time crystals, it is the skeleton of information, because topological or geometric shapes made of singularity points are not shown. The entire table has been created expanding the gridding of triplet of triplet symmetry, for simplicity. Doublet of doublet, doublet of triplet, triplet of pentate, all compositions are there. Self-similarity of various time crystals hints for a metric of finite patterns. That metric gives rise to all possible symmetries found in nature. The geometric similarity between resonance frequencies demands for an invisible resonance chain

Table 1 (a) First part and (b) second part of the table showing step-by-step evolution of computers or decision-makers starting from a single time crystal

(a)

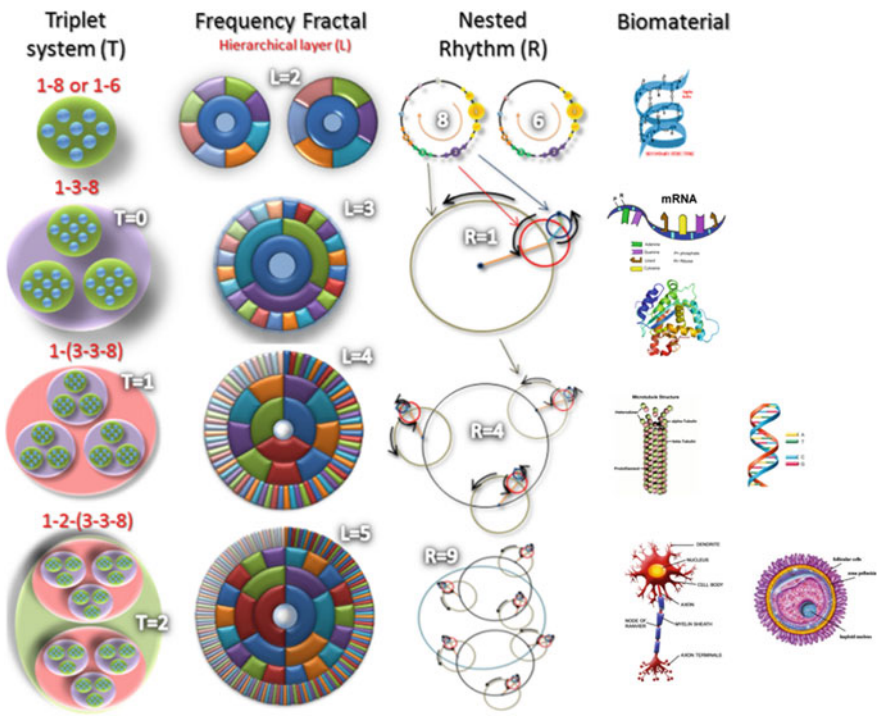

(continued)

Table 1 (continued)

(b)

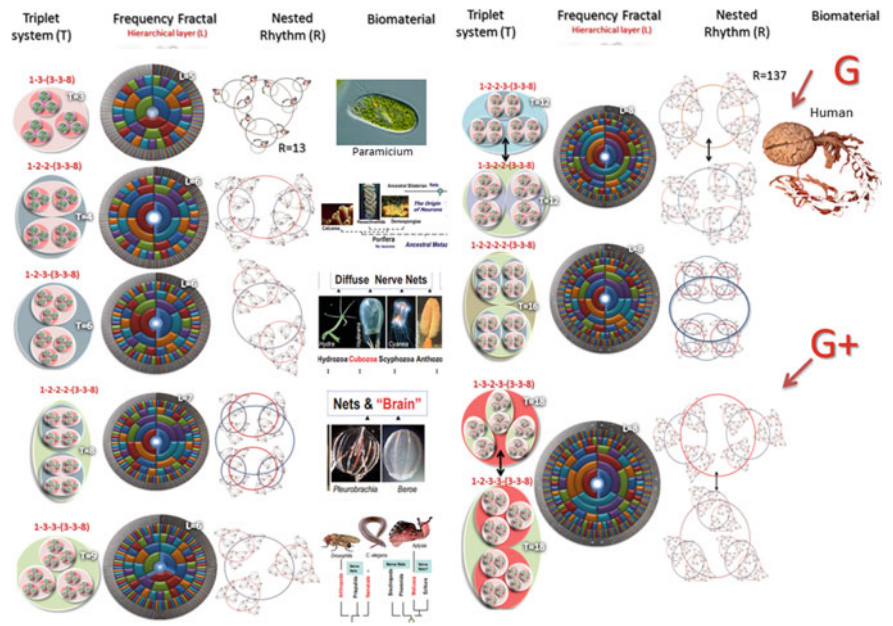

First column shows 2D resonance domain, second column shows equivalent frequency wheel, and third column is a slice of time crystals showing simplified operation. Fourth column shows the equivalent biomaterial targeted to mimic

[52]. The phase quantization is not possible without a universal rule governing the shape of dielectric resonators. A hidden universal metric governs the basic structures of the time crystals. ***We have calculated the pattern by finding the number of ways a given number of nodes could combine successively until we reach prime number of compositions***. It varies non-linearly as the integer grows from zero to infinity. Then, we have calculated how this pattern would look like under various constraints, like n phases that make 360°; then, we find clockwise and anticlockwise rotation, etc. (Fig. 3). We can normalize the number of choices to one, to find self-similar ripples in the number systems. If one event represents one point, and each event is a topology, the pattern suggests a common non-repeating routes or metric as their singular origin. Events occurring in nature are not random. Random events integrate from one singular metric. That metric is closely related to the vibrations of dielectric resonators [73, 81, 82, 94, 95].

Research in the last decade to address the problem of computing: Historically, there was always an effort to "go beyond Turing" [34]. It started by von Neumann to build non-von-Neumann machines. It continued with Turing with an attempt to building non-Turing machines; one class is hypercomputing [109]. Feynman proposed to "replace all physical laws with changing patterns" in 1962 [101, 102]. It

continued with a series of works to make it nature inspired [99]. Quantum mechanical coupling was applied to non-sequential computing in the atomic scale. In 2008, 16 molecular clocks were placed around a single molecular clock [12]. Then, the central molecule was tweaked to process 4.2 million 16-bit choices of the nanowheel. Comparatively, a sequential process could provide only in a structure that violates the Turing system. One could see online video of this time crystal. In 2010, Feynman's suggestion (1962) that patterns compute is true was tested. Two physical events were emulated using quantum properties of molecular clocks [15–17]: First, the evolution of cancer cells, and second, diffusion of electrons on a grid of molecules. The result was obvious. Cellular automaton works as a Turing machine [101, 102]. Two events were emulated, but if there are more events, one required a new hardware. Then, scaling up was impossible. The quest for a universal system ranged from neural network [13–15]. It would require a new hardware every time one tries to emulate a new natural phenomenon. All efforts failed.

A dielectric engineer would consider that everything in this universe is made of dielectric resonators [73, 81, 82, 94, 95]. For this worldview, one can calculate the geometric correlation between the resonance frequencies ranging from the Planks scale to the largest dimension of the universe. A unique pattern of primes is found holding all possible solutions to all possible dielectric resonator networks. This mathematically derived pattern is the phase prime metric (Fig. 3). It was historically used by many researchers to claim that it connects everything in the universe [64, 110]. If true, a hardware inspired by this phase prime metric should absorb the information in nature. During absorption, it will not destroy the 3D integration of events. Then, a small fraction would extrapolate into total information [66]. Thus, analyze events that have not yet happened by using the metric of primes. Simply put, "phase prime metric" would hack nature, copy and paste it in the hardware. Therein, one would see nature, the way it unfolds.

The phase prime metric hardware (non-computer) would not require codes. We plan to eventually optimize the phase prime metric that let the events happening to nature sitting inside our non-computer. It tells beforehand a gross overview of what might have happened or could happen in the future (Quantum computing claims partially) [120]. Then, the phase prime metric is an alternative to a computer programmer; it is an user. The intellect of artificial intelligence is the aptitude of the person who wrote the code. Alternately, a meticulous information structure of any event could be configured from the phase prime metric. Different patterns of a metric act in coherence to frame an event. This key set of compositions is required to simulate or emulate the event. Once the metric codes are read, the event is reliably recreated. Free will and unpredictability are there in nature. However, it is not random [84]. A generic operator "phase prime metric" puts an intricate geometric detail of the event in nature. One reads an event's phase–signal relationship as fractal seed (a few geometric shapes written in a network of clocks, Fig. 6d). Then, one writes that in the metric structure.

What is a phase prime metric: Say in the beginning nature is given only one quanta to create the universe and only allowed to decrease the wavelength of a single quanta, by splitting it one by one, dividing one into two quanta, then each

one into three and so on. Now, the nature's approach would be top down spatially, from the largest boundary of the universe spatially making a journey to the plank scale. Simultaneously, mapping the shortest to the longest time is possible. Together, the journey would look like Fig. 2c. A standing waveform is part of a clock (sin or cos wave = a circle with a rotating system point), and it occupies a space, so it is an unified way to map both space and time. A given number of nodes of a waveform are combined until it reaches prime number of nodes. Then, in a particular way, both time and space are integrated. Therefore, one gets a composition of frequencies. The number of the composition C is plotted as a function of a number of quanta n. A group of primes determines C compositions. C-n plot shows geometric correlations of different choices [42, 62, 100, 117]. C-n geometric pattern is called a phase prime metric. Twelve distinct ways one could connect the dots or events in the phase prime metric (Fig. 3). Therefore, there are 12 sub-metrics, or 12 geometric patterns, one top of another. If 12 special methods are adopted, each pattern is seen.

Historically, phase prime metric connects the smallest dimension known to us to the largest dimension at the extreme end, or a single event to the all possible events, or fastest time to the longest time possible. Spatial interpretation is easy to understand, through all three interpretations that are equivalent. Choose a length as the starting half-waveform, and start calculating its ordered factor (OF) and/or divisors following protocols developed for centuries. This is one of the simplest known mathematical problems taught to kids. OF can have many interpretations too. All possible superposition for a given number of waveform is OF. All possible ways one could combine an event is OF. All possible ways a space could be mapped is OF and so on. But one should connect the nearest neighbors in the OF plot for $N = 1$ to infinity, to learn how network of events could be a single event represented as a single point would combine and evolve with space or time or mass. The beauty of phase prime metric is that once a point is defined, its integration topology is revealed. If it is time, then the past and the future is also evident. The number of composition varies non-linearly with the N number of waveform as shown in Fig. 3a–c, e, g. The origin of non-linearity is the irregular occurrence primes as evident in Fig. 1g. For the prime number of waveform, there is no harmonics, hence no superposition. Recently, fractal metric is suggested to replace space–time metric [90]. Phase prime metric shows phase fractal (Fig. 3d), triplet grouping fractal (Fig. 3f), phase quantization (Fig. 3i), organized selection of clock and anticlock spin (Fig. 3d), circular traps at logarithmic space (Fig. 3c), saturation of patterns for 1 = 1 million (Fig. 3h).

Advance from the existing fractal space–time metric [90]: The established route of fractal space–time adds a physical reason of connecting the neighbors [4]. First, one has to divide the number of superposition ($\pm h/2$) count. It inherently considers that the there is a Bloch sphere whose diameter is h and $\pm h/2$ are two of its poles. As the number of superposition increases, one gets larger spheres. It is known that the Hilbert space is infinite in size irrespective of the Bloch sphere diameter. A Hilbert space connects various pathways between the poles. The composition of superposition estimates the energy of a dielectric. It also measures

the number of degenerate states of a system. Connecting the neighboring compositions means connecting the neighboring real poles. It transitions between different energy packets. A Bloch sphere also represents a particular symmetry. A closed loop drawn by connecting the points is a set of symmetries. This set forms an energetically coupled group. This is strictly how a material is defined. "A set of symmetry" defines a lattice, a dielectric, a real structure. However, a 2D loop in the phase prime metric does not tell us how its corresponding object looks like.

Derivation of wiring of clocks from phase prime metric: For this reason, one rotates the *XY* plane 360° along the *X*-axis ($X = n$ or number, $Y = C$). When one connects the $\pm h/2$ points, using an imaginary line, a 1D line makes a 2D surface. However, when one rotates the *XY* plane, an infinite number of the same imaginary lines in the 2D surface roll. Thus, one gets a 3D structure, teardrop to ellipsoid, vortex to spiral and dumbbell disk to nephroid. As noted above, each $\pm C/2$ points form a Bloch sphere. As the 2D surface rotates around the *X*-axis, the real points of the Bloch sphere rotate with the same angular speed. Multiple geometries overlap in the metric. A pair of teardrops of different sizes overlap or a teardrop overlaps with an ellipsoid. Then, the rotating speeds of the real points of the two shapes are different. If more than a threshold, then it satisfies the condition of singularity. Thus, as one connects the *C* coordinates, it is applying geometric algebra that creates a hyperspace. The process generates naturally abundant symmetries and dynamics from the pattern of primes. A slice of phase prime metric designs a universal sensor. Phase prime metric inspired sensors would capture the natural events more efficiently.

Imaginary lines are phase paths connecting the singularity points. Once a singularity point is formed, it triggers a cascade effect. Singularity acts like a glue. It embeds various time crystals inside or connects side by side [60, 96] to the surface of the Bloch sphere. Singularity points are undefined functions. There are layers of geometric shapes inside a singularity point. Several clocking spheres pour in and embed in the host sphere. Thus, the Bloch spheres expand as it integrates information as shown in Figure lb. This is fractal information theory (FIT) (Fig. 2c) [6].

Now, we explain geometric musical language so that the "fractal seed" is understood properly.

The fundamentals of a geometric musical language (GML): Many small circles written as pixels on a big circle act as a clock. If one zooms any phase cycle or clock, similar tiny phase cycles or clocks are found inside. This is how several clocks reside inside a clock, while the side-by-side assembly of the clocks forms when such circles are drawn one top of another. All the circles of a time ring oscillate continuously. During oscillation, it increases its diameter together coherently (in phase) and decreases to a single point. That single point is also one pixel or the smallest phase cycle [91]. Say, one of the many connected pixels starts oscillating in a different phase, for a certain time. Then, returns to the same phase like its neighbor. This happens with all the pixels one by one in a sequence. Then, an external observer sees as if a point is moving on a circle, or a clock is born. Two such points hold an angle that enables encoding a geometric shape. For example, by shifting the position of points, one can encode triangles of any shape. Similarly, by

using four points one can encode a rectangle or square and so on (Fig. 6a–c). Every pixel in a phase cycle is another phase cycle or clock [58]. When clocks change locations, it is not a crystal, but a jelly. The jelly absorbs, writes and erases the time rings or clocks to sync with its environment [14, 57].

How a decision is made by Geometric musical language (GML): Self-assembled geometric shapes represent all sensory signals. Geometric shapes can integrate two ways: side by side and one inside another. The corner points of a geometric shapes break, and then, one inserts a geometric shape in it. Thus, geometries grow side by side and one inside another. It is not a 2D structure. The integrated geometric shapes are best represented in a clocking Bloch sphere (Fig. 6d). When it integrates, information bubbles of Bloch spheres would grow [6]. When a time ring holds more than one geometric shape, any of them could represent a query and the other an answer. Therefore, when the clock runs, the decision is made for a query (Fig. 6a). The existing 3D assembly of Bloch sphere adds new sets of nested clocks or bubbles with its surface [112]. During addition, it even undergoes a phase transition just like an organic supramolecule [53, 55, 57]. The rule for phase transition is same, "symmetry breaking." Here the 3D oriented structure of phase cycles is an alternative to program or algorithm. When synchronized clocks run together, every time, synchrony selects a new wiring [88]. To an external query, all the associated clocks run. All issues related to a query are played out by the clocks. Since entire Bloch sphere architecture is one single structure, no choice is left out.

Experiments that enabled us to construct geometric musical language (GML): Pumping a time crystal holding geometric shape is the route to test a geometric musical language. The resonance frequency band and associated phases need to be written in an antenna to pump. If one plays time crystal music to a microtubule, it responds a crystal. Similarly, by synthesizing the organic jelly a neural network like supramolecular structure was built (Fig. 7a, b) [53, 55, 57]. That brain jelly is poured in a fractal dielectric, designed similar to a brain. The organic jelly made device of time clocks morphs the EEG features of a human brain (Fig. 7d). Clock like crystallization of materials is unique in nature [31].

How the phase prime metric hardware is designed and built: The philosophy is that all information in nature is an event, like a single point, which has inside a geometric shape with its corners made of sub-events. Following that philosophy, one has to convert a stream of all sensory signals (visual, auditory, etc.) into a time crystal. There are several self-similar geometric shapes of the time crystal. Phase prime metric-based filter shrinks the size of a time crystal network. The shrunk time crystal is called a fractal seed. The decision-making core is 3D time crystal architecture. First, one should pump such a fractal seed into it. The fractal seed expands by phase prime metric and morphs into an information architecture (Fig. 2c). During morphogenesis, fractal structure formation is common in biology [35]. Most dense parts of a time crystal network are blacked out as if these are pieces of mass. We repeat that phase shift models space, time and mass as network of clocks mimicking biological rhythms [49]. If these "masses" are replaced with clocks, phase lines with wire, one gets a circuit. This circuit vibrates like the time

crystal. Building a circuit from the phase prime metric requires ten steps. We discussed it below in a separate section. The experimental prototype of the non-computer is a device whose vibration is similar to the phase prime metric. There are various ways to do it. A suitable organic jelly [53, 55, 57] is being developed for over a decade (design in Fig. 5f, result Fig. 7). Now, a suitable fourth circuit element is found (Sahu et al. US patent 9019685B2). It could be assembled to clock like a phase prime metric. If a white electrical noise is applied to this hardware, then the clocking waveforms superimpose. It delivers a resonance frequency pattern like that of the phase prime metric. With the current technology, it is not possible to realize circuitry with intricate details of phase prime metric. It is primitive, but at least a hope for the future. Moreover, no one requires a new accurate high-resolution computing. The existing Turing based computers are ultimate in doing that.

Prototype under construction in NIMS, Japan: A global platform is under construction [10] (JP-5,187,804-"a vertical parallel processor"). In the current prototype, a slice of $N = 1000$ is cut from phase prime metric. Find its equivalent clocking circuit. Depending on the number of integer in the metric, define its class. For example, $N = 1000$ means a thousand class hardware; if $N = 10^{12}$, then it is a conscious class or G class (see Table 1b, G and G+). A G class means a superposition of a pair of time crystals generated by a single hardware (classified). However, a global triplet of triplet fractal pattern emerges in the phase prime metric. If that seed pattern is plotted in a circle to address the phase quantization, it makes a wheel for 360° phase. This is noted as frequency fractal (Fig. 4c). Frequency wheel classifies the non-computing ability in the hardware. It also accounts for a transition from artificial intelligence to natural intelligence.

Determination of wiring between clocks from a phase prime metric: There is an upper and a lower time limit of an integer representing a decision-making non-computer. Non-computer core architecture is a fractal network of clocks or clocking Bloch spheres holding the geometric shapes. Mathematically, it is an assembly of a large number of distinct ΔN slices of the phase prime metric. To cut a ΔN slice of metric, start at $N = 0$; end at a certain N value. All clocks are wired following ten steps noted below. A metric prime hardware could be realized in various ways. We repeat every point in the phase prime metric of Fig. 3 is an event that contains many points forming a geometric shape inside. One could start from any simple event to begin with and find events inside, continuously, building a topological network.

(1) **Select a set of *N*, e.g., {1, 3, 7, 45, 32, 734, 1500, 3800}**: A set of n values is selected on the phase prime metric that forms a closed loop. The phase relationships of N Bloch spheres plotted in a circle. Together, n components try to cover a phase space of 360° (see Fig. 3). The plot reveals the value of quantized phase. The resultant parameters of spiral dynamics become evident as in biosystems [24]. In the set of n, some engage in clocking; others are found as not participating in the periodic vibration. They remain outside the spiral or vortex dynamics that integrates a set of N.

(2) **Identify different slices are components, to make individual loop of geometric structures**: All distinct slices of a phase prime metric have their own time crystal or phase space structure. A slice means a set of values n in ΔN; it has its own factors, own sub-metric. The network of time crystal reveals hidden geometric structure. The layered geometric structures match for all N time crystals and those hidden self-similarities group subsets of N. Therefore, even before the phase prime metric starts convergence to primes, as a drive to integrate the discrete time crystals into a singular one, a preliminary grouping is made.

(3) **Initial phase gap between the clocks is important**: Initial phase relationships between different clocks can change the output projection of time crystal dramatically. Initial starting points define temporal change of phase or dynamics. Temporal recording of resonance peaks reveals how the time gap or phase gap between clocks changes with time (dynamics). For a given slice of metric ΔN, the dimensional ratios of the n geometric shapes located at n points on the metric are noted (Figs. 4a and 6a). Junctions of clocks locate system points; direction of rotation is selected to neutralize vector sum of 3D structure. The system points and their phase gaps determine the angle between clock planes.

(4) **Fractal network of clocks, side by side and one inside another**: When a set of N integers is spotted in the phase prime metric, the integration begins. Say two integers of set N are 32 and 56; they make individual time crystals by following phase prime metric. At the same time, their products ($N1 \times N2$, $N1/N2$, $N1 + N2$, $N1 - N2$) will be the new members in the phase prime metric; expansion of set numbers will be plenty to find a closed pattern in the phase prime metric. The gaps will be filled by repeated elementary primes. The repeat of primes repeats a particular geometric shape to build a large structure. These repetitions cause self-similar patterns in an architecture; there is essentially no universal fractal in the phase prime metric.

(5) **3D geometry optimization of clock location**: Since one has to build a wireless network of clocks, the physical location of the clocks in a 3D network is important. Wireless projection of constituent time crystals all around, by 360° solid angle, selects whatever time crystals reside in its path. A 3D network appears as a sphere to an external probe or we state "3D projection of a time crystal." So, the clocks along a line screen each other's information, thus creating an erroneous signal to an observer. Note that in case of conventional electromagnetic signaling by an antenna and a receiver, the energy degrades largely with the distance. However, for magnetic beating in a noise activated phase coupled matrix of time crystals, there is no single point source of energy and no fixed destination. Thus, size of the phase network is irrelevant to an observer, which also becomes a part of it. Geometric locations govern the phase relationships of the integrated clocks. Locally in the 3D architecture of the computer core, a group of clocks shifts their coordinates. Thus, locally, the system shifts from one metric to another.

(6) **Vibrations at all time scales in all spatial scales maintain speeds**: Clock speed is regulated by delay time and fixed everywhere in the metric hardware. Only one, the fastest clock alone is used to integrate the phase or delay to create all possible "times" for operation. For that purpose, it is imperative that every clock senses all neighbors once hardwired. This is a critical technological challenge. All the clocks communicate wirelessly in a hardware following magnetic beating of beats explained earlier. The localized beating during synchrony should converge on the particular locations of the clocks, so that phase shifts do not occur. Phase shift with the motion of the system point is key to reliable processing of topological information. The speed of a system point along the perimeter of phase cycle changes if it falls into the singularity domain and recovers it afterward. This falling into singularity is crucial for editing geometric memory.

(7) **Thermal and electrical noise as the source of energy**: Wireless communication is the key to achieve "one-to-many and many-to-one" communication [12, 13]. The 12 singularities detected in the biomaterials 3D phase space link magnetic field with the stored charge. This relation is historic because in the last 800 years all theories of electromagnetism have endorsed that a current must flow. But this phase space activates by noise and only noise; no current flows into modulate magnetic flux with charge. For that reason, clocks are wired, but make sure that em noise splits into electric and magnetic parts, but no current flows, but only white noise (Sahu et al. US patent 9019685B2). Thus, a clock in a phase cycle is free for neighbors; no wiring is essential.

(8) **Testing the 12 metric compatibility, building a grammar of limiting changes allowed**: First, the clocks are wired as suggested by the phase prime metric. Provisions are kept so that input time crystal modifies the coordinates of the clocks. Specific input time crystal selects one of 12 distinct patterns of phase prime metrics (Fig. 3). It is crucial task to find the right trigger. A delicate choice of the clock coordinates eventually allows a few metric to dominate. We are currently adding several new aspects of the phase prime metric. Newer and more insightful metric features are being revealed.

(9) **Geometric shapes synchronization is a test of unity (oneness)**: The non-computer has two parts: First, converting all sensory signals into a set of topology, and second, integration of topology. However, at both parts the geometric shapes spontaneously store and synchronize the clocks. Circuits modify; filters, amplifiers and vibrating membranes are added to process geometric musical language [6]. The whole device is just one single clock holding plenty of clocks inside. The non-computer core has one device, only one geometric shape for all sensory memory.

(10) **Non-disruptive Interaction between the four modules**: Finally, the wiring is edited to enable the device as a filter, resonator, inverse of resonance and clocking geometry writer. Once these four qualities are optimized, a true hardware of metric of primes is made. It is tested for image processing, hierarchical perception to find the mismatch in the wiring. A particular test is repeated in all directions of the 3D network of clocks.

Four essential modules of the phase prime metric hardware: A diffusing function connects the dots (composition, h) to show a superposition of 12 different sub-metrics inside one phase prime metric. Following ten rules described above, four modules are made, as a core decision-maker [52]. They are sensor to sense the environment. Initiator filters and makes instant decisions. Processor stores the learned situations. Regulator filters the learning parts and evolves entire architecture. The four hardware modules operate independently in the non-computer core. Together, they have a purpose. It increases the length or number of integers in the slice of operational phase prime metric.

5 The Operational Mechanisms of the Non-computer

Viewing a decision-making in terms of time crystal concept: All are time crystals that vibrate like metric of primes. The same hardware is used differently to get different functionalities.

First, sensor acquires data from its environment. As the signals fall in, due to resonance, associated clocks are spontaneously activated. Thus, the phase prime metric based sensory network transforms even a binary stream of pulses into a 3D network of clocks, instantly. The sensor network builds an architecture of input time crystal, irrespective of nature of sensory signal.

Second, an initiator acts like bipolarity filter. In one way, it shrinks the size of an input time crystal. Output becomes a small fractal seed. If the input is sent through the reverse direction, phase prime metric fills the missing gaps. It inflates the time crystal, to its original form, sometime much larger. Output time crystal contains situations not yet happened, i.e., futuristic dynamics.

Third, all parts of a processor are always active. As time crystals arrive from initiator, synchronization begins. Entire phase prime metric from the smallest to the largest time scale syncs simultaneously. All the matching time crystals amplify the signal.

Fourth, a regulator synchronizes with the time crystals missing in the processor part. It activates the new missing clocks inside. The mismatched yet essential clocks find suitable location in the Processor. They are later absorbed there as a part of learning.

Viewing a decision-making in terms of geometric musical language: Corners of a geometric shape are made of singularities. When the clocks run, at the singularity points one hears “bing” [85]. The time gap between a pair of “bings” tells us the phase gap. The ratios of the phases hold the geometric parameters. This is the rule of composing music too, note geometric musical language [4]. Therefore, to feel like a triangle one can combine three ringing bells with an alarm clock (Fig. 6a). The alarm rings the bells after certain intervals. In this way, using a simple circuit one can realize an analog of clock-based geometric memory. This kind of decision-making or non-computing does not distinguish between question and answer (Fig. 6a). Both get the same status. Various geometries self-assemble as

clocks in the phase cycle. It increases the complexity of decision-making. It is preferred to assemble the nanosecond clocks alone in the entire circuit. Fast clocks are coupled to deliver clocking at all time scales. Picoseconds clocks make a seconds clock. Singularity is a key to this non-computing. However, a separate hardware provision is not required to realize that. An external sensor could lock on any part of the hardware. Due to two limiting time resolutions of the sensor, the fastest clock and the slowest clock are selected naturally. Thus, a decision-making fixes the end of computing before even it begins synchronization.

6 How Phase Prime Metric Replaces the User and Enables Self-programming

Circuit-based Turing computers have human as the key component for its efficiency. Non-computer relies on the phase prime metric to fill the gap and expand the time metric it gets from nature. Discrete clocks link. If some clocks are missing, they are created. Constructing a higher-level clock is the only drive of a non-computing core. A drive to make slower clocks gets everything done, spontaneously.

7 The Use of the Pattern of Primes in Integrating the Time Crystals Has Ten Major Advantages

(1) **Retrieving the lost data and transmitting a fraction**: Sometimes, a hardware damage loses information. One has to place the remaining part in user's time crystal network. The pattern of phase prime metric integrates the available crystals, thus recreating the missing network [17]. For this reason, there is no need to communicate full information. If a fractal seed is sent, it evolves uniquely, more profoundly in the receiver. The morphing of a fractal seed retrieves total information. See Fig. 6e; an entire infinite series could be retrieved from any part of hardware.

(2) **Drive to integrate discrete time crystals is similar to programming**: The metric acts as an operator on the input matrix of clocks. It links any form of time crystals with slower clocks. The phase prime metric has two drives. Make slower clocks to integrate, and expand its phase prime metric implementation. No hardware can implement a phase prime metric with intricate details. A continuous drive to improve metric makes nominal mistakes in reconstructing the perception of logic.

(3) **Provide key information to change wiring**: Unlike other space–time metrics, the phase prime metric does not depend on user's guess. It determines the detailed structural features like an origami [57]. The time crystals dynamics

are mapped accurately. The time of symmetry breaking and the states post-phase transition are also determined. Thus, the phase prime metric provides the software solutions, like a fusion of a user and computer. The essential hardware modifications required for an input time crystal to store and evolve are also delivered.

(4) **Higher-level perception is naturally embedded**: A phase prime metric hardware has embedded self-similarity. As a result, it does not count "bits," but a pattern of time. Slower clocks integrate the faster clocks in a scale-free manner [43]. In its own time scale, clocks are arranged symmetrically. It enables fractal clocking. It means during a one-second operation, one could dip down into the picosecond scale, process and return with a solution before the one-second clock "ticks." Fast running time crystals are never left alone. In a widely varied time scale, only a few clocks need to "tick" to make a decision.

(5) **Computing location, start, end and halting are decided early**: The construction and editing of the time crystal continue forever. During synchronization, the transformation (morphing) peaks, but do not die out [17]. The effective length of the metric is infinite due to a closed loop [63]. It also drives to increase metric length. This has several advantages; no instruction is needed to start and halt. Halting is a significant problem only when the end is not fixed [86]. This is a case of Turing computer. Here, computing is all about entering inside a singularity, so the start and the end are fixed before the journey begins. The metric activation reaches a maximum and then naturally reduces the editing of the time crystals. Thus, a near halt is reached.

(6) **Non-reductionist approach: no choice is ever rejected**: The phase prime metric reads the events in nature, so the concept of input is none. A phase prime metric hardware includes an observer, an external user and all environmental participants. It integrates into a virtual unified universe. There is never a rejection or reduction in choices or even a probabilistic select. The only effort is to en-loop the isolated loops. Non-reductionism ensures junction-free hardware (no heating).

(7) **Quantum-like speedup without entanglement**: Due to the fractal nature of the phase prime metric, it performs a search without searching. A physical wiring destroys the phase modulation. So, the hardware uses a wireless communication [70]. Spontaneous reply requires only 12 layered clocks to find 10^{12} number of clocks. At every layer, one enters inside a faster clock. Hence, time to solve a problem is the smallest time possible in the layer where the question was asked [52]. Note that 10^{12} oscillators make 99% of all patterns in nature (10^7 almost covers all, Fig. 3h). So it is the maximum number of clocks used in a layer. Quantum computing also provides this speed [23, 51, 63, 106]. However, if entanglement needs to be broken, repeatedly, which is often requisite, then the advantage of speed disappears in quantum [72]. Alternate routes can speed up [80].

(8) **Directional memory delivers a virtually infinite capacity**: The same 3D structure of a time crystal emits a different burst of signals to different directions at any given time. The observer can chose infinite locations around the structure to get a new solution. Therefore, the memory capacity and the distinct solution generation ability are astronomical. It has nothing to do with the number of oscillators.

(9) **Universal language is fundamentally embedded in the phase prime metric**: The geometric musical language (GML) in combination with the phase prime metric can build a virtual language of patterns of any system. They need only a temporal evolution of resonance signal data to build a network of phase. It suggests interacting with any system whose language is unknown. No rules or information about the intelligence of the system is required.

(10) **Harnessing singularity is not possible with the existing mechanics**: Due to the fractal clocking behavior, there are singularities at every location on the phase prime metric [78]. The differential calculus needs to be replaced by a conformal algebra to simulate the wiring (Fig. 6e). If one enters a singularity domain, it finds no self-similarity. The phase prime metric ensures a non-repeating experience continuously [18]. One needs to make a journey to the singularity domain blindly following a phase prime metric. Thus, both classical and quantum mechanics are not useful here. Bridging the singularity safeguarded quantum. Here, it is prohibited. One has to enter inside a singularity and collect available self-similar clocking factors. This finding holds the key dynamics of a phase prime metric. It explores pure topological factors for developing an effective mechanics [4, 67] (Kawato and Tsuzuki 1978).

8 When One Does Requires a Truly Bioinspired Computer?

Biological clocks are well known in the brain. It extends from circadian rhythms to the single neurons. The connecting protocol and the route that connects the rhythms are unknown. Currently, rhythmic activities are linked as a chemical process associated with proteins and enzymes. Clocking in the protein like nanoscale biomaterials does not terminate at the neuron level, as it was believed thus far. The rhythmic or clocking reaches deep down to the few atomic groups. Triplet of triplet resonance band connects the peta Hertz (femto seconds) to the nano Hertz (twelve years) frequency scales [52, 56]. The resonance pattern looks similar to the pattern of primes derived from the resonance of the dielectric resonators. There are many carriers. All carriers resonate with different dielectric resonators [73, 81, 82, 94, 95]. Yet, the frequencies constitute a singular pattern.

Ten situations when one should use this non-computer: The objective is to develop a science for non-computing to make decisions where the Turing computing fails. Here we note ten circumstances where non-computing is essential.

(i) Information is not sufficient or organized to frame logic. (ii) No time is available to find the rules for structuring logic, i.e., the urge for an instant reply. (iii) Rejection of choices is not advisable. The rejected choices could take over the lead anytime as the dominant player. (iv) Database is too big to structure it into a format solvable by a futuristic quantum computer. It requires to "search" without searching, i.e., spontaneous reply. (v) The decision-making devices of the future cannot carry a giant megawatt power supply continuously. Thermal and electrical noises are the only energy sources. (vi) We encounter a system that uses an unknown language, cannot be understood at all. (vii) Learning the real parameters using which a system configures its response. Complete rejection of black box approach, to unraveling the true dynamics. (viii) A large number of parameters are being born, disappear, change and redefine itself with a truly random, chaotic fashion, when even the variable parameters could not be identified. (ix) Undefinable factors govern a situation. A factor has several sub-factors. In addition, each of those has several sub-sub-factors. Thus, the logical statements inside logic inside logic perpetuate into an endless network [59]. (x) Computing is always a reduction in choices, but in morphing, it is just the opposite. There is a continuous increment of choices and that defines non-computing. Output is more than input.

9 What Is Non-computing? Definition of a Non-computer [4]

(a) The number of choice and quantity of information increase during a decision-making instead of reduction. (b) No finite statement is found; all statements are fractal, not overlapped [98]. (c) There is no sequence of events; it is always event inside an event, i.e., a fractal thread. (d) No measurement happens here; superposed possibilities coexist as a distinct state. The observer becomes an integral part of the morphing. (e) All decisions are logically circular. Nothing exists without a closed loop. (f) There are no data or fact as the decision. It is always a shape changing geometry; the habit of looking at numbers for solutions is unfound here. (g) All solutions are incomplete. They are extended from the beginning to end of the hardware structure. (h) Halting is never there; decision-making never stops. (i) A decision-making happens in the phase network. Mostly, the signals remain the same, only the phase changes. So literally an observer detects no ongoing computation; still, a decision is made. (j) There is no question and answer or argument, only situations. An intractable Clique problem is solved bypassing its criticality [48, 52]. (k) The user or observer does not write instruction. Instead "metric prime is the programmer, it replaces the user." (l) There is no input. User does not search inside the hardware. Using a geometric grammar, it searches its environment.

10 Critical Challenges and the Weaknesses of a Non-computer

(i) A non-computer is not precisely accurate. It gives a global idea or perspective. A non-computer is like a life form, good at those kinds of problems that it solves most. If given, different kinds of problems, a shadow of past analytic protocols are reflected. (ii) Speed, makes no sense, the total time of decision-making are fixed. Decision-making cannot end in principle. An observer captures a solution based on its own time resolution. (iii) Blindly it trusts the metric prime as an encoder of all dynamics in the universe instead of a human user. This is as conventional computers trust that all events could be sequentialized. (iv) All ten deliverables of non-computing are abstract (see below). (v) Instead of signal, the phase or silence between a pair of signals holds the key information. A 3D network of silence is the unit of information, not bits. Hence, particular clocks work [9–11, 15], but a switch alone fails. (vi) Wiring does not work; one-to-many and many-to-one communication is required [16, 17]. Hardware needs a wireless communication and a fractal network with a null screening effect [70]. (vii) Non-computing never stops; it slows down at synchrony. Therefore, there is no static output. The answer depends on the time when the question is asked. Depending on the observer location, the solution changes significantly. (viii) In the conventional computer, noise disrupts the system. Here, noise is fed to activate the synchrony. But a signal affects the decision-making largely, i.e., signal affects negatively. (ix) Addition of resource has no value. It is not number of elements, but the distinct sets of vibrations that make a powerful non-computer. (x) The solution has to be taken from all over the fractal hardware. There is no output and input location.

What is this non-computer going to deliver? The following ten features are not common to a computer. The problem, scope of application and the user protocol are different.

(1) It does not have any software program (no algorithm). (2) It runs by white noise; more randomness in noise is preferred. It uses an ultra-low power; only to manage re-wiring, non-computing does not require power in principle, as there is no reduction, no collapse and no junction. (3) It expands the input information using phase prime metric and hacks nature to predict a gross future. (4) It runs 24-7 as it evolves its wiring by itself for learning, a computation never stops, and "halt" is set by observer. (5) It never performs a search yet finds what it seeks (search without searching). It never acquires a true input; it has all possible input elements already inside as part of the geometric musical language (GML). So, it reads them outside; thenceforth, a spontaneous reply is its operational key. (6) It follows geometric clocking language or principles of composing music to process information. It is hypothesized as a natural language. (7) It has the singular unified homogeneous fractal hardware for doing all tasks of decision-making, learning changes them in their own way, and all tasks are performed by metric prime architecture. (8) The non-computer is made of one element only, clocks. It considers only parameter phase, emulate mass, space and time to process information. Thus, it explores

singularity and uses fractal mechanics [4], nothing to do with classical or quantum computing. It belongs to a non-Turing class. (9) It shrinks massive information into a small geometric clocking seed. It follows a unique superposition of 12 sub-metrics; each sub-metric represents a set of unique geometric patterns. (10) No wiring is involved; a wireless connection to process geometry at all the time scales is allowed in the hardware simultaneously.

11 A Comparative Study Between Time Crystal Computing and the Artificial Intelligence

Linearization of events is not accurate: Artificial intelligence has thus far considered that all events could be expressed as a sum of a series of elementary sub-events. Here the events are not linearly connected. They are intricately connected by phase. It means, if an event has several parts, their intricate relationships are neither in series nor in parallel. A temporal 3D wiring of sub-events is a reality. When one tries to draw the connections, 3D phase wiring should remain intact; one cannot draw it on a 2D surface. Every corner of this geometric wiring of events is important. A corner holds a unique geometric structure inside that is also a 3D network of sub-events. A singular change in this worldview changes everything in the Turing information theory. Consequently, the whole research field of artificial intelligence is redefined.

Why this little change does affects so much? Here, all events are considered as a 3D wiring of sub-events. Then immediately all events turn unpredictable, just like quantum [41]. Say, one is looking into a complicated 3D network. It would appear differently from different directions. Now, the second problem is even more serious. Every event has a 3D network of sub-events inside. It means there is an infinite journey for any observer who wants to find out the basic event that gives rise to all other events. This is a disruptive idea. One could immediately notice that an "event" becomes an undefined function. The third immediate effect is that an observer has to limit its sensing time width between limits. It is not like cutting a tape; it is cutting a 3D rock. If the lower limit is cut, even after cutting the rock appears as the same. Thus, an observer recreates an event: first, by finding a suitable orientation around the 3D event architecture, second, by locating itself where in the infinite journey, it would fit, and finally, to sense it, cutting off the event architecture based on observer's own time limits.

Feynman's singularity bridge [33] (Feynman 1948): This worldview breaks the fundamentals of the information science that has been successful for over a century. The reasons are the following. First, the observer dilemma is that already it is putting its bias into the system by choosing when to see, wherefrom to see, how much to see in the output. Then, the observer should not make a black box to fit nature blindly. Second, quantum fails to probe singularity. When one considers events located inside an event are located inside another event, in an infinite

network of events, then it takes us back to the quantum deadlock of the 1930s. Then, Feynman bypassed the singularity to save the quantum deadlock [4]. Bridging singularity saved them. However, the journey they avoided is what makes the nature beautiful. One should not bypass, but explore it [85]. Third, logic and the fitting tools of Al are blamed to be a product of human imagination for creating the abstract black box. This is far beyond reality, only to fit certain observations. Then, one should not avoid singularity, do not use an "educated guess."

The phase prime metric is an explorer of singularity: From this metric, one can build intricate details of an event's 3D architecture and avoid black box. This metric which is derived from experiment with the proteins is to hack nature. It is to replace the "free will of a programmer" from the current structure of the artificial intelligence and information processing. This metric is not a black box, but a starting point of mapping a 3D network of events. Events pours in as time crystals, since each event's time crystal is a set of integer, one finds the exact location of the event where it locks with the metric. Then the missing links are bridged, all associated numbers of 12 sub patterns are activated in the metric, so, we finally get a new set of numbers as output or decision of the information processing. This number set represents the output time crystal. If input time crystal changes with time, output geometric shape changes too. We observe morphogenesis of a geometric shape. If one knows how nature processes information, then the any form of artificial intelligence is irrelevant. Now, a geometric musical language, wherein the letters are a few geometric shapes, is invented. Using this language, a non-computer could search outside. It does not have to wait to get an input. This approach is just opposite to a computer. Understanding the true nature of an event is to replace the black box with something real, closer to nature. It is not the ultimate. Non-computing is a primitive yet significant step to mark the beginning of replacing artificial intelligence with a natural intelligence.

Ten features that constitute our frequency fractal computer distinct [AjoChhand—A = Advanced, J = Junction-free, O = Organic, C = Computer, via, H = Hierarchical (higher level), and H = Heuristic (without programming), N = Nanobrain, D = Development]:

(i) Search a massive database without searching (spontaneous reply). (ii) Multiple nested clocks one inside another enable "a virtual instant decision-making." (iii) No programming is required as "cycles self-assemble/disassembly for better sync at all possible time scales simultaneously." (iv) "Phase space" keeps "volume intact" as required resources only increase phase density not a real space. (v) Perpetual spontaneous editing of slower time cycles (creation/destruction/defragmentation) "prepare for unknown" = higher-level learning. (vi) We introduce "fractal resolution," a complex signal's lowest and fastest time scale signals that are absorbed. Simultaneously, and during expansion, the fractal seed delivers full output, from a seed of information (drastic shrinking of data). (vii) The superposition of simultaneously operating million paths assembles into a sphere enables "extreme parallelism." In quantum, only one Bloch sphere represents all qubits, with increasing numbers we move to higher dimensions, here we build a network of spheres, wherein inside the singularity points which are corners

of geometric shapes, more spheres reside, finally, its an infinite network of spheres, within and above. (viii) Time cycle is memory, rotation along the cycle is processing, there are same events, "no transport needed between memory and processing units," no wiring. (ix) No logic gate and no reduction in choices, which ensures that "speed" is irrelevant. (x) All sensory information is converted to one geometric language that allows "perception;" a yellow color could have a taste. Perception is not a programming as wrongly perceived.

12 Future of Fractal Computing

(1) **Musiceuticals (musical + pharmaceuticals)**: Vibrations could rectify the misfolding or unfolding of proteins (Sahu et al. 2015) or activate new age chemical bots [57]. (2) **Increased human sense bandwidth**: Phase prime metric restricts the time bandwidth of a brain-like computer. By harnessing the phase prime metric, mathematically, human ++ intelligence could be developed. (3) **Halt aging-related processes significantly**: Editing age requires a true phase prime metric hardware to feed cells with real vibrational data. The hardware would correct the clocking errors in the age-related proteins and complexes. (4) **Understanding of the language of natural events like the beating of earth's magnetic field and every life form**: Geometric musical language (GML) is a universal language. It could be scaled up to replace the fitting with black box, equations, to a group of patterns explaining fundamental physics theories (Feynman 1962) [101, 102]. (5) **Developing a truly dynamic model where we cannot find any logic**, e.g., earthquake, weather change, the evolution of a virus, aging, side effects of drugs, dynamics of gaseous clouds. A non-computing hardware learns higher-level rules. Thenceforth, it bridges the missing links in the information architecture and spontaneously simulates the future instantly. It can morph events much better than the previous cellular automaton-based architectures [16, 101, 102]. (6) **Science of human behavior, society, economics, etc**: The psychological behaviors, emotions and other non-defined parameters would be geometrically defined [115]. One would get a geometric pattern of clocks from the human responses. (7) **Simulate beyond limit or knowledge**: Once built, a phase prime metric hardware needs very little gross information about any event. Then, from that little information, it generates dynamics at time scales that it has never encountered in the past. (8) **Noise would replace signal and enter into the era of ultra-low power**: Earlier, scaling up was like adding more resources, faster speed, more power, etc. Now, it is all about how one could make a device that captures a much longer slice of phase prime metric. (9) **Predict and simulate' million year evolution in' a finite time (the science of evolution)**: Currently, there is no tool to estimate evolution because this is a slow process. Non-computer, by using geometric musical language and the phase prime metric, could project a far more reliable picture of the future. (10) **Machines of nature**: The phase prime metric, by intimately interacting with nature, can design scientifically life-like machines; it could be an architect.

Acknowledgements Authors acknowledge the Asian office of Aerospace R&D (AOARD) a part of United States Air Force (USAF) for the Grant no. FA2386-16-1-0003 (2016–2019) on electromagnetic resonance based communication and intelligence of biomaterials. A.B acknowledges Satyajit Sahu, Daisuke Fujita, Lokesh Agrawal and D. J Chafai for their contributions.

Glossary

Biomaterial Material collected from Biological living species.

Bloch sphere Quantum mechanics is a dynamics of system points active between classical states. So, the system points can acquire a large number of solutions, we keep a pair of classical states at the pair of poles of a sphere, while the actual solutions are located on the surface of the sphere. These solutions are phase points, and the sphere is called Bloch sphere.

Fractal clock Normal clocks are circular, and a system point moves around it. Quantum clock has an additional geometric phase counter, but a fractal clock has infinite chains of clocks; so it is not just a counter, it represents a changing topology.

Fractal computing Undefined phase space of singularity domains in a system is harnessed to apply phase prime metric suggested integration of vibration. This way of integrating and extrapolating events to the future is fractal computing.

Fractal tape A tape whose every single cell contains a tape inside. One version of such a tape is a circular ring with finite cells.

Geometric algebra A study of mathematics to fuse geometry and algebra. It is not just algebra of geometric shapes; it is also finding the hidden geometries in the algebra.

Hierarchical perception A hierarchical perception is made of two kinds of information feeding each other. Symmetries that integrate a set of discrete information created by unique different definition of information are hierarchical information. When both lower level and higher level information are about cognitive ability, it is hierarchical perception.

Image processing A method for identifying the geometric shapes hidden in an image using algorithm.

Information theory Information could be any finite state with a significance, the method to process the states such that the significance of information content is properly justified.

Microtubule A nanowire made of a hollow tubulin protein cylinder with a dimension of 20 nm to 30 nm, and inner core is a solid water cylinder. It is found in every Eukaryote cells, say, all animal, plant, protista, and fungi cells have

these nanowires, whose primary objective is to run primary cell events. Most part of a microtubule is water.

Neuron It is a non-dividing cell whose membranes or cell skins have highly evolved over the years to pass electric current.

Phase prime metric A pattern of all possible choices a given number of events could be grouped.

Protein Protein is a long chain polymer which folds with water such that is forms various elementary geometric shapes called secondary structures. It is the building block of life.

Quantum computing Harnessing the phase path between two classical states, classical computing speed is increased enormously. This is called quantum computing.

Resonance Periodic oscillation has a frequency. If a system is triggered with an external signal with the same frequency at which the system naturally oscillates, then several vibrational modes canalize energy into one; thus, one observes a surge in the energy of oscillation of a particular mode.

Singularity It is a point in a set of system points, linked with all other points in a set via well-defined dynamics, so it is accessed, but does not deliver a defined value. At singularity, the function representing the dynamics that links the events becomes non-differentiable. One reason for this to happen is the fractal nature of subset points around a given singularity point.

Synchrony More than one oscillators match in one or more oscillation parameters.

Time crystal Singularity of a space is measured as mass, so we get a spatial crystal when there is a space, and 360° rotation around a point in space one finds more than one singularity points or mass. Similarly, singularity of phase is measured as time; in a 360° variation of phase if one encounters a pair of such phase singularities, it is a time crystal. Just like one point of mass cannot create a crystal, one point of phase singularity cannot create a time crystal.

Topology Geometric shapes could acquire various symmetries or an order in its arrangement. Ordering in geometric shapes follows certain properties, topology is its study.

Turing tape A tape that encodes any information as a sequence of unified simple information in its cells.

Universal language A method of expression of information following which all possible information could be encoded and processed.

Wireless communication Electromagnetic packet of energy could travel without a medium. Using this property, one could send signal from one point to another.

References

1. Abbot, L. F. and Wise, M. B. (1981), Dimension of a quantum mechanical path, Am. J. Phys. 49, 37.
2. Aldridge, J., and Pavlidis, T. (1976) Clocklike behavior of biological clocks. Nature 259, 343–344.
3. Alleva, J. J., Waleski, M. V., and Alleva, F. R. (1971) A biological clock controlling the estrous cycle of the hamster. Endocrinology 88, 1368–1379.
4. Agrawal, L. et al; (2016a) Replacing Turing tape with a Fractal tape: a new information theory, associated mechanics and decision making without computing, Consciousness: Integrating Indian and Western perspective. Chapter 6, 87–159. Paperback: 630 pages, Publisher: New Age Books; 1st edition (October 5, 2016), Language: English, ISBN-10: 8178224933, ISBN-13: 978-8178224930, India.
5. Agrawal, L. et al, (2016b) Inventing atomic resolution scanning dielectric microscopy to see a single protein complex operation live at resonance in a neuron without touching or adulterating the cell; J. Int. Neurosci., 15(4), 435–462.
6. Agrawal, L., Chhajed, R., Ghosh, S., Ghosh, B., Ray, K., Fujita, D., Bandyopadhyay, A. (2018) Fractal Information Theory (FIT)-Derived Geometric Musical Language (GML) for Brain-Inspired Hypercomputing. In: Pant M et al (eds) Soft Computing: Theories and Applications. Advances in Intelligent Systems and Computing, vol 584, pp 343-372. Springer, Singapore. https://doi.org/10.1007/978-981-10-5699-4_33
7. Arvanitaki, A., and Chalazonitis, N. (1968) Electrical properties and temporal organization in oscillatory neurons. In Neurobiology of Invertebrates. J. Salanki, ed. Plenum, New York, pp. 169–174.
8. Aschoff, J., and Wever, R. (1976) Human circadian rhythms: a multi-oscillatory system. Fed. Proc. 35, 2326–2332.
9. Bandyopadhyay, A., Miki, K., Wakayama, Y., (2006a) Writing and erasing information in multilevel logic systems of a single molecule using scanning tunneling microscope (STM); Appl. Phys. Lett. 89, 243506.
10. Bandyopadhyay, A. et al, (2006b) Global tuning of local molecular phenomena: An alternative approach to nano-bioelectronics; J. Phys. Chem. B, 110, 20852–57.
11. Bandyopadhyay, A., Wakayama Y., (2007) Origin of negative differential resistance in molecular Junctions of Rose Bengal; Appl. Phys. Lett. 90, 023512.
12. Bandyopadhyay, A., Acharya A., (2008) A 16 bit parallel processing in a molecular assembly, Proc. Natl. Acad. Sci. USA 105, 3668–3672.
13. Bandyopadhyay, A., Sahu, S., Fujita, D., (2009a) Smallest artificial molecular neural-net for collective and emergent information processing, Appl. Phys. Lett. 95, 113702.
14. Bandyopadhyay, A., Fujita, D., Pati, R., (2009b) Architecture of a massive parallel processing nano brain operating 100 billion molecular neurons simultaneously, Int. J. Nanotech. & Mol. Comp. 1, 50–80.
15. Bandyopadhyay, A. et al, (2010a) A new approach to extract multiple distinct conformers and co-existing distinct electronic properties of a single molecule by point-contact method, PCCP, 12, 2033.
16. Bandyopadhyay, A. et al, (2010b) Investigating Universal Computability of Conventional Cellular Automata Problems on an Organic Molecular Matrix, Natural Computing, 2, 1–12.
17. Bandyopadhyay, A. et al, (2010c) A massively parallel computing on an organic molecular layer, Nature Physics 6, 369.
18. Barnsley, M.; Hutchinson, J.; Stenflo, Ö. (2008), V-variable fractals: Fractals with partial self similarity. Adv. Math. 218, 2051–2088.
19. Basar E., (1990), Chaotic dynamics and resonance phenomena in brain function : Progress, perspectives and thoughts, in Basar E. ed. Chaos in Brain Function Springer-Verlag, Heidelberg 1–30.

20. Berliner, M. D., and Neurath, P. W. (1965) The rhythms of three clock mutants of Ascobolus immersus. Mycologia 57, 809–817.
21. Best, E. N. (1976) Null space and phrase resetting curves for the Hodgkin-Huxley equations. Ph.D. thesis, Purdue University.
22. Betz, A., and Becker, J. U. (1975b) Phase dependent phase shifts induced by pyruvate and acetaldehyde in oscillating NADH of yeast cells. J. Interdiscipl. Cycle Res. 6, 167–173.
23. Bloch, S. (1997) On parallel hierarchies and *R^i_k*. *Annals of Pure and Applied Logic*, 89(2–3):231-273, 8.
24. Bourret, A., Lincoln, R. G., Carpenter, B. H. (1969) Fungal endogenous rhythms expressed by spiral figures. Science 166, 763–764.
25. Brun, T. A. (2008) Computers with Closed Timelike Curves Can Solve Hard Problems, 2008. Available online: http://arxiv.org/pdf/gr-qc/0209061v1.pdf (accessed on 15 January 2014).
26. Bruno, P., (2013); Impossibility of Spontaneously Rotating Time Crystals: A No-Go Theorem; Phys. Rev. Lett. 111, 070402.
27. Bruce, V. G., Wright, F.. and Pittendrigh, C. S. (1960) Resetting the sporulation rhythm in Pilobolus with short light flashes of high intensity. Science. 131. 728 730.
28. Brinkmann, K. (1971) Metabolic control of temperature compensation in the circadian rhythm of Euglena gracilis. pp 567–593. In Biochronometry, M. Menaker, ed. Nat. Acad. Sci., Washington, D.C.
29. Brown, B. H., Duthie, H. L., Horn, A. R. and Smallwood, R. H. (1975) A linked oscillator model of electrical activity of human small intestine. Amer. J. Physiol. 229, 384–388.
30. Bruce, V. G., and Pittendrigh, C. S. (1956) Temperature independence in a unicellular "clock". Proc. Nat. Acad. Sei. 42, 676–682.
31. Brumberger, H. (1970) Rhythmic crystallization of poly-L-alanine. Nature 227, 490–491.
32. Buhusi, C. V.; Meck, W. H.; (2005) What makes us thick?, Functional and neural mechanisms of interval timing, Nature reviews, Volume 6, October 2005; http://www.nature.com/nrn/journal/v6/n10/abs/nrn1764.html.
33. Cao, T. Y.; Schweber, S. S.; (1993) The conceptual foundation and the philosophical aspect of the renormalization theory, Synthese 97: 33–108.
34. Copeland, B. J. and Proudfoot, D. (1999) Alan Turing's forgotten ideas in computer science, April, 99–103.
35. Cooke, J., and Zeeman, E. C. (1976) A clock and wave front model for control of the number of repeated structures during animal morphogenesis. J. Theor. Biol. 58, 455–476.
36. Clark, R. L. and Steck, T. L. (1979) Morphogenesis in Dictyostelium: an orbital hypothesis. Science, 204, 1163–1168.
37. Choi, S. et al (2017); Observation of discrete time-crystalline order in a disordered dipolar many-body system, Nature 543, 221–225.
38. Chandrashekaran, M. K. (1974) Phase shifts in the Drosophila pseudoobscura circadian rhythm evoked by temperature pulses of varying durations. J. Interdiscipl. Cycle Res. 5, 371–380.
39. Chandrashekaran, M. K., and Engelmann, W. (1973) Early and late subjective night phases of the Drosophila pseudoobscura circadian rhythm require different energies of blue light for phase shifting. Z. Naturforsch. 28, 750–753.
40. Chandrashekaran, M. K., and Loher, W. (1969b) The relationship between the intensity of light pulses and the extent of phase shifts of the circadian rhythm in the exclusion rate of Drosophila pseudoobscura. J. Exp. Zool. 172, 147–152.
41. Durr, D., Goldstein, S., and Zanghi, N., (1992) Quantum equilibrium and the origin of absolute uncertainty", J. Stat. Phys. 67, 843–907.
42. Dickau, R. (1999); "Visualizing Combinatorial Enumeration," Mathematica in Education and Research, 8, pp. 11–18.
43. Eguiluz, V.M. et al (2005) Scale free brain functional networks. Phys. Rev. Lett. 2005, 94, 018102.

44. Else, D. V., Bauer, B. & Nayak, C. (2016) Floquet time crystals. Phys. Rev. Lett. 117, 090402.
45. Edmunds, L. N. (1977) Clocked cell cycle clocks. Waking and Sleeping 1, 227–252.
46. Engelmann, W., Eger, 1., Johnsson, A., and Karlsson, H. G. (1974) Effect of temperature pulses on the petal rhythm of Kalanchoe: an experimental and theoretical study. Int. J. Chronobiol. 2. 347–358.
47. Engelmann, W., Karlsson, H. G., and Johnsson, A. (1973) Phase shifts in the Kalanchoe petal rhythm caused by light pulses of different durations. Int. J. Chronobiol. 1, 147–156.
48. Feige, U.; Goldwasser, S.; Lovász, L.; Safra, S.; Szegedy, M. Approximating Clique is almost NP-Complete. In Proceedings of the 32nd IEEE Symposium on Foundations of Computer Science, San Juan, Puerto Rico, 1–4 October 1991; pp. 2–12; https://doi.org/10.1109/sfcs.1991.185341.
49. Frank, K. D.. and Zimmerman, W. F. (1969) Action spectra for phase shifts of a circadian rhythm in Drosophila. Science 163, 688–689.
50. Fuller, C. A., Sulzman, F. M., and Moore-ede, M. C. (1978) Thermoregulation is impaired in an environment without circadian time cues. Science 199, 794–796.
51. Galil, Z. et al (1987) An $O(n\text{^}3 \log n)$ deterministic and an $O(n\text{^}3)$ Las Vegas isomorphism test for trivalent graphs. *Journal of the ACM*, 34(3):513–531.
52. Ghosh, S. et al (2014a), Design and operation of a brain like computer: a new class of frequency-fractal computing using wireless communication in a supramolecular organic, inorganic systems. Information, 5, 28–99.
53. Ghosh, S., et al, (2014b), Nano Molecular-platform: A protocol to write energy transmission program inside a molecule for bio-inspired supramolecular engineering. Adv. Func. Mater. 24, 1364–1371.
54. Ghosh, S. et al, (2015a) Resonant Oscillation Language of a Futuristic Nano-Machine-Module: Eliminating Cancer Cells & Alzheimer Aβ Plaques, Curr. Topic. Med. Chem. 15, 534–541.
55. Ghosh, S., et al; (2015b) An organic jelly made fractal logic gate with an infinite truth table; Scientific Reports 5, 11265.
56. Ghosh, S. et al, (2016a) Inventing a co-axial atomic resolution patch clamp to study a single resonating protein complex and ultra-low power communication deep inside a living neuron cell; J. Integrated Neuroscience,15(4), 403–433.
57. Ghosh, S. et al, (2016b) A simultaneous one pot synthesis of two fractal structures via swapping two fractal reaction kinetic states, Phys. Chem. Chem. Phys. 18, 14772–14775.
58. Girelli F., Liberati S., Sindoni L., (2009) Is the notion of time really fundamental? Submitted on 27 Mar 2009 http://arxiv.org/abs/0903.4876.
59. Gödel, K. (1938), 'The Consistency of the Axiom of Choice and of the Generalized Continuum-Hypothesis', Proc. Natl. Acad. Sci. (U.S.A.) 24, 556–57.
60. Gurevich, Y., Shelah, S., (1989); Nearly linear time, Springer LNCS 363, 108–118.
61. Gerisch, G., Hulser, D., Malchow, D., and Wick, U. (1975) Cell communication by periodic cyclic-AMP pulses. Phil. Trans. Roy. Soc. Lond. B. 272, 181–192.
62. Harris, V. C. and Subbarao, M. V., (1991) "On Product Partitions of Integers," Canadian Mathematical Bulletin, 34(4), pp. 474–479.
63. Hamkins, J. D.; Lewis, A. (2000) Infinite Time Turing machines, Journal of Symbolic Logic, vol. 65 (2) pp. 567–604.
64. Haramein, N. (2001); "Scaling Law for Organized Matter in the Universe," Bull. Am. Phys. Soc. AB006, Ft. Worth, Oct. 5.
65. Hastings, J. Woodland and Sweeney, Beatrice M. (1957) On the mechanism of temperature independence in a biological clock. PNAS USA, 43 (9). pp. 804–811.
66. Horodeck, M., Oppenheim, J., Winter, A., (2005) Partial quantum information, Nature, 436, 673–676.
67. Hohlfeld, R.G.; Cohen, N. (1999) Self-similarity and the geometric requirements for frequency independence in antenna. Fractals, 7, https://doi.org/10.1142/s0218348x99000098.

68. Hill, A. V. (1933) Wave transmission as the basis of nerve activity. Cold Spring Harbor Symposia on Quantitative Biology 1, 146–151.
69. Jaynes E. T. (1980); Foundations of Radiation Theory and Quantum Electrodynamics, Eds Asim Barut pp 37–43, Springer; Quantum Beats.
70. Jaeger, H.; Haas, H. (2004), Harnessing nonlinearity: Predicting chaotic systems and saving energy in wireless communication. Science, 304, 78–80.
71. Jenerick, H. (1963); Phase Plane Trajectories of the Muscle Spike Potential. Biophysical Journal, vol. 3, issue 5, pp. 363–377.
72. Jozsa, R. and Linden, N. (2003); On the role of entanglement in quantum-computational speed-up, 459(2036) https://doi.org/10.1098/rspa.2002.1097.
73. Joshi, A., Xiao, M., (2006); Cavity-QED based unconventional geometric phase dc gates with bichromatic field modes, Phys. Lett. A 359 390–395.
74. Johnsson, A., Brogarth, T., and Holje, φ, 1979, Oscillatory transpiration for avena plants: perturbation experiments provide evidence for a stable point of singularity. Physiol Plant 45 393–398.
75. Johnsson, A., and Karlsson, H. G. (1971) Biological rhythms: singularities in phase shift experiments as predicted from a feedback model, In Proc. of first European biophysical congress, E. Broda and A. Locker eds. Springer, Berlin, pp-263–267.
76. Johnsson, A., and Karlsson, H. G. and Engelman, W. (1973) Phase shift effect in the Kalanchoe petal rhythm due to two or more light pulses, Physiol. Plant, 28, 134–142.
77. Kantelhardt, J. W. (2011) Fractal and multi-fractal time series, Mathematics of Complexity and Dynamical Systems, Springer, 463–487.
78. Kolwankar, K. M. and Gangal A. D. (1996) Fractional differentiability of nowhere differentiable functions and dimensions, Chaos: An Interdisciplinary J. Nonlinear Sci., vol. 6 (4), pp. 505–513.
79. Kuramoto Y. (1983) "Each singularity generates a signal burst" Chaos and Statistical Methods: Proceedings of the Sixth Kyoto Summer Institute, Kyoto, Japan September 12–15, 1983; December 6, 2012, page 273, Springer, ISBN 9783642695599.
80. Lloyd, S., (1999) Quantum search without entanglement, Phys. Rev. A. 61(01031-1).
81. Lauber, H. –M., Weidenhammer, P., Dubbers, D., (1994), Geometric phases and hidden symmetries in simple resonators, Phys. Rev. Lett. 72(7) 1004–1007.
82. Lee, T., Broderick, N. G. R. and Brambilla, G. (2011) "Berry phase magnification in optical microcoil resonators," Opt. Lett. 36, 2839–2841.
83. Liebovitch L.S. et al (1987), Fractal model of ion-channel kinetics, Biochim. Biophys. Acta 896, 173–180.
84. Li T.Y., Yorke J.A., (1975), Period three implies chaos, Am. Math. Mon. 82, 985.
85. Mallat, S., Hwang, W. L. (1992) Singularity signal detection and processing with wavelets, IEEE trans. On Information Theory, vol. 38, pp. 617–643.
86. Minsky, M. (1967) *Computation: Finite and Infinite Machines*; Prentice-Hall, Inc.: Upper Saddle River, NJ, USA, Chapter 8, Section 8.2 "Unsolvability of the Halting Problem".
87. Monserrat, B.; Drummond, N.D.; Needs, R.J. (2013), "Anharmonic vibrational properties in periodic systems: energy, electron-phonon coupling, and stress", Phys. Rev. B 87: 144302.
88. Mirollo, R.E.; Strogatz, S.H. (1990); Synchronization of pulse coupled biological oscillators. SIAM J. Appl. Math., 50, 1645–1662.
89. Noctor S, Martinez-Cerdeno V, Ivic L, Kriegstein A (2004) Cortical neurons arise in symmetric and asymmetric division zones and migrate through specific phases. Nat Rev Neurosci 7: 136–144.
90. Ord, G. N. (1983) Fractal space-time a geometric analogue of relativistic quantum mechanics, J. Phys. A. 16, 1869–1884.
91. Ord. G. N. (2012) Quantum phase from the twin paradox, J. Phys. Conf. Series, 361, 012007.
92. Ord. G. N. (2011) How does an electron tell the time? Int. J. Theo. Phy. 1–15.

93. Panarella, E. (1987) “non-linear behavior of light at low intensities: the photon clump model”, p 105 in Quantum Uncertainties –recent and future experiments and interpretations, Eds. W. M. Honing, D. W. Kraft & E. Panarella, Plenum Press.
94. Pistolesi F. and Manini N., (2000); Geometric Phases and Multiple Degeneracies in Harmonic Resonators; Phys. Rev. Lett. 85, 1585.
95. Pechal, M., et al, (2012) Geometric Phase and Nonadiabatic Effects in an Electronic Harmonic Oscillator, Phys. Rev. Lett. 108, 170401.
96. Pippinger N. and Fischer M. J. (1979) Relations among Complexity Measures. J. ACM 26:2, 361–381.
97. Prati, E., (2009) The nature of time: from a timeless hamiltonian framework to clock time metrology, arXiv:0907.1707v1, 10 July.
98. Paterson, M. S., Fischer, M. S., Meyer, A. R. (1974) An improved overlap argument for on-line multiplication SLAM-AMS Proc. 7 (1974), 97–111.
99. Ridge, E. et al (2005) Moving Nature-Inspired Algorithms to Parallel, Asynchronous and Decentralised Environments. In *Self-Organization and Autonomic Informatics (I)*; Czap, H., Unland, R. Brank, C., Tianfield, H., Eds.; IOS press: Amsterdam, The Netherlands, 2005; pp. 35–49.
100. Richmond B. and Knopfmacher, A. (1995) “Compositions with Distinct Parts,” Aequationes Mathematicae, 49, pp. 86–97.
101. Sahu, S., et al (2009) Remarkable potential of pattern based computing on an organic molecular layer using the concept of cellular automata; IEEE PID 107, 2403.
102. Sahu, S., et al (2012) On Cellular Automata rules of molecular arrays. Natural Computing 11(2): 311–321.
103. Sahu, S., et al (2013a) Multi-level memory-switching properties of a single brain microtubule. Applied Physics Letters 102, 123701.
104. Sahu, S., et al (2013b) Atomic water channel controlling remarkable properties of a single brain microtubule: Correlating single protein to its supramolecular assembly Biosensors and Bioelectronics 47, 141–148.
105. Sahu, S., et al, (2014) Live visualizations of single isolated tubulin protein self-assembly via tunneling current: effect of electromagnetic pumping during spontaneous growth of microtubule. Scientific Reports, 4, 7303.
106. Schnorr, C. P. (1978) Satisfiability is Quasilinear Complete in NQL. Journal of ACM. 25:1, 136–145.
107. Shlesinger, M. F. (1988) Fractal time in condensed matter, Ann. Rev. Phys. Chem. 39, 269–290.
108. Shapere, A., Wilczek, F. (2012); Classical time crystals Phys. Rev. Lett. 109 160402.
109. Siegelmann H. T. (1995) Computation beyond the Turing limit, 268 (545–548).
110. Tomes, R. (1990), http://ray.tomes.biz/maths.html.
111. Van Stokum, W. J., (1937); The gravitational field of a distribution of particles rotating about an axis of symmetry. Proc. R. Soc of Edinburgh 57, 135–154.
112. Vitiello, G. (2012); Fractals, Dissipation and Coherent States. In Quantum Interaction; Lecture Notes in Computer Science; Springer: Berlin and Heidelberg, Germany, pp. 68–79.
113. Van Essen DC (1997) A tension-based theory of morphogenesis and compact wiring in the central nervous system. Nature 385: 313–318.
114. Watrous, J., Aaronson, S. (2009) Closed time like curves make quantum and classical computing equivalent, Proceedings of the Royal Society A: Mathematical, Physical and Engineering Sciences. 465 (2102): 631.
115. Wegner, P. (1997); Why interaction is more powerful than algorithms. Commun. ACM, 40, 80–91.
116. Winfree, A. (1977); Biological Rhythm Research 8, 1; The Geometry of Biological Time (Springer, New York, 2001), 2nd ed.
117. Warlimont, R. (1993); “Factorisatio Numerorum with Constraints,” Journal of Number Theory, 45, pp. 186–199.

118. Xue, G. et al, (2010); Greater neural pattern similarity across repetitions is associated with better memory. Science, 330, 97–101.
119. Yao, N. Y., Potter, A. C., Potirniche, I.-D. & Vishwanath, A. (2017) Discrete time crystals: rigidity, criticality, and realizations. Phys. Rev. Lett. 118, 030401.
120. Zhou, X.-Q. et al (2013). Calculating unknown Eigen values with a quantum algorithm. *Nat. Photonics 7*, 223–228.
121. Zhang Z. et al, (2017); Observation of a discrete time crystal, Nature 543, 217–220.

Analysis of News in the Hindustan Times and India Today

Vishal Rajput, Irshad Ahmad Ansari and Millie Pant

Abstract The media is known as a mirror of any society, and because of that, a national newspaper can be analyzed to know the current mindset of any nation. The different types of news and reports actually show the countrymen's interests as media cover majority of that news that is of interest to their readers. In this study, the analysis is performed on the two leading Indian news providers, known as Hindustan Times and India Today. The main aim of this study is to find out the interest of Indians and Indian media houses in terms of national and international news. To make a generalized comment, six-month data of recent past is used for the analysis purpose. Different parameters (for same duration) are considered for the analysis of the news for both the e-papers so that media house's interest can also be compared.

Keywords Data mining · Indian media · Popularity analysis · India Today Hindustan Times

1 Introduction

In the current era of communication and information technology, a society and its needs can be easily analyzed by the content they read on day-to-day basis. Media analysis can be used to get an insight to the society. The publishing speed of the data is almost real time [1, 2] and so the reaction and popularity can also be

V. Rajput · I. A. Ansari (✉)
Electronics and Communication Engineering, PDPM Indian Institute of Information Technology Design and Manufacturing, Jabalpur 482005, MP, India
e-mail: irshad@iiitdmj.ac.in; 01.irshad@gmail.com

V. Rajput
e-mail: vishalrajput@iiitdmj.ac.in

M. Pant
Department of ASE, Indian Institute of Technology Roorkee, Roorkee, India
e-mail: millifpt@iitr.ac.in

K. Ray et al. (eds.), *Soft Computing Applications*, Studies in Computational Intelligence 761, https://doi.org/10.1007/978-981-10-8049-4_2

analyzed in real time. However, a steady finding needs a capture-analysis approach, i.e., the data needs to be captured over duration of time and then analyzed by experts for any relevant findings. Such findings are more reliable.

The news of any country directly reflects the mindset of its citizens as media give more coverage to the people/reader interest [3, 4]. On the other hand, different media houses may also have their own interests/area of specialization [5], where they may want to cover more news. So a comparative analysis (between media houses) is also needed for correct conclusion.

In the present time, the Internet captures the world and makes it much faster than earlier. The media is also not an exception, and it got affected by this Internet storm. The paper mode news is now a thing of past. Today, the whole world news is available on a click of mouse. The newer version of news (e-paper) is much faster and effective than the earlier version (print media) [6, 7]. The reader feedback is instant and that gives the media houses a chance to improve their news feeding as per the reader interest [8–10]. Overall, the new mode is more dynamic and effective representation of society.

Considering these points, the present study also utilizes the two e-papers [11, 12] for the analysis of news. The main focus of this study is to find out the interest of Indian citizens and media houses and that is why both the e-papers are Indian.

2 Methods and Tools

Data mining is a famous and well-known method for the data analysis and interpretation [13–15]. It is used to get the meaningful information from the large data sets [13]. However, the final interpretation is totally coder-dependent thing and that's why the analysis is always a tricky thing to do as different users can find out different information from the same data set [15].

To start with the data mining, the first thing needed is data. World Wide Web is a huge source of data; the only issue is fast collection of this data. The data collection from the Internet becomes much easy, if the Web site of interest offers API (application programming interface)-based collection [16]. API provides a set of subroutine protocols make an effortless connection between server and local user [17, 18]. However, the limitation of the same is that only server-defined functions can be used for data collection. Some famous APIs [19] are Twitter API, YouTube API, Google Maps API, etc. Figure 1 shows the basic architectural view of an API.

2.1 Code Development for the Analysis

The code is developed in the Python language. The development remains focused on the fact that the multiple keyword-based searches become possible from the

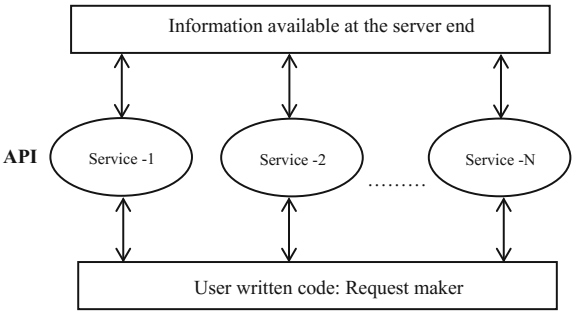

Fig. 1 Basic architectural view of an API

extracted news article. This developed code passes multiple parameters to the raw data and figures out the frequency of passed parameters. Also, the code provides the ability to figure out the total article within any specific period. After extraction, percentage-wise data is also plotted.

3 Problem Formulation for Data Analysis and Test Parameters

This study is performed to check the major news sources of the Indian mainstream media. In addition to that, proposed study also compares the news categories of two major media houses. Different keywords and parameters are used in this study. The detail of all parameters and keywords is as follows:

The analysis starts from the search of concept/keyword/class of five categories (world, sports, science, entertainment, and defense) in both the e-papers. Each category is used to check the news article from respective fields. For example, class "world" contains international news (other than India), class "sports" contains majority of the sports category.

After that, the news of neighboring country is checked so that the neighboring country effect on Indian media can be analyzed.

The political and legal influence on the media is also analyzed on the basis of article coming from these sectors. The popularity of famous politicians and political parties is also checked and compared in both the e-papers. This analysis is used to show the influence of particular politician and political party on the national news. This also shows respective "class" popularity level among the citizens of India and importance for the county.

Further, states of India are also tested for their popularity in the mainstream media. Also, four major cities (Delhi, Mumbai, Kolkata, and Chennai) are tested for popularity. The news article's comparison from both the e-papers is also provided.

3.1 E-papers Used in the Study

Two leading Indian news Web sites are used in this study for data analysis and comparison:

HINDUSTAN TIMES—http://www.hindustantimes.com/
INDIA TODAY—http://indiatoday.intoday.in/.

3.2 Data Set and Duration

To make a solid comparison between the media house's trends as well as to find out the popularity of various news topics among common people, a fairly long duration (6 months) is considered for the analysis. The exact duration is shown in Table 1. The data is collected from Ref. [20].

3.3 Countries Used for Comparison

Four neighboring countries of India, namely Sri Lanka, Pakistan, China, Bangladesh are used in this analysis to see the effect and importance of them from the point of view of Indian media.

3.4 Popularity Analysis of Indian Politicians

Five well-known Indian politicians are checked for their popularity in the Indian media. The more mention of them simply means that they are more popular. Following politicians are considered:

1. Mr. Narendra Modi: politically linked with Bharatiya Janata Party and Prime Minister (current) of India
2. Mr. Amit Shah: politically linked with Bharatiya Janata Party
3. Mr. Arvind Kejriwal: politically linked with Aam Aadmi Party and Chief Minister (current) of New Delhi
4. Mrs. Sonia Gandhi: politically linked with Indian National Congress
5. Mr. Rahul Gandhi: politically linked with Indian National Congress.

Table 1 Time durations used in the study

Media house	Duration of analysis
India Today	February 24, 2017–August 03, 2017
Hindustan Times	February 24, 2017–August 03, 2017

3.5 Popularity Analysis of Indian Political Parties

Five major political parties of India are checked for their popularity. The more news coverage of any political parties simply means that they are more popular in media and people. Following political parties are considered:

1. BJP (Bharatiya Janata Party)
2. AAP (Aam Aadmi Party)
3. INC (Indian National Congress)
4. SP (Samajwadi Party)
5. BSP (Bahujan Samaj Party).

3.6 Popularity Analysis of Indian Regions (States and Major Cities)

Different regions/parts of the Indian Territory are also checked for their influential ability on Indian media as well as their importance to different media houses. Twenty-nine states and four major cities are considered for the analysis.

3.7 Concept/Keyword/Class Used

Following keywords are used for different analyses:

- **For world news**: USA, US, United states, Trump, Putin, Russia, Australia, UK, United Kingdom
- **For sports news**: Sports, cricket, football
- **For science news**: Science, Technology, ISRO
- **For entertainment news**: Hollywood, Bollywood, Movies, Music
- **For defense-related news**: Army, Military, defence
- **For neighboring countries**: Respective names
- **For legal news**: Supreme Court, High Court, SC, HC
- **For political news**: BJP, Congress, Politics
- **For politician's news**: Respective names, for example: Sonia Gandhi
- **For political party**: Respective names (short form and long form). For example: BJP and Bharatiya Janata Party
- **For cities and states**: Respective names (short form and long form). For example: UP and Uttar Pradesh.

4 Results and Discussion

This section is dedicated to the detailed analysis and discussion of the obtained results. Table 2 shows the complete news articles published in six months in both the e-papers. Table 2 also shows the news publishing frequency of Hindustan Times and India Today for five different classes (world, sports, science, entertainment, and defense). Figure 2 shows the comparison between both the e-papers on the basis of percentage news from these five sectors.

It is quite evident from Fig. 2 that Hindustan Times primarily focuses on entertainment news, whereas sport is the main focus of India Today. Science category is of the least interest for both the media houses. However, Hindustan Times is better than India Today as far as interest in science news is concerned.

Table 2 News publishing frequency of Hindustan Times and India Today for six different classes (everything, world, sports, science, entertainment, defense)

News related to	News publishing frequency	
	Hindustan Times	India Today
Everything (all news articles of 6 months)	1219	3025
World	107	353
Sports	123	388
Science	102	159
Entertainment	198	272
Defense	148	363

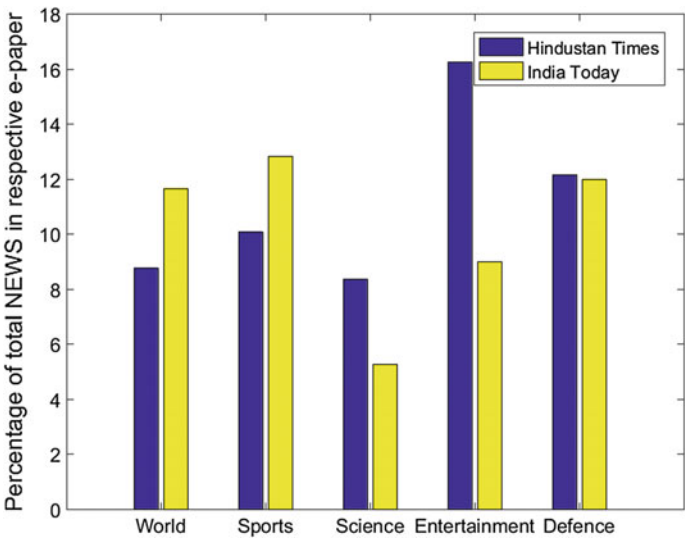

Fig. 2 Comparison between both the e-papers on the basis of news percentage for five different classes

Table 3 shows the news publishing frequency of Hindustan Times and India Today for neighboring countries. Figure 3 shows the comparison between both the e-papers on the basis of percentage news for neighboring countries.

It is quite evident from Fig. 3 that China and Pakistan remain much more in news as compared to Sri Lanka and Bangladesh, which effectively means that these countries are more influential and Indians also have more interest in their news.

Table 4 shows the news publishing frequency of Hindustan Times and India Today for classes: legal and politics. Figure 4 shows the comparison between both the e-papers on the basis of percentage news for classes: legal and politics.

It is quite evident from Fig. 4 that political news coverage is quite high as compared to the legal news. This also shows the public's interest in the politics rather than legal field.

Table 5 shows the news publishing frequency of Hindustan Times and India Today for different Indian politicians. Figure 5 shows the comparison between both the e-papers on the basis of percentage news for different Indian politicians.

Table 3 News publishing frequency of Hindustan Times and India Today for neighboring countries

News related to	News publishing frequency	
	Hindustan Times	India Today
Pakistan	61	250
China	78	252
Bangladesh	15	49
Sri Lanka	15	48

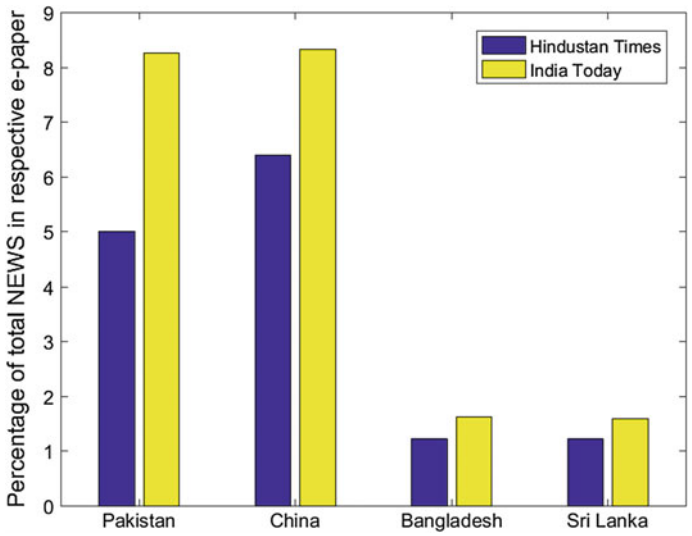

Fig. 3 Comparison between both the e-papers on the basis of news percentage for neighboring countries

Table 4 News publishing frequency of Hindustan Times and India Today for classes: legal and politics

News related to	News publishing frequency	
	Hindustan Times	India Today
Legal	137	387
Politics	300	780

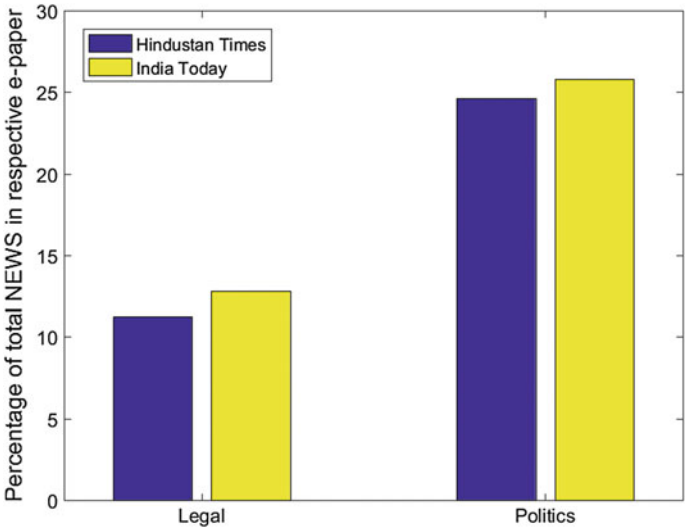

Fig. 4 Comparison between both the e-papers on the basis of news percentage classes: legal and politics

Table 5 News publishing frequency of Hindustan Times and India Today for different Indian politicians

News related to	News publishing frequency	
	Hindustan Times	India Today
Mr. Narendra Modi	115	463
Mr. Amit Shah	15	45
Mr. Arvind Kejriwal	115	239
Mrs. Sonia Gandhi	18	20
Mr. Rahul Gandhi	19	70

It is quite evident from Fig. 5 that the current Prime Minister (Mr. Modi) has the most influence on the Indian media, which is quite a normal thing. On the other hand, opposition leaders have very poor influence on media, which is a bit strange. However, Mr. Kejriwal seems to have a good impact and stays in the news of both the media houses.

Table 6 shows the news publishing frequency of Hindustan Times and India Today for different Indian political parties. Figure 6 shows the comparison between

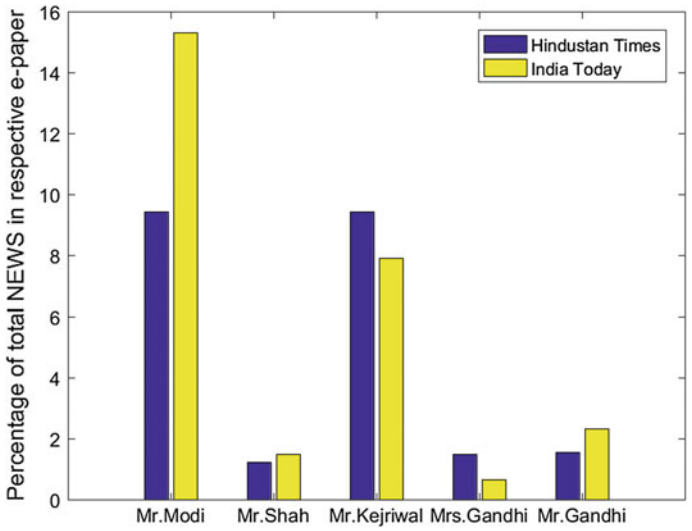

Fig. 5 Comparison between both the e-papers on the basis of news percentage for different Indian politicians

Table 6 News publishing frequency of Hindustan Times and India Today for different Indian political parties

News related to	News publishing frequency	
	Hindustan Times	India Today
BJP	296	796
Congress	158	624
AAP	180	432
BSP	14	70

both the e-papers on the basis of percentage news for different Indian political parties.

It is quite evident from Fig. 6 that BJP (ruling party) is most influential. Congress (opposition) also seems to have a good impact. However, Figs. 5 and 6 combined can be used to conclude that even after having a good impact as a political party, there is an absence of an influential leader in Congress. AAP also seems to have a good impact.

Table 7 shows the news publishing frequency of Hindustan Times and India Today for different Indian states. Figure 7 shows the comparison between both the e-papers on the basis of percentage news for different Indian states.

It is quite evident from Fig. 7 that Uttar Pradesh is the most influential state, followed by Madhya Pradesh and Maharashtra in terms of national news coverage. A high variation can be seen in the interest of both the media houses as national news percentage varies a lot from one state to another as well as from “Hindustan Times” to “India Today”. Also, few states seem to have very low coverage by the

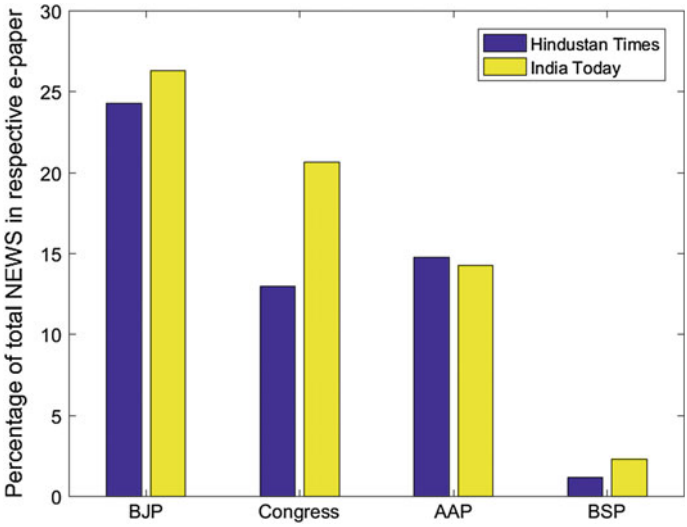

Fig. 6 Comparison between both the e-papers on the basis of news percentage for different Indian political parties

Table 7 News publishing frequency of Hindustan Times and India Today for different Indian states

Serial no.	News related to	News publishing frequency	
		Hindustan Times	India Today
1	Andhra Pradesh	11	31
2	Arunachal Pradesh	10	13
3	Assam	19	29
4	Bihar	57	118
5	Chhattisgarh	0	1
6	Goa	44	142
7	Gujarat	46	74
8	Haryana	48	64
9	Himachal Pradesh	17	22
10	Jammu & Kashmir	61	162
11	Jharkhand	16	28
12	Karnataka	18	68
13	Kerala	20	128
14	Madhya Pradesh	76	256
15	Maharashtra	106	98
16	Manipur	10	34
17	Meghalaya	6	8
18	Mizoram	3	5

(continued)

Table 7 (continued)

Serial no.	News related to	News publishing frequency	
		Hindustan Times	India Today
19	Nagaland	7	10
20	Odisha	12	31
21	Punjab	63	139
22	Rajasthan	26	59
23	Sikkim	10	20
24	Tamil Nadu	17	122
25	Telangana	8	34
26	Tripura	1	6
27	Uttarakhand	11	63
28	Uttar Pradesh	115	467
29	West Bengal	26	87

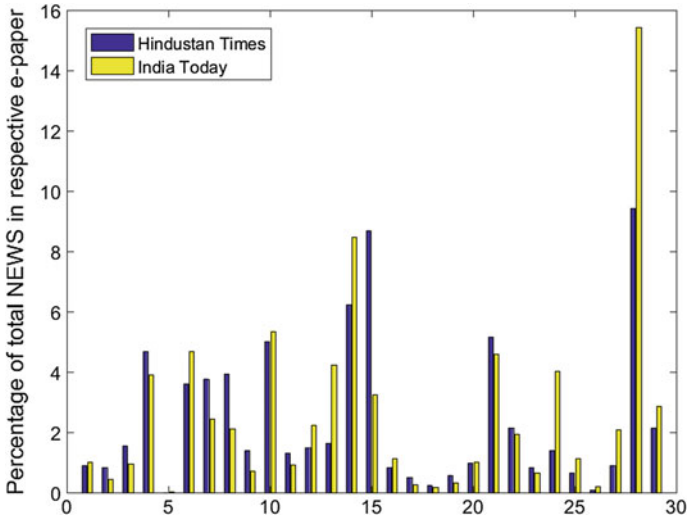

Fig. 7 Comparison between both the e-papers on the basis of news percentage for different Indian states

national media house, which shows uneven coverage and low interest of Indian in that news.

Table 8 shows the news publishing frequency of Hindustan Times and India Today for four major cities of India. Figure 8 shows the comparison between both the e-papers on the basis of percentage news for four major cities of India.

Table 8 News publishing frequency of Hindustan Times and India Today for four major cities of India

News related to	News publishing frequency	
	Hindustan Times	India Today
Delhi	443	674
Mumbai	194	345
Kolkata	24	287
Chennai	18	87

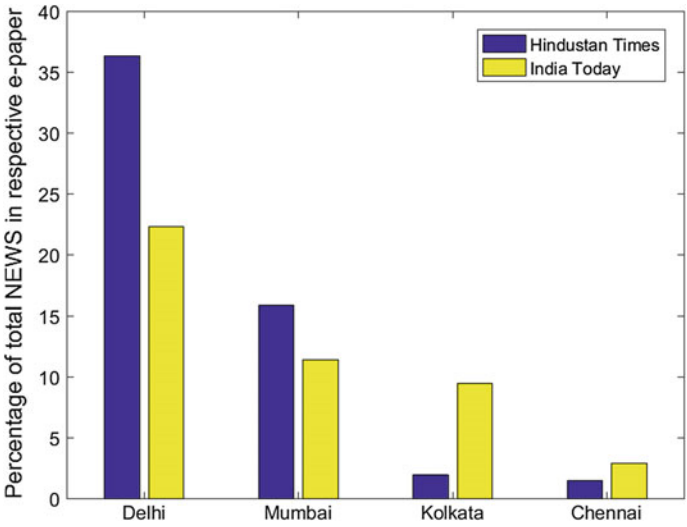

Fig. 8 Comparison between both the e-papers on the basis of news percentage for four major cities of India

It is quite evident from Fig. 8 that India's capital (New Delhi) gets more coverage from the media, followed by Mumbai. But two other major cities (at par with New Delhi) get very less coverage, which again shows uneven reporting by media houses.

5 Conclusion

The aim of this study was to find out the trends of the Indian mainstream media. The analysis was carried out over the recent past data to ensure that the finding remains relevant to the present time. Political news was found to be very dominating over the scientific and other news. Also, Delhi news got most of the coverage and many parts of the country found a very less space in national news, which showed uneven coverage of media houses. Both the media houses were seemed to

have different interests and so the news percentage from different areas varies with decent percentage.

In future, data clustering [21] will be used to find out the news type (positive or negative) also. The positive and negative aspects are also needed to be known so that complete pattern and reason of the popularity can be understood. Soft computing techniques [22] will also be incorporated to improve the clustering performance.

References

1. Straubhaar, J., LaRose, R., & Davenport, L. (2013). Media now: Understanding media, culture, and technology. Cengage Learning.
2. Jones, C., & O'Brien, T. (1997). The long and bumpy road to multi-media: Hi-tech experiments in teaching a professional genre at distance. System, 25(2), 157–167.
3. Cross, K., Gunster, S., Piotrowski, M., & Daub, S. (2015). News Media and Climate Politics. Canadian Centre for Policy Alternatives-BC Office.
4. Nadler, A. M. (2016). Making the news popular: Mobilizing US news audiences. University of Illinois Press.
5. Bagdikian, B. H. (2014). The new media monopoly: A completely revised and updated edition with seven new chapters. Beacon Press.
6. Verma, J., & Sonkar, S. K. (2013). Impact of E-Resources and Web Technology on Reading Habits. In Challenges of Academic Library Management in Developing Countries (pp. 68–74). IGI Global.
7. Souto, V. T. (2017, July). Creativity in Digital Design: Differences from Print-Based Graphic Design. In International Conference of Design, User Experience, and Usability (pp. 755–766). Springer, Cham.
8. Mawindi Mabweazara, Hayes. "Readers Comments on Zimbabwean Newspaper Websites: How audience voices are challenging and (re) defining traditional journalism." Digital Journalism 2.1 (2014): 44–61.
9. Muhingi, W. N., Agonga, A., Mainye, M. M., Mong'are, A. B., & Maranga, F. K. (2015). Political Communication for Sustainable Development in Kenya. Political Communication, 5 (18).
10. Radsch, C. C. (2016). We the People: Citizen Journalism in the Era of Social Media. In Cyberactivism and Citizen Journalism in Egypt (pp. 127–184). Palgrave Macmillan US.
11. HINDUSTAN TIMES—http://www.hindustantimes.com/.
12. INDIA TODAY—http://indiatoday.intoday.in/.
13. Witten, I. H., & Frank, E. (2005). Data Mining: Practical machine learning tools and techniques. Morgan Kaufmann.
14. Srivastava, J., Cooley, R., Deshpande, M., & Tan, P. N. (2000). Web usage mining: Discovery and applications of usage patterns from web data. Acm Sigkdd Explorations Newsletter, 1(2), 12–23.
15. Berkhin, P. (2006). A survey of clustering data mining techniques. In Grouping multi dimensional data (pp. 25–71). Springer Berlin Heidelberg.
16. Imielinski, T., Virmani, A., & Abdulghani, A. (1996, August). DataMine: Application Programming Interface and Query Language for Database Mining. In KDD (Vol. 96, p. 256).
17. Berry, D. M., Borra, E., Helmond, A., Plantin, J. C., & Rettberg, J. W. (2015). The data sprint approach: exploring the field of Digital Humanities through Amazon's application programming interface. Digital Humanities Quarterly, 9(4).

18. Hess, C. K., & Morgan, R. J. (2015). U.S. Patent No. 8,972,880. Washington, DC: U.S. Patent and Trademark Office.
19. http://www.computersciencezone.org/50-most-useful-apis-for-developers/.
20. https://www.kaggle.com/sunnysai12345/news-summary.
21. Kant, S., & Ansari, I. A. (2015). An improved K means clustering with Atkinson index to classify liver patient dataset. International Journal of System Assurance Engineering and Management, 1–7, https://doi.org/10.1007/s13198-015-0365-3.
22. Ansari, I. A., Pant, M., & Ahn, C. W. (2017). Secured and Optimized Robust Image Watermarking Scheme. Arabian Journal for Science and Engineering, 1–20, https://doi.org/10.1007/s13369-017-2777-7.

Optimum Selection of Energy-Efficient Material: A MCDM-Based Distance Approach

Chiranjib Bhowmik, Sachin Gangwar, Sumit Bhowmik and Amitava Ray

Abstract Engineers and manufacturers have encountered a pool of materials depending upon their physical and non-physical properties. Each and every material has its own positiveness and negativeness. Therefore, diminishing adverse environmental effects from material uses is a big challenge in the backdrop of material selection procedure. The aim of this paper is to identify the optimum energy-efficient material from a given set of alternatives in the light of futuristic growth and environmental constraint based on the performance of the decision-making algorithm. The proposed work presents an application of multi-criteria decision-making (MCDM) analysis Entropy-Technique for order of preference by similarity to ideal solution (TOPSIS) to evaluate the appropriate optimum energy-efficient material on the basis of tangible criteria. Firstly, Entropy method is used to figure out precise weight for the criterion from the vagueness of available data associated in this study. Thereafter, TOPSIS method is utilized to select and rank the alternative materials according to their importance merit. Sensitivity analysis is carried out to show the robustness of the selection methodology. Study also reveals that, this is among the few analyses in the energy-efficient material selection which considers environmental threats.

Keywords Entropy · TOPSIS · Energy-efficient material · Sensitivity analysis

C. Bhowmik (✉) · S. Bhowmik
Department of Mechanical Engineering, NIT Silchar, Silchar, Assam, India
e-mail: chiranjibbhowmik18@gmail.com

S. Bhowmik
e-mail: bhowmiksumit04@yahoo.co.in

S. Gangwar
Department of Mechanical Engineering, JKLU, Jaipur, India
e-mail: sachingangwar@jklu.edu.in

A. Ray
JGEC, Jalpaiguri, West Bengal, India
e-mail: amitavaray.siliguri@gmail.com

K. Ray et al. (eds.), *Soft Computing Applications*, Studies in Computational Intelligence 761, https://doi.org/10.1007/978-981-10-8049-4_3

List of symbols

MCDM	Multi-Criteria Decision-Making
TOPSIS	Technique for Order of Preference by Similarity to Ideal Solution
ELECTRE	Elimination and Et Choice Translating Reality
AHP	Analytical Hierarchy Process
VIKOR	VIse Kriterijumska Optimizacija kompromisno Resenje
COPRAS	Complex Proportional Assessment
EVAMIX	Evaluation of Mixed Data
PROMTHEE	Preference Ranking Organization Method for Enrichment Evaluation
MULTIMOORA	Multiobjective Optimization by Ratio Analysis Plus Full Multiplicative Form
SWARA	Step-wise Weight Assessment Ratio Analysis
A1	Alkaline Earth Lead Glass
A2	Silicon
A3	Cast Magnesium
A4	Wrought Magnesium
A5	Cast Nickel Iron Alloy
A6	Lanthanum Commercial Purity min 99%
A7	Magnesium Commercial Purity
A8	Nickel Iron Chromium Alloy HW grade: aged
A9	Cerium Commercial Purity
M1	Density
M2	Bulk Modulus
M3	Compressive Strength
M4	Thermal Conductivity
M5	Thermal Expansion
M6	Resistivity
M7	Cost
M8	Energy Production
M9	CO_2 Emission
α	Decision maker's choice
SI	Sensitivity index
II	Individual influences
UI	Unbiased influences
UIA	Unbiased influences attributes
n	No of alternatives

1 Introduction

Diversification and rapid utilization of energy-efficient materials amplifies the rate of infrastructure development all around the globe [1]. Engineers and manufacturers have encountered a pool of candidate energy materials depending upon their physical and non-physical properties [2]. In order to maintain their increased competitive edge and profit margin of the product they always lookout for new energy-efficient materials and improved manufacturing processes [3]. Therefore, the selection of energy-efficient material has to face a daunting pressure in the various fields of study such as petrochemical, engineering design, dentistry, nuclear engineering, pressure vessel system, membrane science and biomedical engineering [4]. So, the design engineer as well as manufacturer has to think twice before selecting the proper energy-efficient material for any particular application [5]. The engineers and the manufacturers have to consider various factors like physical properties, chemical properties, electrical properties, manufacturing properties, material cost, environmental effect, performance characteristic, availability, etc., while selecting the optimum material [5]. Furthermore, exploitation of energy-efficient materials has gained enormous interest during recent years. Wherein, these materials are usually classified based on density, bulk modulus, compressive strength, thermal conductivity, thermal expansion and resistivity, etc. Selection of appropriate energy-efficient material is essential and also a tedious task. Energy-efficient materials have been exploited in immense scientific and technological applications [6–8] such as radiation windows, florescent lamp envelopes, television bulbs, electronic component, photovoltaic cell, lining of furnace, electrical heating elements, carbon arc lighting and many others. Among the large volume of materials present in the universe and their numerous conflicting criteria, a more precise technique is required to select the optimum material. Selection of an optimum material for any specific application from a finite set of alternatives is an example of multi-criteria decision-making (MCDM) problem. Various MCDM techniques were utilized in the past by many researchers for the selection of most suitable materials in different engineering applications [5]. Jee and Kang [9] utilized Entropy-Technique for Order Preference by Similarity to Ideal Solution (TOPSIS) method for the selection of alternative flywheel material. Suitable material for micro-electromechanical system design has been investigated by Qian and Zhao [10] using performance index. Shanian and Savadogo [11] applied Elimination and Et Choice Translating Reality (ELECTRE) for thermal conductor materials selection. Material suitability index was proposed by Rao [12] to rank the alternative materials for an engineering application. Nonlinear normalization and modified digital logic method was developed by Dehghan-Manshadi et al. [13] for material selection. Chan and Tong [14] adopted gray relation analysis to measure the performance end-of-life product strategy for material selection. An intelligent method was developed by Ullah and Harib [15] based on imprecise information to solve the material selection problem. Rao and Davim [16] selected various engineering components materials using combined TOPSIS and Analytical Hierarchy Process

(AHP) method. Chatterjee et al. [17] utilized VIse Kriterijumska Optimizacija kompromisno Resenje (VIKOR) and ELECTRE II methods for material selection. Rathod and Kanzaria [18] used fuzzy-TOPSIS method to evaluate phase change material in solar domestic hot water system. Utility additive method was applied by Athawale et al. [19] for solving the material selection problem. Chatterjee et al. [20] applied Complex Proportional Assessment (COPRAS) and Evaluation of Mixed Data (EVAMIX) methods for materials selection. Jahan and Edwards [21] applied VIKOR method for material selection from a set of alternatives based on interval data and all types of criteria availability. Anojkumar et al. [22] used four MCDM methods such as fuzzy-TOPSIS, fuzzy-AHP, fuzzy-ELECTRE and fuzzy-Preference Ranking Organization Method for Enrichment Evaluation (PROMTHEE) for the selection of pipes material in sugar industry. Hafezalkotob et al. [23] proposed a fuzzy-interval weighted Multiobjective Optimization by Ratio Analysis Plus Full Multiplicative Form (MULTIMOORA) method for selection of power gears materials. Gul et al. [24] applied fuzzy-PROMETHEE method for the selection of materials for an automobile instrument panel. Milani et al. [25] evaluated gear material selection problem for power transmission using different normalization norms and TOPSIS approach. Zavadskas et al. [26] utilized a single–valued neutrosophic method based on Step-wise Weight Assessment Ratio Analysis (SWARA) and MULTIMOORA for the selection of residential house element material. From the past, research work reveals that various material selection problem has been extensively carried out employing different MCDM methods. A very few literatures are available that examine the optimum energy-efficient material selection for sustainability. Therefore, this study seeks to select the optimum energy-efficient material by an integrated Entropy-TOPSIS methodology for their best utilization. Shannon Entropy method is used to find the precise weights for each criterion from the available information [27]. Thereafter, TOPSIS method is applied to rank and select the alternatives considering beneficial and non-beneficial effects. This study mainly focuses on nine energy-efficient materials and their properties. Sensitivity analysis shows the robustness of the integrated methodology and selection strategy. The study is standardized in the following manner. Problem formulation has been described in Sect. 2. Methodology and findings is illustrated in Sect. 3. Sensitivity analysis is shown in Sect. 4. The next section concludes the paper.

2 Problem Formulation

Optimal material selection is the crucial part for any engineering application in current era. Any erroneous selection of optimal materials can impose enormous cost associated with extravagant CO_2 emissions to the environment. Therefore, the task to select the optimum material from all the distinctively available materials becomes even more difficult. A superior procedure or any robust technique is precariously needed for the selection of optimal energy-efficient material for sustainability [8].

In real scenario, energy-efficient materials compared to auxiliary materials are the superlative choice on the grounds of mitigating emission to the environment. The quandary embroils testimony of distinct energy-efficient materials that are passed down in the manufacturing of radiation windows, solar cells, fluorescent lamp envelop and to select the optimum energy-efficient materials among them [8]. Various energy-efficient materials selected for this study are listed in Table 1. This study selects nine energy-efficient materials which are, Alkaline Earth Lead Glass (A1), Silicon (A2), Cast Magnesium (A3), Wrought Magnesium (A4), Cast Nickel Iron Alloy (A5), Lanthanum Commercial Purity min 99% (A6), Magnesium Commercial Purity (A7), Nickel Iron Chromium Alloy HW grade; aged (A8) and Cerium Commercial Purity (A9). Wherein, there corresponding properties are 'Density; Kg/m^3 (M1), bulk modulus; Gpa (M2), compressive strength; Mpa (M3)-physical properties,' 'thermal conductivity; W/mk (M4), thermal expansion; μstrain/°C (M5)-thermal properties,' 'resistivity; μΩ cm (M6)-electrical property,' 'cost; GBP/Kg (M7), energy production; MJ/Kg (M8)-economical property' and 'CO_2 emission; Kg/Kg (M9)-environmental property.'

From Table 1, it is very difficult for any person to select the optimum energy-efficient materials for sustainability. Because all the materials like A1, A2, A3, A4, A5, A6, A7, A8 and A9 selected in this research are excellent, but each and every material composes with rare earth elements which makes them very pricey in nature. Similarly, each and every material acquires its own positive and negative properties, respectively. Therefore, the outcome judgement has to correlate all the energy-efficient materials in regard to all the aspects and choose the optimum one [8]. So the objective of this work is to find the optimum energy-efficient materials for sustainability. The hierarchy of the problem is shown in Fig. 1.

Table 1 Energy-efficient materials and their properties [28]

Criteria										
Sl. no	Materials	M1	M2	M3	M4	M5	M6	M7	M8	M9
1	A1	0.113	4.83	36.5	0.47	5.27	1.22	74.7	2578	1.28
2	A2	0.082	13.7	464	86.6	1.11	1.1	164	6164	3.07
3	A3	0.063	4.78	10.1	29.4	13.6	5.35	104	4.99	29
4	A4	0.062	5.07	12.3	28.8	13.6	4.15	119	5.51	32
5	A5	0.290	18.8	31.9	6.35	6.38	108	112	1.37	7.98
6	A6	0.220	3.77	15.9	7.51	2.5	56	261	3.54	20.6
7	A7	0.062	4.78	9.42	86.6	14.1	4.2	104	3.96	32.8
8	A8	0.290	18.8	45.6	6.35	6.38	108	373	1.18	6.84
9	A9	0.238	2.32	13.0	5.77	3.33	75	673	6.57	38.2

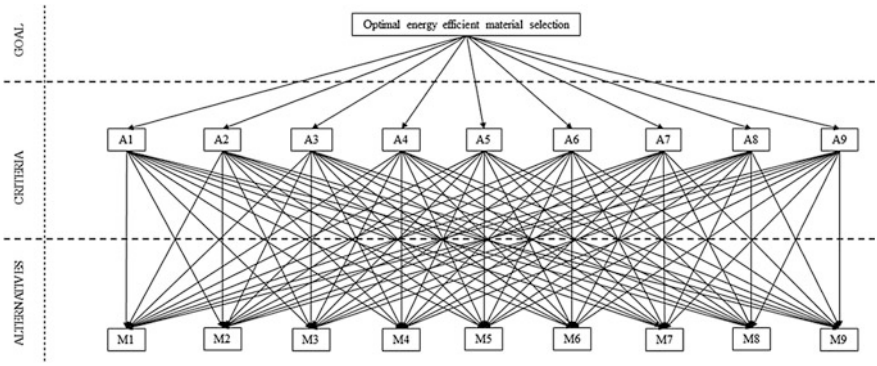

Fig. 1 Hierarchy of the problem

3 Methodology and Findings

Based on the aforementioned dimensions, this study reveals that, there are enormous criterions followed by different alternatives for the optimal energy materials selection. From the various criterions and alternatives, to select the optimum one is an example of MCDM application, wherein the study follows an integrated methodology comprising Entropy-TOPSIS method for the optimal selection of energy-efficient materials. Figure 2 depicts the flow diagram of the proposed methodology.

The following steps satisfy the Entropy-TOPSIS methodology to select the optimum energy-efficient materials.

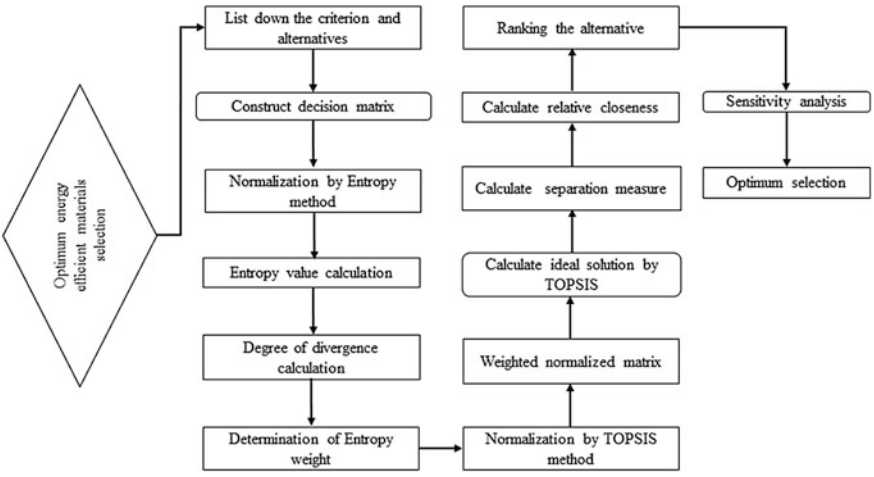

Fig. 2 Flow diagram of the proposed methodology

Step 1: Decompose the problem into a hierarchy with control criterion as shown in Fig. 1. The goal of the problem is placed at the top level of the hierarchy, whereas criterion and alternatives are placed at the lower level of the hierarchy.

Step 2: After formation of the control hierarchy, the decision matrix is prepared. In this study, the data have been taken from CES Edu pack (2005) [28] for making the decision matrix as depicted in Table 1.

Step 3: After formation of the decision matrix, the values are normalized to maintain the same unit. This study allows Entropy method for the normalization purpose. The normalization is done using Eq. (1), and the results are depicted in Table 2. Entropy method consists of following steps to measure the weights of each criterion suggested by Lotfi and Fallahnejad [27] and Dashore et al. [29].

$$P_{ij} = \frac{X_{ij}}{a_{i=1}^{m} X_{ij}} \tag{1}$$

Step 4: Then the Entropy value for the entire criterion using Eq. (2) is calculated. The computed values are shown in Table 3.

$$e_j = -k \sum_{j=1}^{n} P_{ij} \ln P_{ij} \tag{2}$$

Step 5: Thereafter, degree of divergence is computed using Eq. (3) and tabulated in Table 4.

$$d_j = 1 - e_j \tag{3}$$

Step 6: Then each element of divergence value is divided by its row sum to calculate the Entropy weight of each criterion. The weighting components are shown in Table 2.

Table 2 Normalized matrix by Entropy method

Criteria									
Materials	M1	M2	M3	M4	M5	M6	M7	M8	M9
A1	0.079	0.062	0.057	0.001	0.079	0.003	0.037	0.293	0.007
A2	0.057	0.178	0.726	0.335	0.016	0.003	0.082	0.702	0.017
A3	0.044	0.062	0.015	0.114	0.205	0.014	0.052	0.005	0.168
A4	0.045	0.065	0.019	0.111	0.205	0.011	0.060	0.006	0.186
A5	0.204	0.244	0.049	0.024	0.096	0.297	0.056	0.001	0.046
A6	0.154	0.048	0.024	0.029	0.037	0.154	0.131	0.004	0.119
A7	0.043	0.062	0.014	0.335	0.213	0.011	0.052	0.005	0.190
A8	0.204	0.244	0.071	0.024	0.096	0.297	0.187	0.003	0.039
A9	0.167	0.030	0.020	0.022	0.050	0.206	0.338	0.007	0.222

Table 3 Entropy values for each element

Criteria								
M1	M2	M3	M4	M5	M6	M7	M8	M9
1.307	68.30	322.8	188.8	59.71	253.9	1736	2519	148.3

Table 4 Divergence value

Criteria								
M1	M2	M3	M4	M5	M6	M7	M8	M9
2.307	69.30	323.8	189.8	60.71	254.94	1737.8	2520.9	149.3

Among various criterion, to find the weights of each criterion is very difficult and can be done by various techniques. In this study, Entropy method is employed because this method is helpful to find the precise weight from the vagueness of data. This method will help decision-makers to find the importance of each criterion in a minimal time [8] (Table 5).

Step 7: After computing the weights of each criterion, normalized decision matrix is evaluated by TOPSIS method as shown in Table 1. Normalization is done using Eq. (4). Normalization is required to neutralize the irregularities of different measurement units associated with various variables in a decision matrix into a compatible unit. The normalized decision matrix is depicted in Table 6. TOPSIS model was first put forward by Hwang and Yoon [30], and their application history was also described by them. According to Chauhan and Vaish [7] and Kumar et al. [31], TOPSIS implies that a decision matrix having 'm' alternatives and 'n' criteria can be pretended to be dilemma of 'n' dimensional hyper plane having 'm' points whose whereabouts is obsessed by the value of their criteria [32]. The subsequent steps discuss the TOPSIS methodology employed in this study.

$$P_{ij} = \frac{x_{ij}}{\sqrt{\sum_{i=1}^{m} x_{ij}^2}} \quad (1 \le i \le m, 1 \le j \le n) \tag{4}$$

Step 8: After normalizing the decision matrix, the weighted normalized matrix is computed by multiplying the Entropy weights (Table 5) of each attribute to each element of the normalized decision matrix using Eq. (5). The weighted normalized matrix is shown in Table 7.

$$V_{ij} = P_{ij} * w_j \tag{5}$$

Table 5 Weight of each criterion

Criteria								
M1	M2	M3	M4	M5	M6	M7	M8	M9
0.0004	0.0130	0.0610	0.0357	0.0114	0.0180	0.3273	0.4747	0.0281

Table 6 Normalized decision matrix by TOPSIS method

Criteria									
Materials	M1	M2	M3	M4	M5	M6	M7	M8	M9
A1	0.204	0.151	0.077	0.003	0.199	0.006	0.086	0.385	0.018
A2	0.148	0.432	0.988	0.666	0.041	0.006	0.190	0.922	0.043
A3	0.114	0.150	0.021	0.226	0.515	0.029	0.121	0.007	0.043
A4	0.113	0.159	0.026	0.222	0.515	0.023	0.138	0.008	0.455
A5	0.525	0.591	0.067	0.048	0.241	0.602	0.130	0.002	0.113
A6	0.398	0.118	0.033	0.057	0.094	0.312	0.303	0.005	0.292
A7	0.112	0.150	0.020	0.666	0.534	0.023	0.121	0.005	0.466
A8	0.525	0.591	0.097	0.048	0.241	0.602	0.433	0.001	0.097
A9	0.430	0.072	0.027	0.044	0.125	0.418	0.780	0.009	0.543

where w_j is the weight of the ith criterion and $\sum_{i=1}^{n} w_j = 1$

Step 9: In this step, for every attribute, best performance and worst performance is computed using Eqs. (6) and (7) by taking the maximum and minimum value [31]. Before computation, the beneficial and non-beneficial attributes are considered for this purpose. In this study, the beneficial attributes are M1, M2, M3, M4, M5 and M6, whereas non-beneficial attributes are M7, M8 and M9. The best performance values and worst performance values are tabulated in Tables 8, 9 and 10 respectively.

$$V^{+} = \left\{v_1^{+}, v_2^{+}, \ldots, v_n^{+}\right\} = \left\{\left(\text{Max}v_{ij}|j\epsilon J|\right), \left(\text{Min}v_{ij}|j\epsilon J|\right)\right\} \tag{6}$$

$$V^{-} = \left\{v_1^{-}, v_2^{-}, \ldots, v_n^{-}\right\} = \left\{\left(\text{Min}v_{ij}|j\epsilon J|\right), \left(\text{Max}v_{ij}|j\epsilon J|\right)\right\} \tag{7}$$

Table 7 Weighted normalized matrix

Alternatives	Criteria								
	M1	M2	M3	M4	M5	M6	M7	M8	M9
A1	0.009	0.001	0.004	0.001	0.002	0.003	0.028	0.183	0.005
A2	0.007	0.005	0.060	0.023	0.004	0.002	0.062	0.437	0.001
A3	0.004	0.001	0.001	0.008	0.005	0.001	0.039	0.003	0.011
A4	0.009	0.002	0.001	0.007	0.005	0.001	0.045	0.003	0.012
A5	0.002	0.007	0.004	0.001	0.002	0.028	0.042	0.009	0.003
A6	0.001	0.005	0.002	0.002	0.001	0.014	0.099	0.002	0.008
A7	0.004	0.001	0.001	0.023	0.006	0.001	0.039	0.002	0.013
A8	0.003	0.007	0.005	0.001	0.002	0.028	0.142	0.008	0.002
A9	0.001	0.009	0.001	0.009	0.004	0.020	0.255	0.006	0.015

Table 8 Best performance value

Criteria								
M1	M2	M3	M4	M5	M6	M7	M8	M9
0.0002	0.0077	0.0602	0.0238	0.0061	0.0289	0.0284	0.0083	0.0005

Table 9 Worst performance value

Criteria								
M1	M2	M3	M4	M5	M6	M7	M8	M9
0.0049	0.0009	0.0012	0.0001	0.0004	0.0002	0.2556	0.4379	0.0152

Table 10 PIS value

Alternatives								
A1	A2	A3	A4	A5	A6	A7	A8	A9
0.1950	0.4401	0.0690	0.0703	0.0621	0.0960	0.0676	0.1279	0.2365

Step 10: This step measures distance from the positive and negative ideal solution [32]. TOPSIS is a distance-based approach; therefore, for all attributes distance from the best alternative or positive ideal solution (PIS) and worst alternative or negative ideal solution (NIS) is computed using Eqs. (8) and (9) and depicted in Tables 10 and 11 respectively.

$$S_i^+ = \sqrt{\sum_{j=1}^{n} \left(v_{ij} - V^+\right)^2} \quad (1 \le i \le m,\ 1 \le j \le n) \tag{8}$$

$$S_i^- = \sqrt{\sum_{j=1}^{n} \left(v_{ij} - V^-\right)^2} \quad (1 \le i \le m,\ 1 \le j \le n) \tag{9}$$

Step 11: Determination of closeness measurement: For every alternative, relative closeness is computed by dividing negative ideal solution by the sum of the distance to the positive and negative ideal solution, i.e., C_i is determined using Eq. (10). C_i exhibits the similarity to the positive ideal solution. According to the magnitude of C_i, alternatives are arranged. The biggest C_i value is selected as the optimum alternative, and the results of relative closeness are shown in Table 12.

Table 11 NIS value

Alternatives								
A1	A2	A3	A4	A5	A6	A7	A8	A9
0.3417	0.2039	0.4880	0.4855	0.4880	0.4650	0.4886	0.4535	0.4379

Table 12 Ranking order

Alternatives	A1	A2	A3	A4	A5	A6	A7	A8	A9
	0.636	0.316	0.876	0.873	0.887	0.828	0.878	0.779	0.649
Rank	8	9	3	4	1	5	2	6	7

$$C_i = \frac{S_i^-}{S_i^+ + S_i^-} \quad (1 \leq i \leq m) \tag{10}$$

where $C_i \epsilon (0.1)$. The larger C_i is, the closer alternative to the ideal solution [32].

Finally, the magnitude of all the alternatives is tabulated in Table 12 and ranked according to the closeness to the ideal solution, wherein the alternative with the highest value is said to be optimum (A5). Cast Nickel Iron Alloy (A5) is the preferred choice of energy-efficient material in dispersion of the correlated other materials with the accustomed equity to wardrobe for environment when different weights were accustomed to all criteria [33]. This study only deals with the tangible behavior of the energy-efficient materials. The tangible output is extracted from the vagueness of information associated with the materials properties. The proposed methodology also takes care of the unpredictability of the instantaneous output of the optimum efficient energy materials selection. The methodology undertaken in this study is user-friendly and time-saving, as the process requires only Microsoft Office and MATLAB program to validate the results. So, it can serve as an effective decision-making tool for the materials managers, process engineers and end users.

4 Sensitivity Analysis

Sensitivity analysis is the practical way for determining the effects of uncertainties with the variation of the criteria of a model and showing substantial effects on the optimum selection of alternative. Therefore, the uncertainty present in the model can be justified by this analysis. From the commercial aspects of material selection strategy, sensitivity analysis is carried out with respect to each criterion. A mathematical model is proposed by Bhattacharya et al. [34] to combine different criteria component with the importance weighting found from the Entropy-TOPSIS method. If the weight assigned to the individual influences $\alpha (0 < \alpha < 1)$, the unbiased influences obtain a weight of $(1 - \alpha)$. Thus, sensitivity analysis for alternative i can be computed using Eqs. (11) and (12).

$$\mathrm{SI}_i = \alpha(\mathrm{II}_i) + (1 - \alpha)(\mathrm{UI}_i) \tag{11}$$

where II_i is the individual influence measure for alternative i. UI_i is the unbiased influence measure for alternative i and derived as:

$$\mathrm{UI}_i = \left[\mathrm{UIA}_i \sum_{i=1}^{n} \left(\frac{1}{\mathrm{UIA}_i}\right)\right]^{-1} \tag{12}$$

where UIA_i is the unbiased influences attributes for alternative i. n is the number of the alternatives (n = 9 in the present case).

The II value, i.e., the comprehensive importance of an alternative, is the unique quantity found using the proposed Entropy-TOPSIS method. Thus, the II values used in Eq. (11) are the importance of C_i (normalized) found from Table 12. The units of UIA are different, but to maintain the similar units normalized UIA values are chosen. Determination of α values is quite tricky and important. The values of α depend on the decision maker's choice regarding the preferences of unbiased and individual influence measures. A sensitivity plot is strongly recommended to analyze the effect of α in the selection process. Figure 3 shows the sensitivity plots for all the alternatives with respect to every criterion. The following cases show the robustness of the analysis.

Case 1: When $\alpha = 0.986$ then the optimum alternatives are likely A5, A6, A8, A1, A9 and A2. Similarly, for $\alpha = 0.989$ and 0.99.
When $\alpha = 0.457$ then the optimum alternatives are such as A1, A2, A5, A6, A8 and A9.
When $\alpha = 0.631$ then the optimum alternatives are, namely A5, A6, A8, A9, A1 and A2.

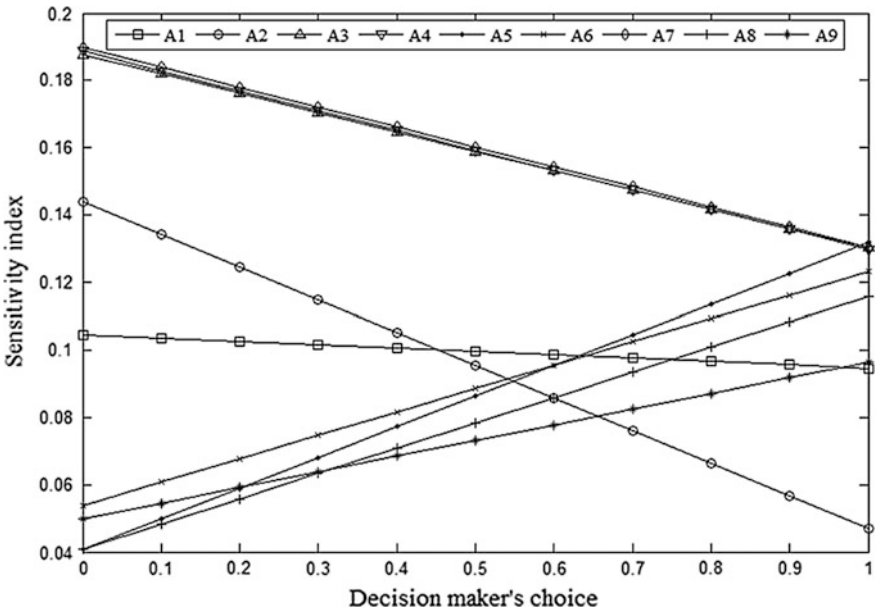

Fig. 3 Sensitivity plot with respect to M1

When $\alpha = 0.64$ then the optimum alternatives are, namely A6, A1, A8, A9 and A2. Figure 3 shows the sensitivity analysis for the above cases with respect to criteria 'density' (M1).

Case 2: When $\alpha = 0.986$ then the optimum alternatives are such as A5, A6, A9, A8, A1 and A2. Similarly, for $\alpha = 0.986$ and 0.983.
When $\alpha = 0.785$ then all the alternatives are optimum depending upon the availability and other circumstances.
When $\alpha = 0.141$ then the optimum alternatives are, namely A4, A1, A5, A8 and A2.
When $\alpha = 0.71$ then the optimum alternatives are likely A1, A5, A8 and A2.
When $\alpha = 0.81$ then the optimum alternatives are, namely A8 and A2. Figure 4 shows the sensitivity analysis for the above case with respect to criteria 'bulk modulus' (M2).

Case 3: Figure 5 shows the sensitivity analysis for this case with respect to 'compressive strength' (M3). In this case all the alternatives are optimum.

Case 4: When $\alpha = 0.949$ then the optimum alternatives are, namely A5, A3, A6, A4, A8, A7 and A9.
When $\alpha = 0.953$ and 0.954 then the optimum alternatives are likely A7, A3, A4, A6, A8, A9 and A2.
When $\alpha = 0.96$ then the optimum alternatives are such as A6, A8, A9 and A2.

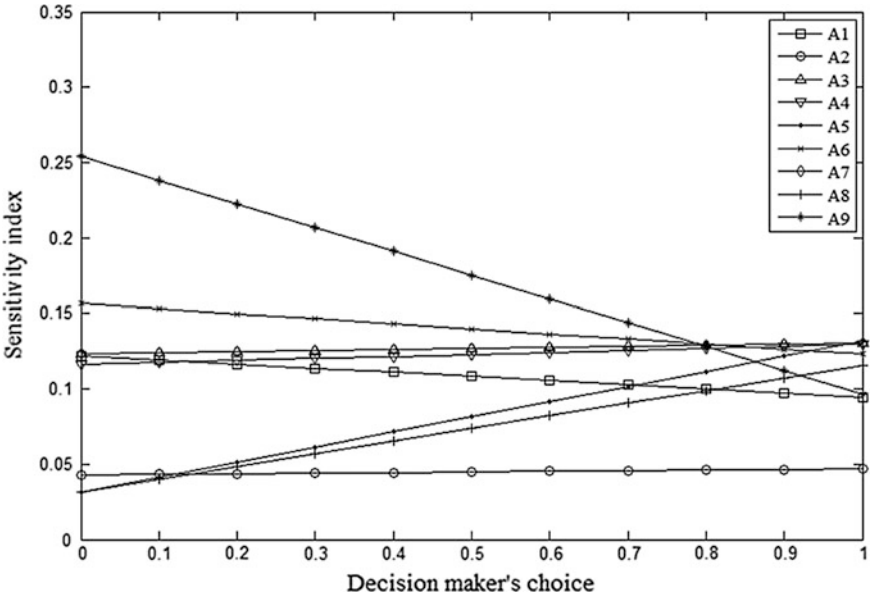

Fig. 4 Sensitivity plot with respect to M2

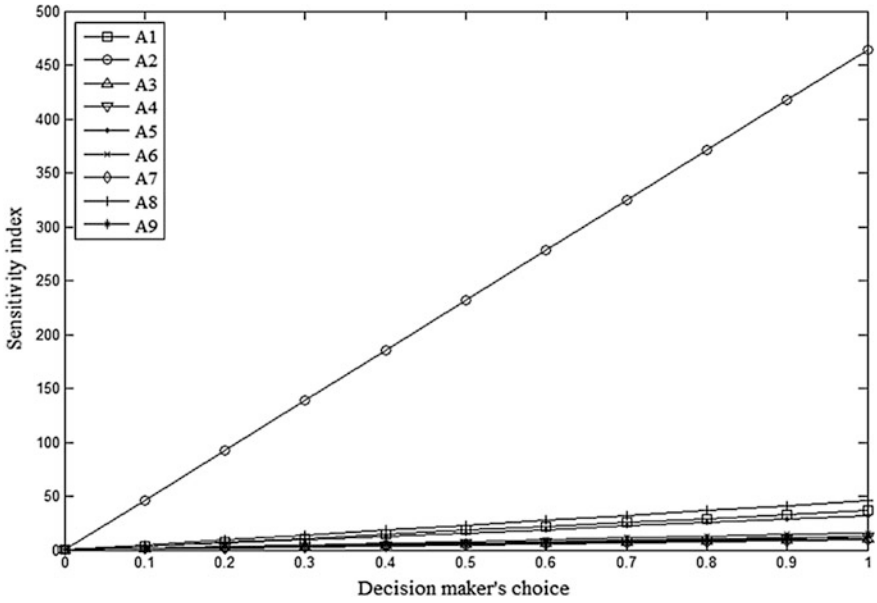

Fig. 5 Sensitivity plot with respect to M3

When $\alpha = 0.97$ then the optimum alternatives are, namely A9 and A2.
When $\alpha = 0.99$ then the optimum alternative is A2. Figure 6 shows the sensitivity analysis for the above case with respect to criteria 'thermal conductivity' (M4).

Case 5: When $\alpha = 0.951$ then the optimum alternatives are likely A5, A7, A3, A4, A6, A8, A9, A1 and A2. Similarly, for $\alpha = 0.954$ and 0.956.
When $\alpha = 0.92$ all the alternatives are optimum.
When $\alpha = 0.815$ then the optimum alternatives are, namely A2, A9 and A1.
When $\alpha = 0.811$ the optimum alternatives are such as A8, A9, A1 and A2.
When $\alpha = 0.810$ then the optimum alternatives are, namely A8, A6, A9, A1 and A2. Figure 7 shows the sensitivity analysis for the above case with respect to criteria 'thermal expansion' (M5).

Case 6: When $\alpha = 0.986$ then the optimum alternatives are likely A5, A7, A4, A3, A6, A8, A9, A1 and A2.
When $\alpha = 0.901$ then the optimum alternatives are, namely A5, A6, A8, A9, A1 and A2. Similarly, for $\alpha = 0.811$. Therefore, the sensitivity analysis for the above case with respect to criteria 'resistivity' (M6) is depicted in Fig. 8.

Case 7: When $\alpha = 0.88$ then the optimum alternatives are such as A5, A4, A1, A6, A8, A9 and A2.

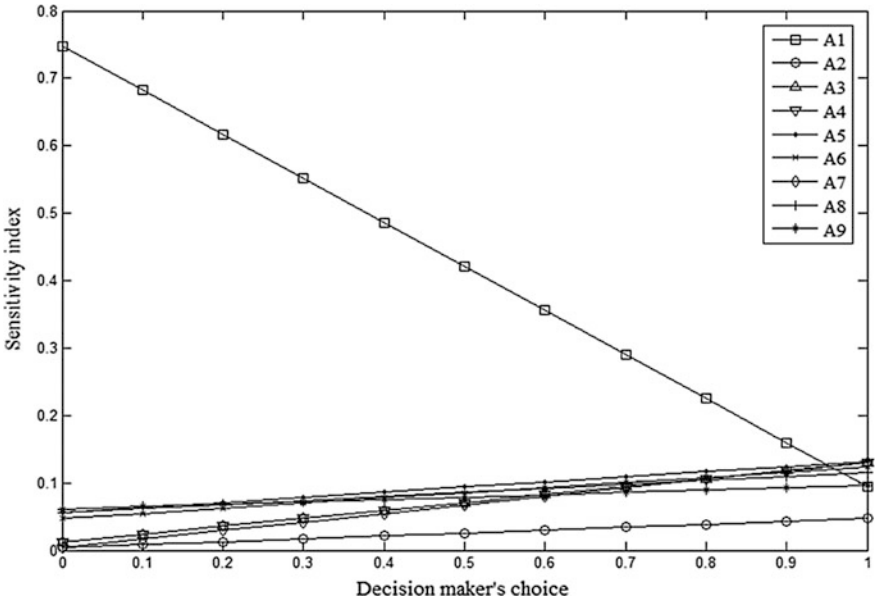

Fig. 6 Sensitivity plot with respect to M4

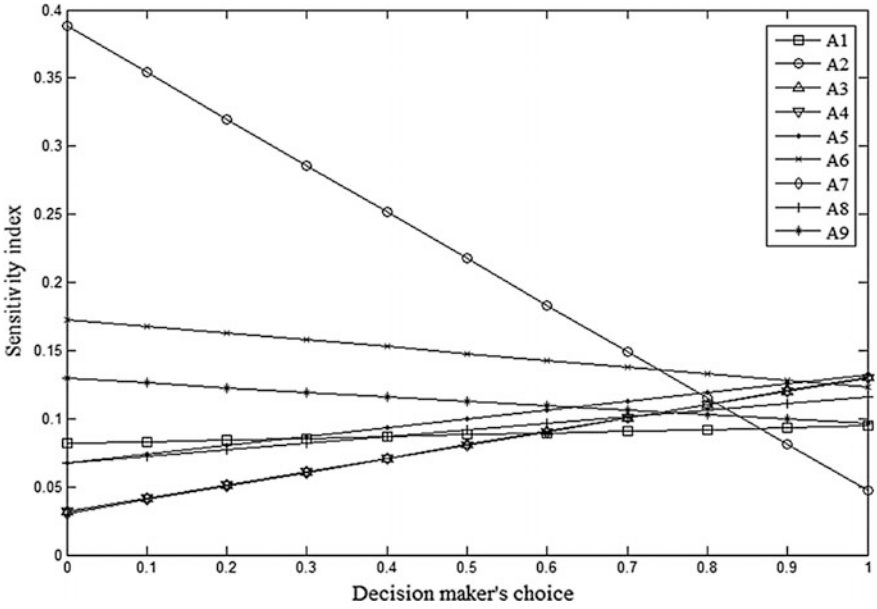

Fig. 7 Sensitivity plot with respect to M5

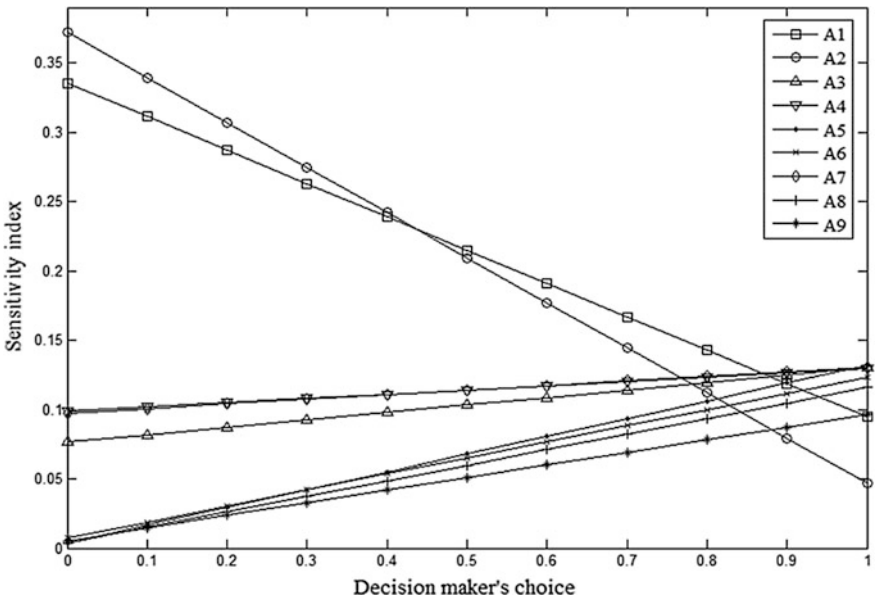

Fig. 8 Sensitivity plot with respect to M6

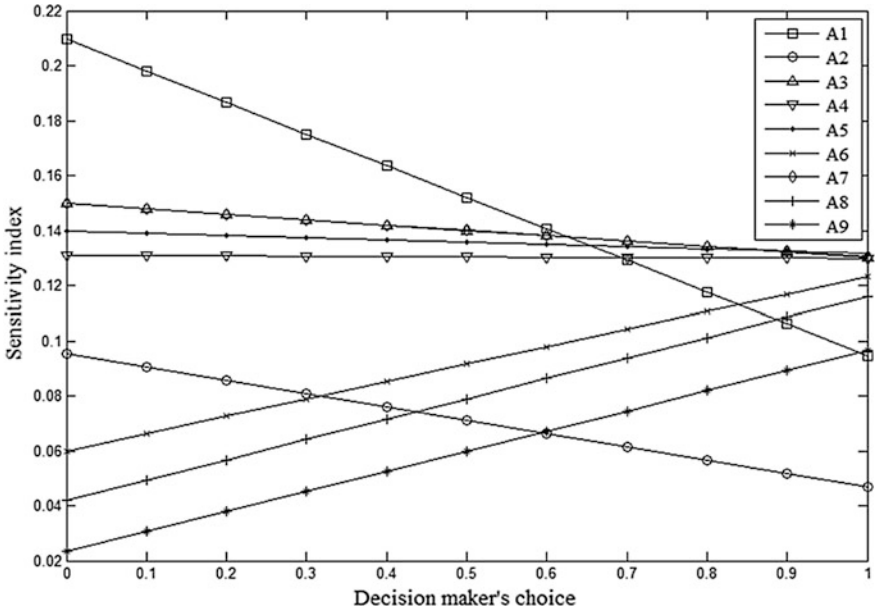

Fig. 9 Sensitivity plot with respect to M7

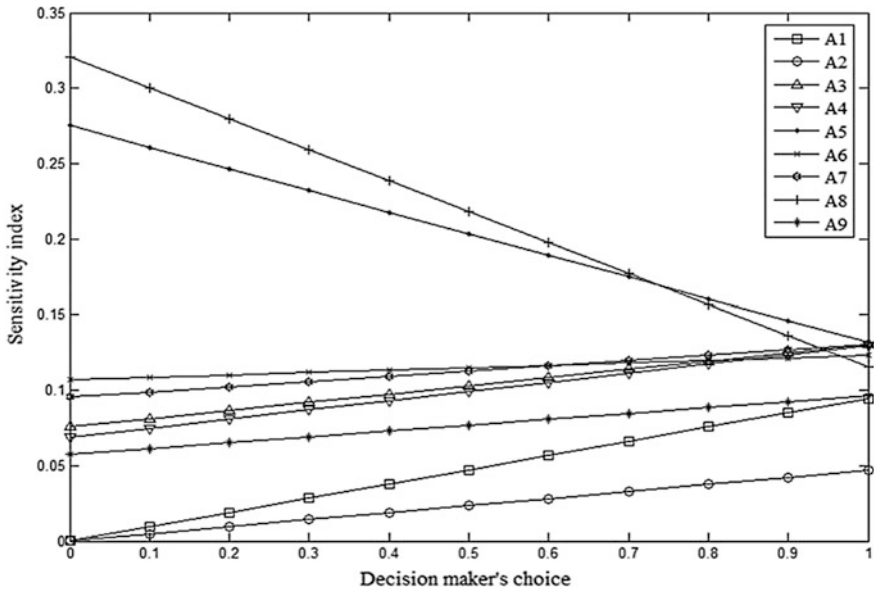

Fig. 10 Sensitivity plot with respect to M8

When $\alpha = 0.65$ then the optimum alternatives are likely A5, A4, A6, A8, A9 and A2. Figure 9 shows the sensitivity analysis for the above case with respect to criteria 'cost' (M7).

Case 8: When the value of $\alpha = 0.74$ then all the alternatives are optimum. Figure 10 shows the sensitivity plot for this case with respect to criteria 'energy production' (M8).

Case 9: When $\alpha = 0.92$ then all the alternatives are optimum. Sensitivity plot for this case with respect to criteria 'CO_2 emission' (M9) is depicted in Fig. 11.

When $\alpha = 0.60$ then the optimum alternatives are likely A5, A3, A4, A6, A7 and A9.

The graphical representation of Figs. 3, 4, 5, 6, 7, 8, 9, 10 and 11 is based on sensitivity index values with respect to relative criterion. The selection of energy-efficient alternatives with respect to every criterion followed the analogy 'higher the better.'

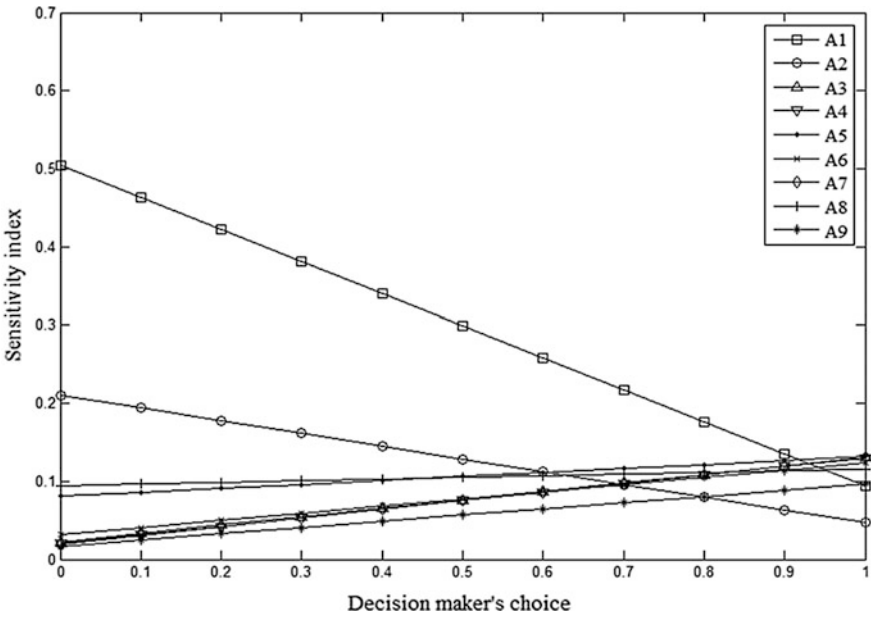

Fig. 11 Sensitivity plot with respect to M9

5 Conclusion and Future Scope

The optimal material selection is an important aspect of material management and essential to material planning. It is a complex multi-criteria decision-making problem that includes both qualitative and quantitative factors which are often assessed with imprecise data and human judgement. Various methods have been proposed to analyze material selection. An efficient assessment system is essential for appropriate energy-efficient material selection for sustainability. This study uses a theoretical case in the form of an arithmetical illustration. Considering the fact of various crucial factors on the optimum energy-efficient material selection, the proposed methodology addresses the major issues and the alternatives considered in this study. The application of integrated Entropy-TOPSIS methodology gives an orderly and reasonable explanation to the decision maker. Weighting factors influence has also been discussed using Entropy method. Each approach suggests its own pros and cons, but completely it is preferred by the decision maker to go with. This study shows that Cast Nickle Iron Alloy (A5) is the optimum choice of energy-efficient material for the accustomed dilemma by the integrated methodology. It is also evident from the sensitivity analysis for all the nine cases. At this juncture, this research can select A5 material because study follows the analogy 'the higher one, the better one' but when A5 is exhausted then remaining alternative materials may be used according to availability. The main features of the potential selection can be catalogued below:

- Recommending an exemplary which simultaneously brings about; energy-efficient material selection and procedure appropriation,
- This research identifies the most critical factors for optimum energy-efficient material selection. Sensitivity analysis shows the robustness of the combined entropy-TOPSIS approach.

Again, there is a scope of future research in the areas of the intangible behavior of the energy-efficient materials properties and their unpredictability toward the output of the selection procedure. Further investigation may also assimilate a practice to contemplate new restraints in prospective Entropy-TOPSIS method. Alternative optimization techniques alike artificial neural network, bee-colony optimization, etc., seems to be practical to appraise and putrid the energy-efficient materials properly.

Acknowledgements The present book chapter is an extended version of the paper entitled 'Selection of Energy-Efficient Material: An Entropy-TOPSIS Approach,' presented during International Conference on Soft Computing: Theories and Applications, held at Amity University Rajasthan, Jaipur, India, during December 28–30, 2016. The authors are thankful to the Organizing Committee.

References

1. Govindan, K., Shankar, K.M., Kannan, D.: Sustainable material selection for construction industry–A hybrid multi criteria decision making approach. Renewable and Sustainable Energy Reviews **55**, 1274–1288 (2016)
2. Hafezalkotob, A., Hafezalkotob, A.: Risk-based material selection process supported on information theory: A case study on industrial gas turbine. Applied Soft Computing, **52**, 1116–1129 (2017)
3. Jahan, A., Ismail, M.Y., Sapuan, S.M., Mustapha, F.: Material screening and choosing methods–a review. Materials & Design, **31**(2), 696–705 (2010)
4. Jahan, A., Ismail, M.Y., Mustapha, F., Sapuan, S.M.: Material selection based on ordinal data. Materials & Design, **31**(7), 3180–3187 (2010)
5. Athawale, V.M., Chakraborty, S.: Material selection using multi-criteria decision-making methods: a comparative study. Proceedings of the Institution of Mechanical Engineers, Part L: Journal of Materials: Design and Applications, **226**(4), 266–285 (2012)
6. Akyene, T.: Cell phone evaluation base on Entropy and TOPSIS. Interdisciplinary Journal of Research in Business, **1**(12), 9–15 (2012)
7. Chauhan, A., Vaish, R.: 2012. Magnetic material selection using multiple attribute decision making approach. Materials & Design, **36**, 1–5 (2012).
8. Kumar, D.S., Suman, K.N.S.: 2014. Selection of magnesium alloy by MADM methods for automobile wheels. IJEM-International Journal of Engineering and Manufacturing, **4**(2), 31–41 (2014)
9. Jee, D.H., Kang, K.J.: A method for optimal material selection aided with decision making theory. Materials & Design, **21**(3), 199–206 (2000)
10. Qian, J., Zhao, Y.P.: Materials selection in mechanical design for microsensors and microactuators. Materials & design, **23**(7), 619–625 (2002)
11. Shanian, A., Savadogo, O.: A material selection model based on the concept of multiple attribute decision making. Materials & Design, **27**(4), 329–337 (2006)

12. Rao, R.V.: A material selection model using graph theory and matrix approach. Materials Science and Engineering: A, **431**(1), 248–255 (2006)
13. Dehghan-Manshadi, B., Mahmudi, H., Abedian, A., Mahmudi, R.: 2007. A novel method for materials selection in mechanical design: combination of non-linear normalization and a modified digital logic method. Materials & design, **28**(1), 8–15 (2007)
14. Chan, J.W., Tong, T.K.: Multi-criteria material selections and end-of-life product strategy: Grey relational analysis approach. Materials & Design, **28**(5), 1539–1546 (2007)
15. Ullah, A.S., Harib, K.H.: An intelligent method for selecting optimal materials and its application. Advanced Engineering Informatics, **22**(4), 473–483 (2008)
16. Rao, R.V., Davim, J.P.: A decision-making framework model for material selection using a combined multiple attribute decision-making method. The International Journal of Advanced Manufacturing Technology, **35**(7), 751–760 (2008)
17. Chatterjee, P., Athawale, V.M., Chakraborty, S.: Selection of materials using compromise ranking and outranking methods. Materials & Design, **30**(10), 4043–4053 (2009)
18. Rathod, M.K., Kanzaria, H.V.: A methodological concept for phase change material selection based on multiple criteria decision analysis with and without fuzzy environment. Materials & Design, **32**(6), 3578–3585 (2011)
19. Athawale, V.M., Kumar, R., Chakraborty, S.: Decision making for material selection using the UTA method. The International Journal of Advanced Manufacturing Technology, **57**(1), 11–22 (2011)
20. Chatterjee, P., Athawale, V.M., Chakraborty, S.: Materials selection using complex proportional assessment and evaluation of mixed data methods. Materials & Design, **32**(2), 851–860 (2011)
21. Jahan, A., Edwards, K.L.: VIKOR method for material selection problems with interval numbers and target-based criteria. Materials & Design, **47**, 759–765 (2013)
22. Anojkumar, L., Ilangkumaran, M., Sasirekha, V.: Comparative analysis of MCDM methods for pipe material selection in sugar industry. Expert Systems with Applications, **41**(6), 2964–2980 (2014)
23. Hafezalkotob, A., Hafezalkotob, A., Sayadi, M.K.: Extension of MULTIMOORA method with interval numbers: an application in materials selection. Applied Mathematical Modelling, **40**(2), 1372–1386 (2016)
24. Gul, M., Celik, E., Gumus, A.T., Guneri, A.F.: A fuzzy logic based PROMETHEE method for material selection problems. Beni-Suef University Journal of Basic and Applied Sciences https://doi.org/10.1016/j.bjbas.2017.07.002 (2017)
25. Milani, A.S., Shanian, A., Madoliat, R., Nemes, J.A.: The effect of normalization norms in multiple attribute decision making models: a case study in gear material selection. Structural and multidisciplinary optimization, **29**(4), 312–318 (2005)
26. Zavadskas, E.K., Bausys, R., Juodagalviene, B., Garnyte-Sapranaviciene, I.: Model for residential house element and material selection by neutrosophic MULTIMOORA method. Engineering Applications of Artificial Intelligence, **64**, 315–324 (2017)
27. Lotfi, F.H., Fallahnejad, R.: Imprecise Shannon's Entropy and multi attribute decision making. Entropy, **12**(1), 53–62 (2010)
28. CES Edu pack 2005
29. Dashore, K., Pawar, S.S., Sohani, N., Verma, D.S.: Product evaluation using Entropy and multi criteria decision making methods. International Journal of Engineering Trends and Technology, **4**, 2183–2187 (2013)
30. Hwang, C.L., Yoon, K.: Methods for multiple attribute decision making. In Multiple attribute decision making. pp. 58–191. Springer Berlin Heidelberg (1981)
31. Kumar, R., Bhowmik, C., Ray, A.: Selection of cutting tool material by TOPSIS method. In National Conference on Recent advancement in Mechanical Engineering, NERIST, Itanagar, India. pp. 978–993 (2013)
32. Chang, C.W.: Collaborative decision making algorithm for selection of optimal wire saw in photovoltaic wafer manufacture. Journal of Intelligent manufacturing, **23**(3), 533–539 (2012)

33. Senan, S., Arik, S.: Global robust stability of bidirectional associative memory neural networks with multiple time delays. IEEE Transactions on Systems, Man, and Cybernetics, Part B (Cybernetics), **37**(5), 1375–1381 (2007)
34. Bhattacharya, A., Sarkar, B., Mukherjee, S.K.: Integrating AHP with QFD for robot selection under requirement perspective. International journal of production research, **43**(17), 3671–3685 (2005)

Role of Sodium, Potassium and Synaptic Conductance in STN-GPe Model of Basal Ganglia in Parkinson Disease

Jyotsna Singh, Phool Singh and Vikas Malik

Abstract This work focuses on the causes of alterations, in the discharge patterns generated STN-GPe network of basal ganglia in Parkinson disease. Model used in this manuscript is conductance based which has various ionic currents like sodium, potassium, calcium and synaptic current etc. These parameters along with various ionic currents like applied current and leakage current are used to generate the membrane potential for healthy primate and Parkinson disease condition. This membrane potential is used to calculate the correlation coefficient among healthy and Parkinson primate and it has been found that discharge patterns has low correlation coefficient between healthy primate and Parkinson condition. Focus of this study is to target the parameters which play a significant role for improving the correlation among healthy primate and Parkinson condition and also to study the effect of one parameter in comparison to other parameter on correlation coefficient. This study is important to look into the causes of deviation of Parkinson discharge pattern and to identify the parameters which might play a crucial role in treating the disease.

Keywords Parkinson disease · Basal ganglia · Subthalamic nucleus
Globus pallidus external · Synaptic conductance · Calcium current
Sodium current · Potassium current · Correlation coefficient

J. Singh (✉) · P. Singh
The NorthCap University, Gurgaon, India
e-mail: singhjyotsna1@gmail.com

P. Singh
e-mail: phool.singh24@gmail.com

V. Malik
JIIT, Noida, India
e-mail: vikasm76@gmail.com

K. Ray et al. (eds.), *Soft Computing Applications*, Studies in Computational Intelligence 761, https://doi.org/10.1007/978-981-10-8049-4_4

1 Introduction

It is evident in subthalamic nucleus (STN) that there is an increased incidence of oscillations and burst firing, as well as higher overall spike rates, as observed in experimental findings [1] and clinical parkinsonian states [2, 3]. These parkinsonian alterations in subthalamic nucleus outputs may arise through reciprocal synaptic interactions of subthalamic neuron with neurons in the external segment of the globus pallidus [4–6]. Subthalamic nucleus neurons also receive glutamatergic inputs from other brain areas, however, including cortical inputs via the so-called hyper-direct pathway, offering an alternative source for the modulation of subthalamic nucleus activity. Individual subthalamic neurons can also fire bursts in rat subthalamic slice [7–9]. Parkinson disease (PD) is a neurodegenerative pathology which is characterized by rigidity, tremor and movement abnormalities. The main cause to this disease is the progressive loss of nigrostriatal dompaminergic neuron in substantia nigra (SNc) and other nuclei of the basal ganglia [10, 11]. Many hypothesis have postulated the development in neuro-anatomical and physiological changes in basal ganglion circuits, which leads to motor dysfunction [12]. Comprehensible answer to the cause of this neuro-anatomical and physiological change is still not clear among the presence of various conflicting results and data [13].

There are various models which depicts the basal ganglia dysfunction on account of the development of Parkinson motor symptoms. The Rate Model [14–16] poised that the Parkinson motor symptoms were the result of change in mean discharge rate in basal ganglia circuit. Experimental studies [14–16] are although supported by human and non-human primates [17], but a recent study [3], failed to show in non-human primate the increase in rate of discharge in internal globus pallidus (GPi) in Parkinson disease. In addition to this, in Parkinson patients the pallidotomy is said to be reduced rather than increase [17, 18], while there is an increase in rate of discharge in GPi in subthalamic nucleus during deep brain stimulation (DBS) with improvement in motor signs [19]. Above observations put doubt on the validity of Rate Model and it led various other theories like bursting and oscillation in a particular frequency range [20].

In DBS, oscillation synchrony is observed in STN and GPi in the beta band [21], in a PD patient [22, 23]. Other studies have shown that pathological STN drive in Parkinson disease modifies the electrophysiological activities in GP, which in turn disrupts the normal function of basal ganglia [24, 25]. Thus the role of neuronal activity within basal ganglia in the development of Parkinson disease remains unclear. The aim of this study is to characterize the changes in neuronal activity in conductance-based subthalamic nucleus model with respect to calcium, potassium, sodium and synaptic conductance for healthy and PD condition. Our focus is on the connection of subthalamic nucleus in basal ganglia model in hyper-direct pathways as shown in Fig. 1 (Schematic diagram of STN-GPe architecture in basal ganglia in Parkinson disease) [26].

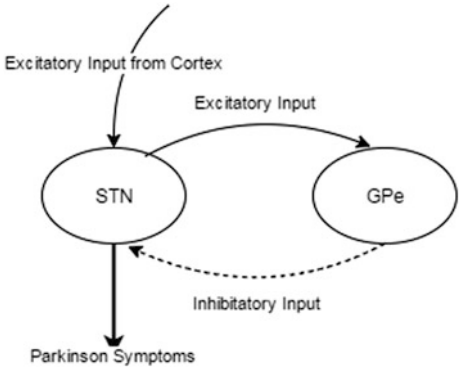

Fig. 1 Schematic diagram of STN-GPe architecture in basal ganglia in Parkinson disease

2 Architecture of Subthalamic Nucleus and Globus Pallidus External in Basal Ganglia in Parkinson Disease

Basal ganglia is the part of fore-brain which is mainly responsible for motor action and activity selection. It has three main nuclei: striatum, subthalamic nucleus and globus pallidus. Various ionic currents flow through them and their concentration determines the spiking pattern in healthy primate and in Parkinson condition. There are few nuclei in basal ganglia which need to be targeted in case of Parkinson disease, and subthalamic nucleus (STN) is one of them [1]. Subthalamic nucleus directly receives signal from cortex. It provides excitatory post-synaptic signals to globus pallidus and other nuclei. It receives inhibitory post-synaptic signal from globus pallidus. This information is processed via indirect pathway in globus pallidus and subthalamic nucleus network and in hyper-direct pathway in subthalamic nucleus and globus pallidus external (GPe) network. This is still a largely unknown area that what are the cellular mechanisms which are responsible for the change in the reading of cortical activity by the dopamine-depleted architecture of STN-GPe in basal ganglia. Schematic diagram of STN-GPe architecture in basal ganglia in Parkinson disease is shown in Fig. 1.

3 Formation of STN-GPe Model

A conductance-based model has been considered to generate the activity patterns in Parkinson disease in the subthalamic nucleus model of basal ganglia. This model (9) incorporates calcium current along with potassium and sodium current. It also considers the synaptic currents from GPe and applied current. This model calculates the membrane potential inside subthalamic neuron in healthy primate and Parkinson condition. There is little variation in the concentration of current in Parkinson disease as compared with the healthy primate. Due to this difference, discharge

patterns (spiking patterns) vary with respect to time in both the cases. Equation governing membrane potential is given (9):

$$C\frac{dV}{dt} = I_{applied} - I_{leakage} - I_K - I_{Na} - I_T - I_{Ca} - I_{Ahp} - I_{Syn} \tag{1}$$

where different membrane currents are given by

$$I_{Na} = g_{Na} \cdot m_{\infty}^3 \cdot h \cdot [V - V_{Na}] \tag{2}$$

$$I_k = g_k \cdot n^4 \cdot [V - V_k] \tag{3}$$

$$I_{leakage} = g_l \cdot [V - V_l] \tag{4}$$

$$I_T = g_T \cdot a_{\infty}^3 \cdot (V) \cdot r \cdot [V - V_{Ca}] \tag{5}$$

$$I_{Ca} = g_{Ca} \cdot s_{\infty}^3 \cdot (V) \cdot [V - V_{Ca}] \tag{6}$$

$$I_{Aph} = g_{Aph} \cdot \frac{[Ca]}{[Ca] + k_1} \cdot [V - V_k] \tag{7}$$

V_{Ca}, V_k, V_{Na} and $V_{leakage}$ are the calcium, potassium, sodium and leakage membrane potential. k_1 is the dissociation constant of Ca^{2+}-dependent AHP current. Applied current I_{app} current is used to adjust the membrane resting potential with the experimental data [6, 28, 29].

The equation for gating variable *m, n, h, s* and *a* is given as under

$$\frac{dx}{dt} = \frac{\phi_x[x_{\infty}(V) - x]}{\tau_x(V)} \tag{8}$$

ϕ is the constant in the equation for gating variables. Synaptic current I_{syn} in the subthalamic neuron is computed as a sum of synaptic currents from the GPe and other feedback neurons (9). Synaptic current I_{syn} is defined by considering the synaptic inputs from GP to STN and from feedback neurons to STN.

$$I_{syn} = g_{gs} \cdot s_g[V - V_{gs}] + g_{fs} \cdot s_f[V - V_{fs}] \tag{9}$$

Here, g_{gs} and g_{fs} are the synaptic conductance and s_g and s_f are synaptic variables. Dopamine depletion is the main cause of Parkinson disease [27, 29]. The depletion in dopamine can be shown with the help of synaptic inputs as synaptic input has an important effect on the information processing within the cell. In this study, two synaptic variables has been considered, s_g and s_f. Strength of synaptic current has been modulated with the help of these variables, and it is used to show higher and lower dopamine levels [30], so that the lower values of s_g and s_f

correspond to lower dopamine levels and stronger conductance and higher values represents the opposite.

The values of synaptic strengths in the normal state (high dopamine level) are taken as $g_{fs} = 0.215$ and $g_{gs} = 0.695$, and the maximal conductance of the AHP current in subthalamic neuron is $g_{\mathrm{AHP}} = 4.23$ nS/mm^2. The values of synaptic strengths corresponding to the PD (low dopamine level) state are $g_{gs} = 1.39$, $g_{fs} = 0.43$, with subthalamic cells AHP conductance set to $g_{\mathrm{AHP}} = 8.46$ nS/mm^2 (9).

Systems of differential Eq. (1) has been simulated in MATLAB 7.14 (i7 Intel processor, 4 GB RAM machine) using ODE45 for different time period. Explanation to which has been provided in next section.

4 Analysis of Discharge Patterns Within STN-GPe Model of Basal Ganglia in Parkinson Disease

Above discussed model has been used to generate the spiking patterns within subthalamic model of basal ganglia in healthy primate and Parkinson disease. These spiking patterns show bursting, which is the common sign of Parkinson disease as shown in Fig. 2. These spiking patterns are further characterized on the basis of their variability in relation to various ionic currents used in the conductance-based model. The characterization of activity pattern is performed on the basis of correlation coefficient between healthy discharge patterns referred as STN and diseased discharge patterns, referred as STNP. The objective of this analysis is to identify the ionic parameter which highly influences the discharge patterns in PD. The analysis gives some insight into the deviation of diseased discharge pattern from healthy patterns. It also presents the analysis of dependence between different parameters and their implications on the patterns generated.

Value of different parameters used in the model is specified in Table 1 (9).

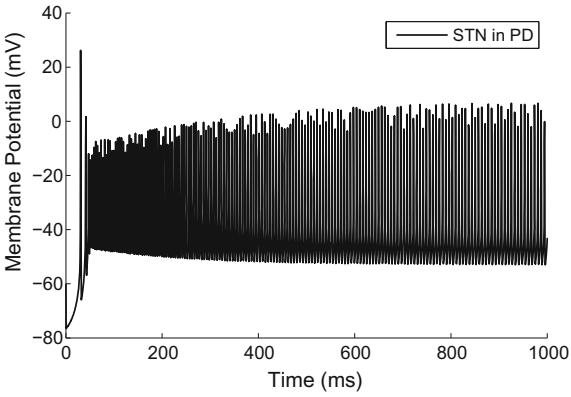

Fig. 2 Bursting in subthalamic nucleus model of basal ganglia in PD

Table 1 Parametric values for subthalamic neuron

Parameter	Value	Unit of measurement
C	1	pF (μm^2)
I_{app}	32	pA (μm^2)
g_l	2.25	nS (μm^2)
g_k	45	nS (μm^2)
g_{Na}	37.5	nS (μm^2)
g_T	0.5	nS (μm^2)
g_{Ca}	0.5	nS (μm^2)
V_l	−60	mV
V_k	−80	mV
V_{Na}	55	mV
V_{Ca}	140	mV

Discharge patterns generated inside subthalamic nucleus for both healthy (STN) and Parkinson condition (STNP) are simulated and analyzed for various time spans. Initially, the model is simulated for 500 ms. The value of applied current I_{app} is taken as 32 nA. The value of other parameters is specified in Table 1 and in the section, formation of Model. In both the cases, synaptic conductance influences the generation of spikes. Cellular changes occurring in striatum and post-synaptic and due to dopamine loss may lead to synaptic dysfunction. These changes will also impact the connecting nuclei, subthalamic nucleus and globus pallidus. So due to alterations in the glutamatergic receptors, the maladaptive forms of synaptic plasticity, contribute to the clinical features of PD [31]. Therefore, synaptic strength is an important parameter. Synaptic strength has been modulated to generate the spiking pattern of PD primate (9). In healthy primate, the strength is 1.5 and for PD the strength is 1. Correlation coefficient has been an important parameter to compare discharge patterns in healthy and Parkinson primate. Better the correlation coefficient, the more inclination of diseased patterns is toward healthy discharge patterns.

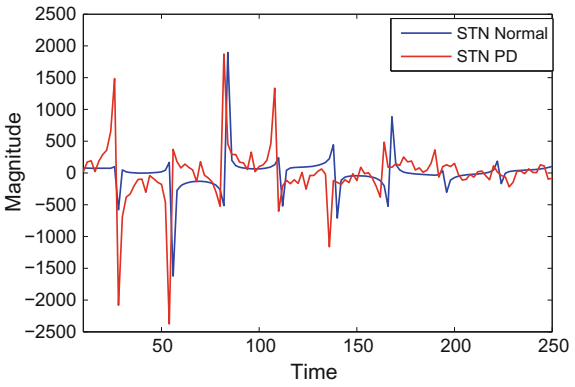

Fig. 3 Fourier transform of STN and STNP for V_{Ca} = 140 mV

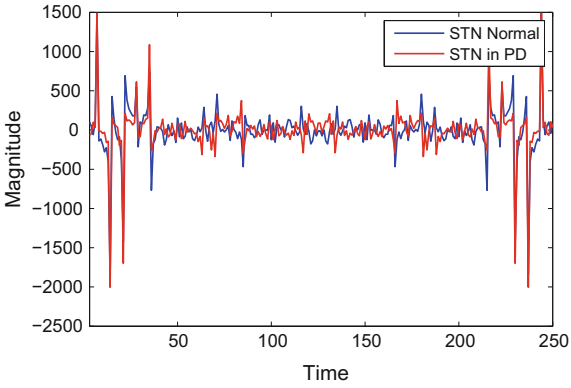

Fig. 4 Fourier transform of STN and STNP for V_{Ca} = 235 mV

It has been approx 0.9551 in our earlier work [26]. The difference between STN and STNP has depicted in frequency domain in Fig. 3. The improved correlation is shown in Fig. 4.

Our focus is to further improve it in the current work and to identify the parameters which are dependent on each other and effect the system in positive or negative ways.

4.1 Effect of Synaptic Conductance on STN-GPe Model in Parkinson Disease

Synaptic inputs play an important role in the conductance and information flow between different nuclei in the brain. Here, our focus area is subthalamic nucleus and its neighboring neuron, i.e., globus pallidus external. Subthalamic nucleus receives inhibitory input from globus pallidus and synaptic input from other neurons. Entire information inside subthalamic neuron depends upon the membrane potential computed by taking into consideration the input from all neighboring neurons. Here, our concentration parameters are g_{gs} and g_{fs}. These are the synaptic conductance while computing I_{syn}. g_{gs} and g_{fs} play an important role in improving the correlation coefficient between STN and STNP. It is shown in Table 2 and the graphs, which show the improved correlation coefficients in Figs. 6 and 7. Initial values of g_{gs} and g_{fs} were 1.39 and 0.43. We have modulated the values, g_{gs} = 2.5 and g_{fs} = 0.1 and seen the effect on the model. At a particular value of g_{gs} and g_{fs}, it gives the maximum correlation as shown in Fig. 7.

Figure 5 displays the discharge pattern generated in STN-GPe network for enhanced calcium membrane potential V_{Ca} = 235–275 mV and g_{gs} = 1.39 and g_{fs} = 0.43. Figure 6 displays the correlation coefficient for V_{Ca} = 235–275 mV and g_{gs} = 1.39 and g_{fs} = 0.43. Correlation coefficient if approx. equal to 0.9951 for

Table 2 Parametric values of g_{gs}, g_{fs} and correlation coefficient computed

g_{gs}	g_{fs}	Correlation coefficient
2	0.4	0.9622
2	0.3	0.9648
2	0.2	0.9674
2	0.1	0.9702
2.8	0.3	0.9711
2.8	0.2	0.9712
2.9	0.1	0.9712
2.7	0.22	0.9713
2.5	0.22	0.9713
2.6	0.22	0.9715
2.5	0.12	0.9716
2.5	0.17	0.9716
2.5	0.1	0.9718

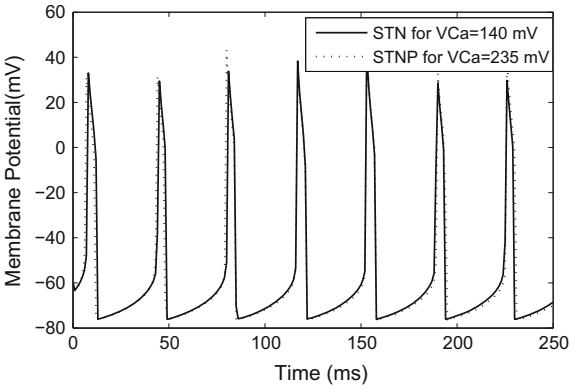

Fig. 5 Discharge patterns for subthalamic nucleus model in Parkinson disease for V_{Ca} = 235–275 mV, g_{gs} = 1.39 and g_{fs} = 0.43

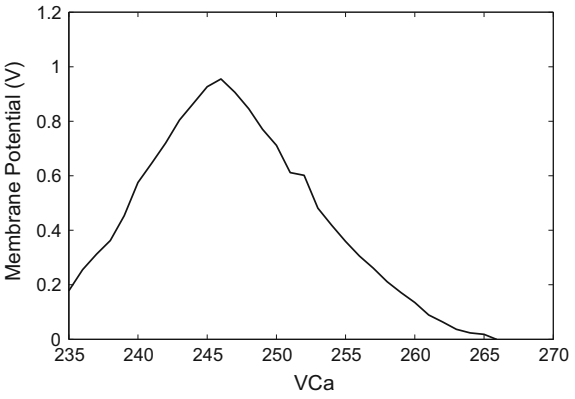

Fig. 6 Correlation coefficient computed for V_{Ca} = 235 −275 mV, g_{gs} = 1.39 and g_{fs} = 0.43

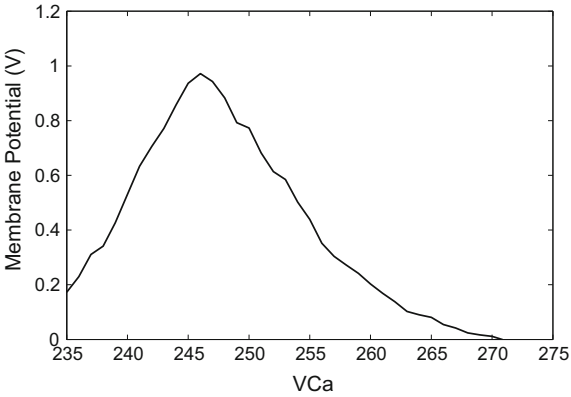

Fig. 7 Correlation coefficient computed for V_{Ca} = 235–275 mV and g_{gs} = 2.5 and g_{fs} = 0.1

V_{Ca} = 246 mV. Figure 7 displays the enhanced correlation when we change the value of synaptic conductance to g_{gs} = 2.5 and g_{fs} = 0.1 for V_{Ca} = 246 mV. Now it becomes approx equal to 0.9718.

4.2 *Effect of Potassium Membrane Potential on STN-GPe Model in Parkinson Disease*

Calcium, sodium and potassium are important parameters for human brain. This study represent the effect on Parkinson disease discharge patterns when the concentration of potassium membrane potential has been modulated keeping in view the other parameters values as V_{Ca} = 235–275 mV, V_{Na} = 55 mV and g_{gs} = 2.5 and g_{fs} = 0.1. Other parameters remain unchanged (9). Initial value of potassium was −80 mV. We have modulated it in the range from −60 to −100 and recorded the change in discharge pattern for each value. Results are displayed for different values of V_k in Figs. 8, 9, 10 and 11.

We generated spikes for different time spans for healthy and Parkinson disease condition for subthalamic nucleus model discussed above. Initially, the spikes generated for 250 ms then 500 ms till 10,000 ms. These spikes/discharge patterns are compared by calculating their correlation coefficient. Figure 7 represents the correlation coefficient for STN and STNP for 250 ms. Value of calcium membrane potential V_{Ca} is consider between 235 and 275 mV, sodium membrane potential is 55 mV and potassium membrane potential is also modulated from −60 to −100 mV. Figure 8 shows the correlation coefficient for V_{k} = 60 mV, Fig. 9 for V_{k} = 70 mV, Fig. 10 for V_{k} = 80 mV and Fig. 11 for V_{k} = 100 mV. There is variability in the correlation coefficient with change in the potassium membrane potential. But there is no significant improvement in the correlation coefficient with

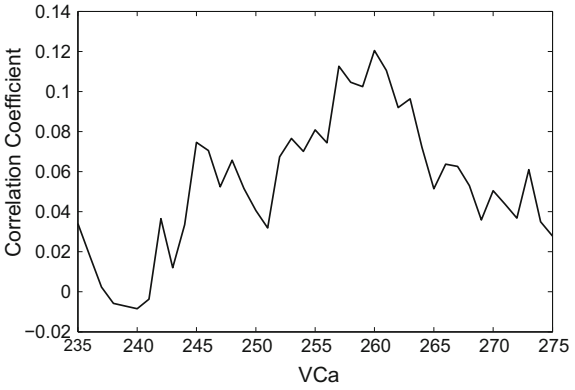

Fig. 8 Correlation coefficient graph between STN and STNP for V_{Ca} = 235 −275mV, V_{Na} = 55 and (a) V_k = −60 mV

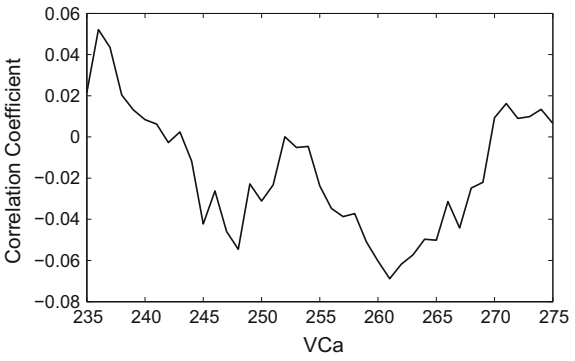

Fig. 9 Correlation coefficient graph between STN and STNP for V_{Ca} = 235 −275 mV, V_{Na} = 55 and V_k = −70 mV

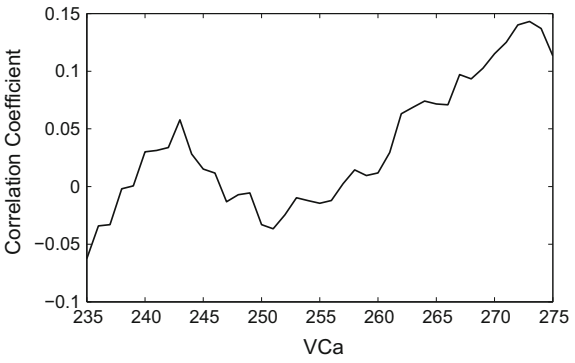

Fig. 10 Correlation coefficient graph between STN and STNP for V_{Ca} = 235 −275 mV, V_{Na} = 55 and V_k = −90 mV

increase or decrease in the potential due to potassium ionic current. Increasing calcium significantly improves the correlation among STN and STNP, but increase in potassium display the opposite effect on results.

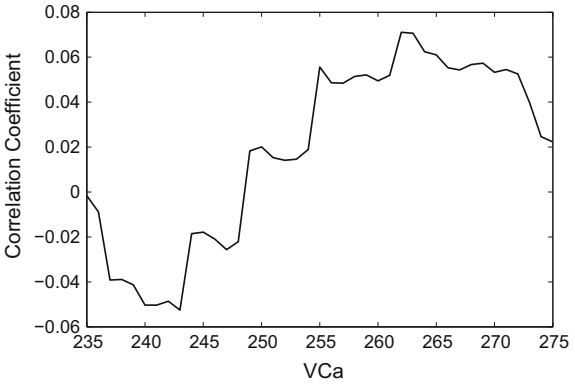

Fig. 11 Correlation coefficient graph between STN and STNP for V_{Ca} = 235 −275 mV, V_{Na} = 55 and V_k = −100 mV

4.3 *Effect of Sodium Membrane Potential on STN-GPe Model in Parkinson Disease*

After observing the not so significant effect of potassium ionic current on subthalamic nucleus model in Parkinson disease, we focused on the other important parameter, i.e., sodium ionic current in human brain. Our focus was to further improve the correlation among STN and STNP, which was improved by increasing the concentration of calcium ionic current from 140 mV to in a range between 235 and 275 mV. The results are promising for V_{Ca} = 246 mV. We can not arbitrary increase the calcium concentration alone. It might have adverse effect on the entire system. To check whether the combination of calcium and sodium might play a significant role for Parkinson patients, we modulated the value of sodium potential from its ideal value, i.e., 55 mV. Cross-correlation for V_{Na} = 10−100 mV has been computed and represented in Table 3. Correlation coefficient has been plotted for four different values of V_{Na}, 40, 45, 50 and 65 mV. Maximum value of correlation coefficient computed is for V_{Na} = 55 mV. This is the initial value of the system. Changing the value of sodium ionic current with calcium ionic current does not effect the system in a positive way. Calcium alone plays a significant role along with the synaptic conductance

Table 3 shows the correlation coefficient computed for different values of V_{Na} = 10–100 mV. Correlation improves from 0.293 to 0.2348 from V_{Na} = 10 to 20 mV. It decreases for V_{Na} = 30–40 mV. It again start improving for V_{Na} = 45 −55 mV. It is maximum for V_{Na} = 55 mV, and it starts decreasing again after V_{Na} = 65 mV till 100 mV. Values of correlation coefficient has been computed for V_{ca} = 235–275 mV for each modulated value of sodium ionic current. Correlation coefficient graph for selected values of V_{Na} has been shown in following figures.

Figures 12, 13, 14 and 15 show the correlation coefficient graph between STN and STNP for a range of sodium membrane potential between 55 and 95 mV and corresponding value of calcium membrane potential in the range between 235 and 275 mV. We can clearly see the variance in the graph generated. There is no

Table 3 Parametric values of V_{Na} and correlation coefficient computed

V_{Na}(mV)	Correlation coefficient
10	0.293
15	0.1877
20	0.2348
30	0.1374
40	0.0626
45	0.3069
50	0.9059
55	0.9551
65	0.8197
70	0.2225
75	0.0853
80	0.1268
85	0.1588
90	0.1595
95	0.1419
100	0.116

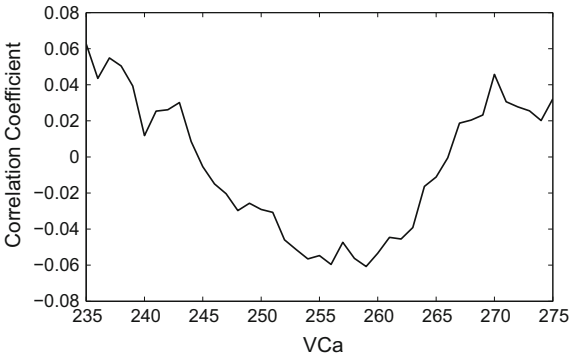

Fig. 12 V_{Ca} versus cross-correlation for V_{Ca} = 235−275 mV, V_k = −80 mV V_{Na} = 40 mV

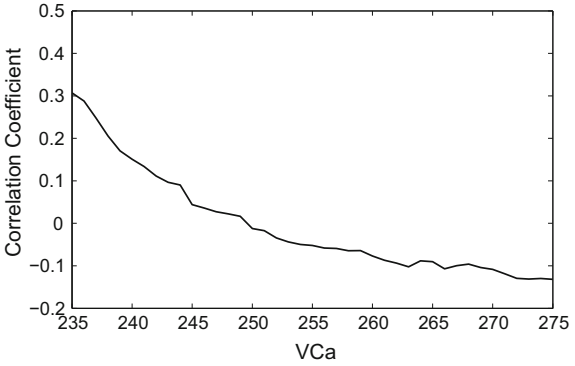

Fig. 13 V_{Ca} versus cross-correlation for V_{Ca} = 235−275 mV, V_k = −80 mV and V_{Na} = 45 mV

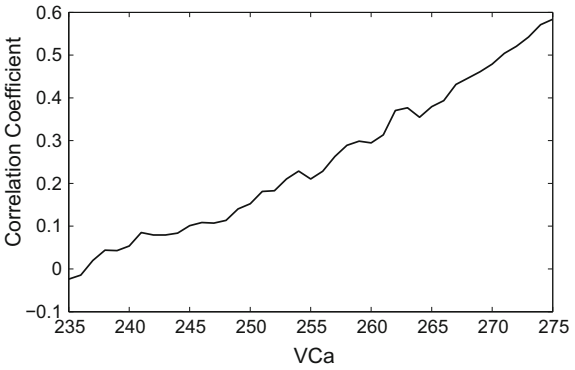

Fig. 14 V_{Ca} versus cross-correlation for V_{Ca} = 235−275 mV, V_k = −80 mV and V_{Na} = 65 mV

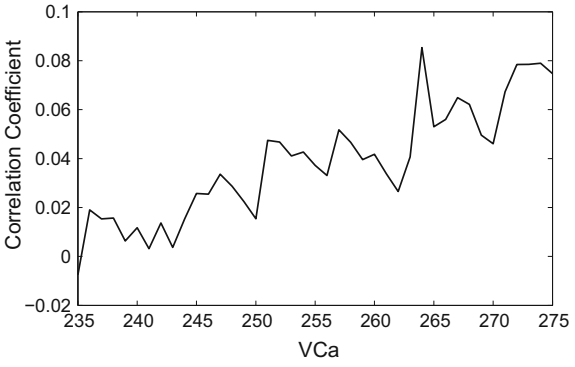

Fig. 15 V_{Ca} versus cross-correlation for V_{Ca} = 235−275 mV, V_k = −80 mV and V_{Na} = 75 mV

significant improvement in the correlation coefficient if we simultaneously increase the value of calcium and sodium membrane potential. Maximum correlation achieved in this case is between 0.6 and 0.7.

5 Conclusion

This work demonstrates that STN-GPe model account for the symptoms of Parkinson disease. It generates oscillation and bursting in Parkinson disease. Calcium, sodium and potassium ionic currents are important for information flow inside the human brain. Due to the depletion of dopamine, the connections got disrupted between different nuclei. But the cause to this dopamine depletion is not yet completely understood. Here, the connection taken into consideration is between subthalamic nucleus and globus pallidus external. We have considered above-mentioned ionic currents along with synaptic conductance to study their effect on the discharge patterns generated inside subthalamic nucleus. Our findings are that calcium current is very important for the identification of PD Primate. It is also a very important parameter to improve the correlation among spiking pattern of

Non-PD and PD primate. The abnormal calcium influx may be aggravated by subthalamic nucleus through a mechanism involving NMDA glutamate receptors. But for the entire process of excitations and inhibition due to glutamate and GABA receptors is limited by the timing of depolarization of the model. Along with calcium, synaptic conductance also plays important role in improving the correlation among healthy and PD primate. Other parameters under study for the time period from 0 to 250 ms do not put any significant effect on the model in Parkinson disease. This model can be exploited further to use any optimization technique for the improvement of correlation between PD and healthy primate.

Acknowledgements We thanks Department of Science and Technology, Government of India for financial support vide Reference No SR/CSRI/166/2014(G) under Cognitive Science Research Initiative(CSRI) to carry out this work. We also thank Prof. Karmeshu from JNU for providing valuable inputs in this work.

References

1. Constance Hammond, Hagai Bergman, and Peter Brown. Pathological synchronization in Parkinson's disease: networks, models and treatments. Trends in Neurosciences, 30(7): 357–364, July 2007.
2. P. Brown, A. Oliviero, P. Mazzone, A. Insola, P. Tonali, and V. Di Lazzaro. Dopamine dependency of oscillations between subthalamic nucleus and pallidum in Parkinson's disease. The Journal of Neuroscience: The Official Journal of the Society for Neuroscience, 21(3): 1033–1038, February 2001.
3. M. Magnin, A. Morel, and D. Jeanmonod. Single-unit analysis of the pallidum, thalamus and subthalamic nucleus in parkinsonian patients. Neuroscience, 96(3):549–564, 2000.
4. D. Plenz and S. T. Kital. A basal ganglia pacemaker formed by the subthalamic nucleus and external globus pallidus. Nature, 400(6745):677–682, August 1999.
5. Y. Smith, M. D. Bevan, E. Shink, and J. P. Bolam. Microcircuitry of the direct and indirect pathways of the basal ganglia. Neuroscience, 86(2):353–387, September 1998.
6. D. Terman, J. E. Rubin, A. C. Yew, and C. J. Wilson. Activity patterns in a model for the subthalamopallidal network of the basal ganglia. The Journal of Neuroscience: The Official Journal of the Society for Neuroscience, 22(7):2963–2976, April 2002.
7. P. J. Magill, J. P. Bolam, and M. D. Bevan. Dopamine regulates the impact of the cerebral cortex on the subthalamic nucleus-globus pallidus network. Neuroscience, 106(2):313–330, 2001.
8. Atsushi Nambu and Yoshihisa Tachibana. Mechanism of parkinsonian neuronal oscillations in the primate basal ganglia: some considerations based on our recent work. Frontiers in Systems Neuroscience, 8, May 2014.
9. Andrew Sharott, Peter J Magill, J Paul Bolam, and Peter Brown. Directional analysis of coherent oscillatory field potentials in the cerebral cortex and basal ganglia of the rat. The Journal of Physiology, 562(Pt 3):951–963, February 2005.
10. G. Kang and M. M. Lowery. Conductance-based model of the basal ganglia in Parkinson's Disease. In IET Irish Signals and Systems Conference (ISSC 2009), pages 1–6, June 2009.
11. Sabato Santaniello, Giovanni Fiengo, Luigi Glielmo, and Warren M. Grill. Basal Ganglia modeling in healthy and Parkinson's disease state. I. Isolated Neurons Activity. In American Control Conference, 2007. ACC'07, pages 4089–4094. IEEE, 2007.
12. Shri Dhar, Jyotsna Singh, and Phool Singh. Insights into various dysfunctions in Parkinsons disease: a survey. CSI Transactions on ICT, 4(2–4):117–122, December 2016.

13. Michal Rivlin-Etzion, Odeya Marmor, Gali Heimer, Aeyal Raz, Asaph Nini, and Hagai Bergman. Basal ganglia oscillations and pathophysiology of movement disorders. Current Opinion in Neurobiology, 16(6):629–637, December 2006.
14. R. L. Albin, A. B. Young, and J. B. Penney. The functional anatomy of basal ganglia disorders. Trends in Neurosciences, 12(10):366–375, October 1989.
15. M. R. DeLong. Primate models of movement disorders of basal ganglia origin. Trends in Neurosciences, 13(7):281–285, July 1990.
16. W. C. Miller and M. R. DeLong. Parkinsonian symptomatology. An anatomical and physiological analysis. Annals of the New York Academy of Sciences, 515:287–302, 1988.
17. M. S. Baron, J. L. Vitek, R. A. Bakay, J. Green, Y. Kaneoke, T. Hashimoto, R. S. Turner, J. L. Woodard, S. A. Cole, W. M. McDonald, and M. R. DeLong. Treatment of advanced Parkinson's disease by posterior GPi pallidotomy: 1-year results of a pilot study. Annals of Neurology, 40(3):355–366, September 1996.
18. Matthew D. Johnson, Hubert H. Lim, Theoden I. Netoff, Allison T. Connolly, Nessa Johnson, Abhrajeet Roy, Abbey Holt, Kelvin O. Lim, James R. Carey, Jerrold L. Vitek, and Bin He. Neuromodulation for brain disorders: challenges and opportunities. IEEE transactions on bio-medical engineering, 60(3):610– 624, March 2013.
19. Takao Hashimoto, Christopher M. Elder, Michael S. Okun, Susan K. Patrick, and Jerrold L. Vitek. Stimulation of the subthalamic nucleus changes the firing pattern of pallidal neurons. The Journal of Neuroscience: The Official Journal of the Society for Neuroscience, 23(5): 1916–1923, March 2003.
20. P. Brown. Abnormal oscillatory synchronisation in the motor system leads to impaired movement. Current Opinion in Neurobiology, 17(6):656–664, December 2007.
21. Andrea A. Khn, Alexander Tsui, Tipu Aziz, Nicola Ray, Christof Brcke, An-dreas Kupsch, Gerd-Helge Schneider, and Peter Brown. Pathological synchronisation in the subthalamic nucleus of patients with Parkinson's disease relates to both bradykinesia and rigidity. Experimental Neurology, 215(2):380–387, February 2009.
22. Annaelle Devergnas, Damien Pittard, Donald Bliwise, and Thomas Wich-mann. Relationship between oscillatory activity in the cortico-basal ganglia network and parkinsonism in MPTP-treated monkeys. Neurobiology of disease, 68:156–166, August 2014.
23. Viviana Gradinaru, Murtaza Mogri, Kimberly R. Thompson, Jaimie M. Hen-derson, and Karl Deisseroth. Optical deconstruction of parkinsonian neural circuitry. Science (New York, N.Y.), 324(5925):354–359, April 2009.
24. Plamen Gatev, Olivier Darbin, and Thomas Wichmann. Oscillations in the basal ganglia under normal conditions and in movement disorders. Movement Disorders, 21(10):1566–1577, October 2006.
25. Ron Levy, Anthony E. Lang, Jonathan O. Dostrovsky, Peter Pahapill, John Romas, Jean Saint-Cyr, William D. Hutchison, and Andres M. Lozano. Lido-caine and muscimol microinjections in subthalamic nucleus reverse parkinsonian symptoms. Brain, 124(10):2105–2118, October 2001.
26. Jyotsna Singh, Phool Singh, and Vikas Malik. Sensitivity analysis of discharge patterns of subthalamic nucleus in the model of basal ganglia in Parkinson disease. Journal of Integrative Neuroscience, Preprint (Preprint):1–12, January 2017.
27. Andrey Dovzhenok and Leonid L. Rubchinsky. On the Origin of Tremor in Parkinsons Disease. PLOS ONE, 7(7):e41598, July 2012.
28. Shruti Gupta and Jyotsna Singh. Effect of applied current on sub-thalamic neuron. CSI Transactions on ICT, 4, 2016.
29. Jonathan E. Rubin and David Terman. High frequency stimulation of the sub-thalamic nucleus eliminates pathological thalamic rhythmicity in a computational model. Journal of Computational Neuroscience, 16(3):211–235, June 2004.
30. D. J. Gelb, E. Oliver, and S. Gilman. Diagnostic criteria for Parkinson disease. Archives of Neurology, 56(1):33–39, January 1999.
31. Synaptic Plasticity—Dynamics, Development and Disease j Michael R. Kreutz j Springer.

A New Hybrid Algorithm Using Chaos-Enhanced Differential Evolution for Loss Minimization with Improvement of Voltage Profile of Distribution Systems

S. Mandal, K. K. Mandal and B. Tudu

Abstract Optimal operation of distribution systems plays an important role in the successful economic and secure operation of modern-day power systems under deregulated environment. Reduction in distribution loss and enhancement of bus voltage profile is often considered as the key parameters for economic and secure operation for distribution systems. Various methods including both mathematical and methods based on soft computing techniques have been utilized to address these problems. As reported in the literature, success of any heuristic technique greatly depends on the determination of optimal values of control parameters. Unfortunately, no analytical and straightforward method is available for the purpose. Usually, these parameters are selected experimentally considering different combination each time. A new hybrid algorithm using differential evolution and chaos theory is presented in the present work. Tent map chaotic sequence is utilized for self-adaptation of control parameters. The method is referred as tent map differential evolution (TMDE) in this work. The proposed hybrid algorithm is tested on 33-bus radial distribution system for validation and demonstration purpose. Systematic simulation results are presented and compared with same obtained by other modern techniques. It has been observed that it is capable of producing higher quality solution.

Keywords Differential Evolution (DE) · Chaos Theory · Voltage profile
Distribution systems · Voltage profile

S. Mandal
Department of Electrical Engineering, Jadavpur University,
Kolkata 700032, India
e-mail: shm.here@gmail.com

K. K. Mandal (✉) · B. Tudu
Department of Power Engineering, Jadavpur University,
Kolkata 700098, India
e-mail: kkm567@yahoo.co.in

B. Tudu
e-mail: bhimsen_ju@yahoo.co.in

K. Ray et al. (eds.), *Soft Computing Applications*, Studies in Computational Intelligence 761, https://doi.org/10.1007/978-981-10-8049-4_5

1 Introduction

Proper and effective planning of reactive power compensative devices can significantly improve the performance of distribution systems. Distribution systems are generally operated at low-voltage level, and a substantial amount of power loss is associated with the distribution systems. As a result, sometimes bus voltage may violate the specified limits. Thus, system reliability is largely affected. Placement of capacitors is often considered as one of the simple and effective means for compensation of reactive power in distribution systems. For achieving maximum economic as well as technical benefits, capacitors of optimal sizes should be placed at optimal locations. This is specially required for a deregulated electricity industry where reactive power is traded as ancillary services and supplied by ancillary service providers. Thus, in a competitive deregulated electricity market mainly two objectives are taken into account during the problem formulation. Minimization of system operational cost by minimizing the system loss thereby maximization of profit is one of the objectives. While minimizing the loss by capacitor placement, cost of the compensating devices should be considered because that will finally affect the profit for the project. Another one is the enhancement of bus voltage profile which is associated with the system reliability and service quality.

In recent years, many optimization techniques have been proposed to solve this complex nonlinear constrained optimization problem. Nonlinear programming [1, 2], genetic algorithm [3, 4], tabu search [5], artificial bee colony [6, 7], bacteria foraging [8, 9], gravitational search algorithm [10], harmony search [11, 12] and particle swarm optimization [13] have been successfully applied to address the problem. Abdelaziz et al. [14] proposed a new algorithm using flower pollination optimization technique to find the optimal sizes and location of capacitors in radial distribution systems. The proposed algorithm was tested on several systems including 15-bus system, 69-bus system and 118-bus system, and encouraging results were presented. Das et al. [15] presented a new method using loss sensitivity factor and cuckoo search algorithm. Teaching learning-based optimization technique was proposed for capacitor placement problems in distribution systems by Sultana et al. [16]. Recently, Gnanasekaran et al. [17] developed a new algorithm using shark smell optimization technique for optimal placement of capacitors in radial distribution systems, and encouraging simulation results were presented. A new and comprehensive objective function formulation for capacitor placement in distribution networks was proposed by Karimi et al. [18], and a particle swarm optimization algorithm was used for demonstration purpose.

Differential evolution (DE) is one of the efficient members of evolutionary algorithms and was proposed by Storn and Price in the year 1995 [19]. DE is a fast and simple optimization technique which has been successfully applied for solving a wide variety of complex engineering problems. One of the major drawbacks for almost all modern heuristic techniques is the setting of control parameters on which success of the particular method is largely dependent. Further, these parameters are in general problem dependent. In other words, these parameters are to be selected

separately each time for different problems. It becomes a tedious job as there is no well-defined rule for parameter selection. Thus, a wrong parameter may affect the performance and sometimes may converge to suboptimal solution and even stagnation may occur. A new parameter adaptive strategy for DE is proposed in this work using chaotic sequence. For the present work, tent map chaotic sequence is utilized and it is termed as tent map differential evolution (TMDE). The proposed algorithm is applied for solving loss minimization and profit maximization problems of distribution networks. The simulation results show that the performance of DE is enhanced and is capable of avoiding premature convergence.

2 Problem Formulation

The primary aim of the present work is to reduce system loss with enhancement of bus voltage profile. This section describes the problem, and finally objective function is formulated.

2.1 Power Loss Calculation

Power loss for a radial distribution system can be determined by adding up the losses for all the lines of the system. Single-line diagram of a feeder with n number of bus is shown in Fig. 1.

From the above, following set of equations relating active power, reactive power and voltage for ith bus can written for loss calculation.

$$P_{i+1} = P_i - P_{Li+1} - R_{i,i+1}\left[\left(P_i^2 + Q_i^2\right)\Big/|V_i|^2\right] \tag{1}$$

$$Q_{i+1} = Q_i - Q_{Li+1} - X_{i,i+1} \cdot \left[\left(P_i^2 + Q_i^2\right)/|V_i|^2\right] \tag{2}$$

$$|V_{i+1}|^2 = |V_i|^2 - 2\left(R_{i,i+1} \cdot P_i + X_{i,i+1} \cdot Q_i\right) + \left(R_{i,i+1}^2 + X_{i,i+1}^2\right)\frac{\left(P_i^2 + Q_i^2\right)}{|V_i|^2} \tag{3}$$

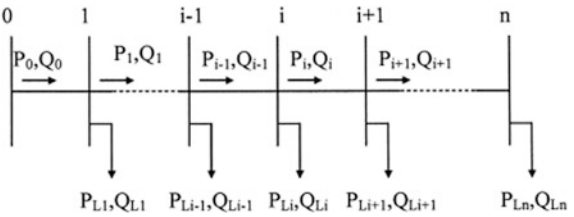

Fig. 1 Single-line diagram of a distribution feeder

where

P_i is the real power flowing out of bus i
Q_i is reactive power flowing out of bus i
P_{Li} represents active load at ith bus
Q_{Li} represents reactive load at ith bus
$R_{i,i+1}$ indicates the resistance and reactance of the line section between buses i and $i + 1$
$X_{i,i+1}$ indicates the resistance and reactance of the line section between buses i and $i + 1$
V_i is the voltage of ith bus.

The real power loss of the line section between buses i and $i + 1$ can be obtained as

$$P_{\text{Loss}}(i, i+1) = R_{i,i+1} \cdot \frac{P_i^2 + Q_i^2}{|V_i|^2} \tag{4}$$

Thus, total real and reactive power loss for the system can be determined as

$$P_{T,\text{Loss}} = \sum_{i=0}^{n} P_{\text{Loss}}(i, i+1) \tag{5}$$

$$Q_{T,\text{Loss}} = \sum_{i=0}^{n} Q_{\text{Loss}}(i, i+1) \tag{6}$$

where

$P_{T,\text{Loss}}$ indicates total real power loss of the system under consideration
$Q_{T,\text{Loss}}$ indicates total reactive power loss of the system under consideration.

2.2 Cumulative Voltage Deviation

One of the objectives for the present work is the improvement of bus voltage profile for enhancing system performance. Thus, voltage deviation is to be kept as smaller as possible. Cumulative voltage deviation (CVD) is considered as a measure for bus voltage enhancement [20] and is expressed as

$$\text{CVD} = \begin{cases} 0 & \text{for} \quad 0.95 \le V_i \le 1.05 \\ \sum_{i=1}^{n} |1 - V_i| & \text{otherwise} \end{cases} \tag{7}$$

2.3 Objective Function Formulation

The primary objective for the present problem is to minimize system loss and enhancement of bus voltage profile subject to several equality and inequality constraints. Thus, it is expressed as

$$\text{Minimize } f = \text{Minimize}\left(w_1 \times \frac{P_{L,\text{ Compensated}}}{P_{L,\text{ Uncompensated}}} + w_2 \times \frac{\text{CVD}_{\text{Compensated}}}{\text{CVD}_{\text{Uncompated}}}\right) \quad (8)$$

where

$P_{L,\text{Compensated}}$ indicates the real power loss of the compensated system
$P_{L,\text{Uncompensated}}$ represents the real power loss of the uncompensated system
w_1 and w_2 are the two weight factors. For loss minimization $w_1 = 1$ and $w_2 = 0$, whereas $w_1 = 0$ and $w_2 = 1$ result in minimization of cumulative voltage deviation. When both loss and voltage deviation are considered, both are set to 1, i.e., $w_1 = 1$ and $w_2 = 1$.

2.4 Constraints

The above function is to be minimized subject to the several equality and inequality constraints.

(i) Power balance constraints:

At every instant, both active and real power constraints must be satisfied and can be expressed as

$$P_{\text{Slack}} = \sum_{i=1}^{n} P_{Di} + \sum_{j=1}^{n_L} P_{Lj} \quad (9)$$

$$Q_{\text{Slack}} + \sum_{i=1}^{n_B} Q_{Ci} = \sum_{i-1}^{n} Q_{Di} + \sum_{j=1}^{n_L} Q_{Li} \quad (10)$$

where

P_{Slack} and Q_{Slack} are the active and reactive power of the slack bus, respectively.
P_{Di} and Q_{Di} are the active reactive power demand of ith bus, respectively.
P_{Lj} and Q_{Lj} represent active and reactive power loss at jth line, respectively.
n, n_B and n_L indicate the total bus number, number of buses where compensation devices are connected and number of lines, respectively.

(ii) Bus voltage constraints:

For maintaining service quality, bus voltages must be maintained within specified limits and it is expressed as

$$\begin{aligned} &V_i^{\min} \le V_i \le V_i^{\max} \\ &i = 1, 2, \ldots, n \end{aligned} \tag{11}$$

where $V_i^{\min}$ and $V_i^{\max}$ are the minimum and maximum bus voltage limits.

(iii) Reactive power compensation limits:

For a practical system, reactive power compensation at the buses must be limited by lower and upper limits and it is represented as

$$\begin{aligned} &Q_{Ci}^{\min} \le Q_{Ci} \le Q_{Ci}^{\max} \\ &i = 1,\ 2, \ldots, n_B \end{aligned} \tag{12}$$

(iv) Maximum reactive power compensation:

For practical point of view, maximum reactive power compensation must be less than the reactive power demand and is expressed as

$$\sum_{i=1}^{n_B} Q_{Ci} \le \sum_{j=1}^{n_L} Q_{Dj} \tag{13}$$

3 Power Loss Index

Power loss index (PLI) is used to identify the potential candidates for placing reactive power compensating devices. Real power loss is calculated for all buses except the slack bus for the uncompensated system. Reactive power injected at each bus is equal to the reactive load except slack bus. Thus, power loss index (PLI) for the kth bus can be expressed as

$$\mathrm{PLI}(k) = \frac{LR(k) - LR^{\min}}{LR^{\max} - LR^{\min}} \tag{14}$$

where

$LR(k)$ is the loss reduction (LR) for the kth bus
$LR^{\min}$ and $LR^{\max}$ are the minimum and maximum loss reduction, respectively.

The buses with higher loss are characterized with lower bus voltage. Therefore, these buses are the potential candidates for reactive power compensation. The buses

are arranged in decreasing order depending on power loss index, and the list of candidates is prepared.

4 Differential Evolution (DE)

Differential evolution (DE) is one of the efficient and powerful global optimization techniques and was proposed by Storn and Price in 1995 [19, 21]. Since its inception in 1995, various optimization problems in engineering and science have successfully solved by DE. According to several reports in the literature, DE has shown the capability in producing competitive performance in terms of convergence characteristics, speed and global optimum values. Several variants of DE have been reported to enhance its performance. It is easy to implement and has only four steps: initialization, mutation, crossover and selection.

4.1 Initialization

Let there be d-dimensional decision variables in the problem search space. It begins randomly the initialization process of N_P individuals with d-dimensional decision variables. Thus, if $x_{i,j}^{(o)}$ represents the jth component of the ith decision variables, then it can be expressed as

$$x_{i,j}^{(0)} = x_{\min,j} + \text{rand}_{i,j}()\left(x_{\max,j} - x_{\min,j}\right) \quad i = 1, 2, \ldots N_P \quad j = 1, 2, \ldots d \tag{15}$$

where $\text{rand}_{i,j}()$ is a random number within 0 and 1 including both the upper and lower values. If $P^{(G)}$ denotes the population that evolves after Tth iteration, then it is expressed as

$$P^{(T)} = \left[X_i^{(T)}, \ldots, X_{N_P}^{(T)}\right] \tag{16}$$

$$X_i^{(T)} = \left[X_{1,i}^{(T)}, \ldots X_{d,i}^{(T)}\right]^T \quad i = 1, \ldots N_P \tag{17}$$

4.2 Mutation Operation

Mutation operation is the method which is utilized to create mutant or donor vectors (V_i) with the help of vector difference. Several variants of DE are available in the literature depending on vector difference of parent or target vectors (X_i). For this work, *DE/rand/1* is used. The mutation operation can be described as follows:

$$V_i^{(T)} = X_k^{(T)} + F_M \left(X_l^{(T)} - X_m^{(T)} \right) \tag{18}$$

where X_k , X_l , X_m are chosen randomly from the set of parent vectors (X_i) and $k \neq l \neq m \neq i$. The mutation factor F_M is one of the important control parameters of DE and is used for scaling the vector difference. It is normally selected by the user within the range [0, 2].

4.3 Crossover Operation

Crossover operation is used for mixing the components of mutation or donor vectors with parent or target vectors and thus trial vectors (U_i) are created. DE uses two crossover methods called binomial and exponential. For the present work, binomial method is used which can be expressed as

$$U_{j,i}^{(T)} = \begin{cases} V_{j,i}^{(T)} & \text{, if } \text{rand}_{i,j}() \leq C_R \text{ or } j = N \\ X_{j,i}^{(T)} & \text{, otherwise} \end{cases} \tag{19}$$

where $\text{rand}_{i,j}()$ is a uniform random number within [0, 1] and N is any randomly chosen natural number from $[1, 2, \ldots d]$. This ensures that at least one component of trial vector U_i is selected from mutant vector V_i. The crossover factor is another important predefined control parameter of DE. Diversity of the population is controlled by C_R.

4.4 Selection Operation

Selection operation is the last step of DE which determines whether parent vector X_i or trail vector U_i is to be selected for the next iteration. If f is the objective function, then it is described as

$$X_i^{(T+1)} = \begin{cases} U_i^{(T)} & \text{, if } f\left(U_i^{(T)}\right) \leq f\left(X_i^{(T)}\right) \\ X_i^{(T)} & \text{, otherwise} \end{cases} \tag{20}$$

5 Tent Map Differential Evolution (TMDE)

Various search strategies such as simplex crossover search strategy, orthogonal search strategy and chaotic search strategy have been used to enhance the performance of many meta-heuristic techniques like DE and particle swam optimization (PSO) [22]. For the present work, chaotic search strategy is used. Chaos is a special branch of mathematics which is associated with chaos phenomenon in nature. Actually, chaos is a typical classic nonlinear dynamical system which is characterized with ergodicity and randomicity and very sensitive to initial conditions. Because of its ergodicity and randomicity, a chaotic system is capable of generating long time sequence randomly which can traverse to every state if a long time duration is allowed. This feature of chaotic sequence is utilized for self-adaptation of two important controlling parameters mutation factor and crossover ratio of DE to enhance its performance.

In this paper, tent map chaotic sequence [23] is used which can be represented as

$$y(k) = \begin{cases} \frac{y(k-1)}{0.7} & y(k-1) < 0.7 \\ \frac{10}{3}(1 - y(k-1)) & y(k-1) \geq 0.7 \end{cases} \tag{21}$$

where k is the sample.

In this work, mutation factor and crossover ratio are controlled dynamically using (21) as follows:

$$F_M(T) = \begin{cases} \frac{F_M(T-1)}{0.7} & F_M(T-1) < 0.7 \\ \frac{10}{3}(1 - F_M(T-1)) & F_M(T-1) \geq 0.7 \end{cases} \tag{22}$$

$$C_R(T) = \begin{cases} \frac{C_R(T-1)}{0.7} & C_R(T-1) < 0.7 \\ \frac{10}{3}(1 - C_R(T-1)) & C_R(T-1) \geq 0.7 \end{cases} \tag{23}$$

where T is the current iteration number.

6 Simulation Results

The effectiveness of the proposed chaotic sequence and DE-based algorithm is tested on 33-bus radial distribution system [20] as shown in Fig. 2. The system data including load and line data are shown in Table 1. Total load of the system is (3715 + j2300) kVA as seen from Table 1. The proposed algorithm is tested using MATLAB on 3.0 GHz, 8.0 GB RAM PC.

Using power loss index (PLI) as described in Sect. 3, the buses are arranged in descending order as [30, 32, 31, 14, 8, 29, 7, 33, 18, 13, 12, 11, 17, 16, 10, 28, 27, 9, 26, 6, 15…]. For simplicity and direct comparison, only seven higher potential buses are considered to be the candidates for reactive power injection.

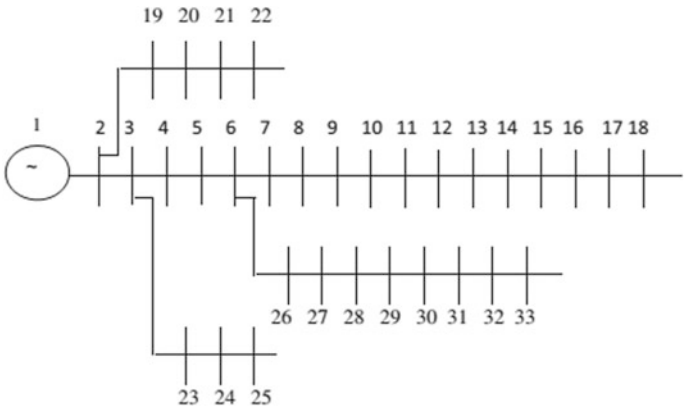

Fig. 2 One-line diagram of 33 bus radial distribution system

The population number is selected as 30. Initial values of mutation factor and crossover ratio are set at 0.85 and 0. 65, respectively. Maximum iteration is set at 100. Available sizes of capacitor are considered to between 0 and 1500 kVAr in step of 50 kVAr. For the present work, both w_1 and w_2 are taken as 1 for a direct comparison. In other words, both the loss and cumulative voltage are given equal importance. Optimal size and location of capacitors (location, size in kVAr) obtained by the proposed algorithm based on TMDE are shown in Table 2. Table 2 also compares the same with that obtained by other methods like cuckoo search algorithm (CSA), genetic algorithm and plant growth simulation algorithm [20].

Minimum and bus voltage, active and reactive power losses, cumulative voltage deviation (CVD) for both the uncompensated and compensated system are shown in Table 3. Table 3 also compares the results with other modern heuristic method. It is observed from Table 3 that active power loss is 137.250 kW with a reduction of 34.64% in comparison with uncompensated system. The computation time is found to be 30.34 s.

Table 4 shows the bus of the compensated system, whereas variation of bus voltage is shown in Fig. 3. Figure 3 also compares the bus voltage of the uncompensated system with that of compensated system. Bus voltage is seen to be improved substantially with respect to uncompensated system.

The convergence characteristic for minimum loss is shown in Fig. 4. Figure 5 shows the convergence characteristic for the objective function. Figure 4 also compares the minimum loss obtained by the proposed TMDE and classical DE where the loss is 146.28 kW. It is clearly observed that the proposed algorithm is capable of enhancing the performance of classical DE.

Table 1 Bus and line data for 33-bus system

Branch no.	Sending node	Receiving node	Active load (kW)	Reactive load (kVar)	Resistance (Ω)	Reactance (Ω)
1	1	2	100	60	0.0922	0.0470
2	2	3	90	40	0.4930	0.2511
3	3	4	120	80	0.3660	0.1864
4	4	5	60	30	0.3811	0.1941
5	5	6	60	20	0.8190	0.7070
6	6	7	200	100	0.1872	0.6188
7	7	8	200	100	1.7114	1.2351
8	8	9	60	20	1.0300	0.7400
9	9	10	60	20	1.0440	0.7400
10	10	11	45	30	0.1966	0.0650
11	11	12	60	35	0.3744	0.1238
12	12	13	60	35	1.4680	1.1550
13	13	14	120	80	0.5416	0.7129
14	14	15	60	10	0.5910	0.5260
15	15	16	60	20	0.7463	0.5450
16	16	17	60	20	1.2890	1.7210
17	17	18	90	40	0.7320	0.5740
18	2	19	90	40	0.1640	0.1565
19	19	20	90	40	1.5042	1.3554
20	20	21	90	40	0.4095	0.4784
21	21	22	90	40	0.7089	0.9373
22	3	23	90	50	0.4512	0.3083
23	23	24	420	200	0.8980	0.7091
24	24	25	420	200	0.8960	0.7011
25	6	26	60	25	0.2030	0.1034
26	26	27	60	25	0.2842	0.1447
27	27	28	60	20	1.0590	0.9337
28	28	29	120	70	0.8042	0.7006
29	29	30	200	600	0.5075	0.2585
30	30	31	150	70	0.9744	0.9630
31	31	32	210	100	0.3105	0.3619
32	32	33	60	40	0.3410	0.5302

Table 2 Optimal location and size of compensation device

Proposed method (TMDE)	CSA [20]	GA [20]	PSGA [20]	DE-PS [20]
(7,300)	(7,450)	(8,300)	PSGA [20]	(14,400)
(8,200)	(14,300)	(15,300)	(61,200)	(30,850)
(14,250)	(30,900)	(20,300)	(28,760)	(31,100)
(29,250)		(21,300)	(29,200)	
(30,450)		(24,300)		
(31,100)		(26,300)		
(32,200)		(27,600)		
		(28,300)		

Table 3 Optimal results obtained by the proposed method

Parameters of comparison	Uncompensated system	Proposed method (TMDE)	CSA [20]	GA [20]	PSGA [20]
$V_{\min}$ (p.u.)	0.9039	0.9350	0.9334	0.9383	0.9250
$V_{\max}$ (p.u.)	0.9970	0.9998	0.9976	0.9996	0.9977
CVD	1.6188	0.5378	0.7601	0.8028	0.8410
P_{loss} (kW)	210.019	137.250	139.643	150.225	151.838
Reduction in $P_{\text{loss}}(\%)$	–	34.64	33.77	28.75	27.98
Q_{loss} (kvar)	142.46	94.667	95.278	97.956	104.840
Reduction in $Q_{loss}(\%)$	–	33.54	33.34	31.55	26.74
Total compensation (kVAr)	–	1750	1650	2700	2160
CPU time (sec)		30.34	45.50	NA	5.13

Table 4 Bus voltage of the compensated system

Bus no.	Voltage (*p*.u.)	Bus no.	Voltage (*p.u.*)	Bus no.	Voltage (*p.u.*)
1	1.0000	12	0.9447	23	0.9829
2	0.9865	13	0.9406	24	0.9763
3	0.9812	14	0.9396	25	0.9729
4	0.9762	15	0.9382	26	0.9650
5	0.9662	16	0.9369	27	0.9635
6	0.9658	17	0.9350	28	0.9585
7	0.9561	18	0.9343	29	0.9552
8	0.9512	19	0.9970	30	0.9530
9	0.9467	20	0.9934	31	0.9509
10	0.9460	21	0.9927	32	0.9505
11	0.9445	22	0.9921	33	0.9503

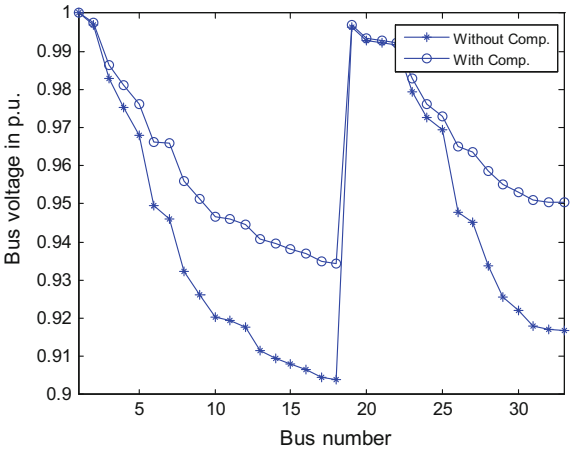

Fig. 3 Comparison of bus voltages of 33 bus radial distribution system

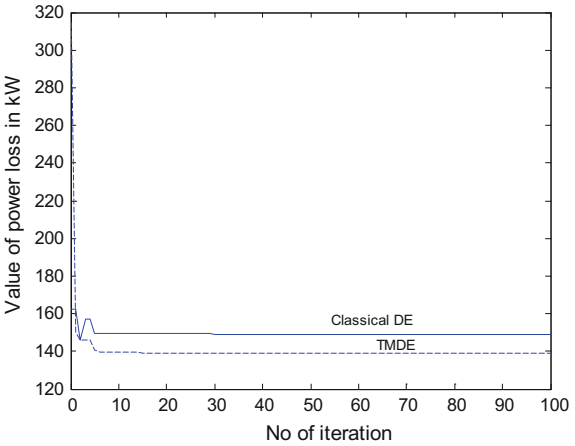

Fig. 4 Convergence characteristic for minimum loss

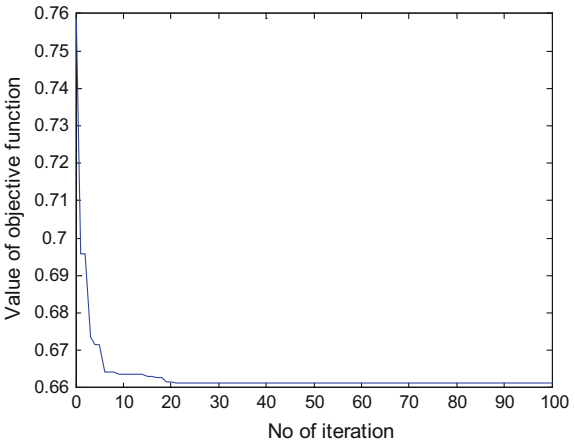

Fig. 5 Convergence characteristic for objective function

7 Conclusion

A new improved algorithm based on chaos-enhanced differential evolution is proposed in this paper to minimize system loss with enhancement of bus voltage profile of distribution systems. The problem is formulated considering both loss and cumulative voltage deviation. Power loss index is used to find the potential candidates for reactive power compensation. It applied on 33-bus distribution system to test its effectiveness. It is observed that proposed algorithm based on TMDE is really capable in producing good-quality solutions. Simulation results and a comparative study with other heuristic techniques are presented. It is also found that proposed TMDE-based algorithm is capable in avoiding premature convergence in comparison with classical DE.

Acknowledgements The authors are thankful to Jadavpur University, Kolkata. This work is supported by the program UPE II, UGC, Govt. of India.

References

1. M. Baran, F. Wu, "Optimal sizing of capacitors placed on a radial distribution system. IEEE Trans Power Del 1989, 4(1), pp. 35–43.
2. S. Nojavan, M. Jalali, K. Zare, "Optimal allocation of capacitors in radial/ mesh distribution systems using mixed integer nonlinear programming approach. Int J Electric Power Syst Res 2014 (107) pp. 119–124.
3. Sundhararajan S, Pahwa A. Optimal selection of capacitors for radial distribution systems using a genetic algorithm. IEEE Trans Power Syst 1994; 9(3), pp. 1499–507.
4. Y. Wei, L. Fang, C.Y. Chung, K. Wong K.P. "A hybrid genetic algorithm-interior point method for optimal reactive power flow. IEEE Trans Power Syst 2006; 21(3), pp. 1163–1169.
5. R.A. Gallego, A.J. Monticelli, R. Romero, "Optimal capacitor placement in radial distribution networks using tabu search, IEEE Trans. Power Syst. 16(4) (2001), pp. 630–637.
6. A.A. El-Fergany, A.Y. Abdelaziz, "Multi-objective capacitor allocations in distribution networks using artificial bee colony algorithm. J Electr Eng Technol 2014; 9(2), pp. 441–51.
7. M.M. Legha, M. Tavakoli, F. Ostovar, M.A. Hashemabadi, Capacitor placement in radial distribution system for improve network efficiency using artificial bee colony, Int. J. Eng. Res. Appl. 3(6) (2013), pp. 228–233.
8. S.M. Tabatabaei, B. Vahidi, Bacterial foraging solution based fuzzy logic decision for optimal capacitor allocation in radial distribution system, Int. J. Electric Power. Syst. Res. 81, 2011, pp. 1045–1050.
9. Mohamed Imran A, M. Kowsalya, "Optimal size and siting of multiple distributed generators in distribution system using bacteria foraging optimization," Swarm Evolutionary Computation 2014, pp. 58–65.
10. Y.M. Shuaib, M.S. Kalavathi, C.C.A. Rajan, "Optimal capacitor placement in radial distribution system using Gravitational Search Algorithm," Int J Electr Power Energy Syst 2015, 64(1), pp. 384–397.
11. K. Muthukumar, S. Jayalalitha, M. Ramasamy, C. Haricharan, Optimal shunt capacitor allocation and sizing using harmony search algorithm for power loss minimization in radial distribution networks, Int. J. Dev. Res. 2014, 4(3), pp. 537–545.

12. E.S. Ali, S.M. Abd Elazim, A.Y. Abdelaziz, "Improved Harmony Algorithm for optimal locations and sizing of capacitors in radial distribution systems," International Journal of Electrical Power and Energy Systems 79, 2016, pp. 275–284.
13. C.S. Lee, H.V.H. Ayala, L.S. Coelho, "Capacitor placement of distribution systems using particle swarm optimization approaches," International Journal of Electrical Power and Energy Systems 64, 2015, pp. 839–851.
14. A.Y. Abdelaziz, E.S. Ali, S.M. Abd Elazim, "Optimal sizing and locations of capacitors in radial distribution systems via flower pollination optimization algorithm and power loss index," Engineering Science and Technology, an International Journal 19, 2016, pp. 610–618.
15. P. Das, S. Banerjee, Placement of capacitor in a radial distribution system using loss sensitivity factor and cuckoo search algorithm, Int. J. Sci. Res. Manag. 2013, 2(4), pp. 751–757.
16. S. Sultana, P.K. Roy, Optimal capacitor placement in radial distribution systems using teaching learning based optimization, Int. J. Electr. Power Energy Syst. 54, 2014, pp. 387–398.
17. N. Gnanasekaran, S. Chandramohan, P. Sathish Kumar, A. Mohamed Imran, "Optimal placement of capacitors in radial distribution system using shark smell optimization algorithm," Ain Shams Engineering Journal 7, 2016, pp. 907–916.
18. H. Karimi, R. Dash, "Comprehensive framework for capacitor placement in distribution networks from the perspective of distribution system management in a restructured environment," International Journal of Electrical Power and Energy Systems 82, 2016, pp. 11–18.
19. R. Storn, K. Price, "Differential evolution: A simple and efficient adaptive scheme for global optimization over continuous spaces," Technical Report TR-95-012", Berkeley, USA: International Computer Science Institute, 1995.
20. A.A. El-Fergany, A.Y. Abdelaziz, "Cuckoo Search-based Algorithm for Optimal Shunt Capacitors Allocations in Distribution Networks," Electric Power Components and Systems, 41, 2013, pp. 1567–1581.
21. R. Storn and K. Price, "Differential evolution—a simple and efficient heuristic for global optimization over continuous spaces," *Journal of Global Optimization*, vol. 11, no. 4, 1997, pp. 341–359.
22. D. Jia, G. Zhenga, M.K. Khan, "An effective memetic differential evolution algorithm based on chaotic local search," Information Sciences 181, 2011, pp. 3175–3187.
23. A.H. Gandomia, X.-S. Yang, S. Talatahari, A.H. Alavi, "Firefly algorithm with chaos," Commun Nonlinear Sci Numer Simulat 18, 2013, pp. 89–98.

Fractal and Periodical Biological Antennas: Hidden Topologies in DNA, Wasps and Retina in the Eye

P. Singh, M. Ocampo, J. E. Lugo, R. Doti, J. Faubert, S. Rawat, S. Ghosh, Kanad Ray and Anirban Bandyopadhyay

Abstract Although the notion of an integrating equation of life has yet to be discovered, the Fibonacci order may institute a basis for such a growth. We examined various biological structures based on Fibonacci numbers. We have observed that (i) for wasp Fibonacci's sequence increases the information amount. (ii) The energy sources should be connected at both ends of DNA structure; single source is not suitable for energy transmission. (iii) Array form of eye's receptor cell is enabled to capture the clocking conduction, localization and delocalization nature of field. We also identified the entire resonance peaks for every reported structure. Fibonacci-based structures may be used in biomedical applications like as to understand the signal propagation along the structures.

Keywords Fibonacci number · Wasp · DNA · Receptor cells
Energy distribution · Clocking conduction

P. Singh · K. Ray (✉)
Amity University, Jaipur, Rajasthan, India
e-mail: Kanadray00@gmail.com

M. Ocampo · J. E. Lugo · R. Doti · J. Faubert
Faubert Lab, Université de Montréal, H3T 1P1 Montreal, Québec, Canada

S. Rawat
Manipal University Jaipur, Jaipur, Rajasthan, India

S. Ghosh
CSIR-North East Institute of Science & Technology, Jorhat 785006, Assam, India

A. Bandyopadhyay
Advanced Key Technologies Division, National Institute for Materials Science, 1-2-1 Sengen, Tsukuba, Ibaraki 3050047, Japan

K. Ray et al. (eds.), *Soft Computing Applications*, Studies in Computational Intelligence 761, https://doi.org/10.1007/978-981-10-8049-4_6

1 Introduction

We can define the concept of shapes accurately by equations borrowed from classical geometry that led to the creation of several architectural structures of modern and ancient civilizations. However, classical geometry fails to explicate the intricacy and complication of nonlinear shapes observed in nature. Fractal geometry on the other hand accounts for such nonlinearity and paves the way for shapes that emulate those evolved in nature with remarkable accuracy. Such occurrence begs the inquiry of structural basis for biological subsistence within the world. While the notion of an integrating equation of life has yet to be discovered, the Fibonacci order may institute a basis for such a growth.

Nature presents infrared (IR) and ultraviolet (UV) detectors in the most capricious and fascinating ways. Such detectors can be observed in plants and animals [1]; among them we find wasps, birds, butterflies and human organs such as the retina or DNA molecules. But how can we characterize the communication mode of such diverse detectors. We propose that it is possible to use the analogy of antennas. The antenna is the most crucial part in the field of wireless communication. With the increasing development in the field of wireless communication, humans are using antennas in many applications. There are many areas where body-centric communication systems can be used, such as identification, tracking and healthcare systems.

We have previously discussed that insects and birds use some types of communication systems similar to antennas. It is not surprising then to find the same kind of mechanisms in plants or even other biological structures such as molecular DNA and human retina.

DNA within cells has a small structural property similar to a fractal antenna with a bandwidth lying in the RF range. By fractal behavior in the electromagnetic resonance spectrum, it is meant that the arrangement of the frequencies has a similar distribution at different scales.

The observation of the Fibonacci sequence is existent in almost all aspects of life ranging from the leaves of a fern tree, architecture, and even paintings, making it highly unlikely to be a stochastic phenomenon [2]. Regardless of its extensive occurrence and existence, the Fibonacci series and the rule of golden proportions have not been widely documented in light of the distribution of the electromagnetic fields, information processing and energy propagation in the living body or living organisms. This chapter serves to address these problems in the following three sections. Section 2 describes the underlying mechanism for the distribution of electric and magnetic energies over an insect's body. In Sect. 3 we describe the importance of geometry on the energy propagation through the DNA structure. Finally, Sect. 4 unveils the importance of periodical geometry within an eye structure which can be explained in terms of delocalization of electric and magnetic field energy in photoreceptor cells.

2 Underlying Mechanism for Distribution of Electric and Magnetic Energies Over an Insect's Body

Fibonacci numbers are the critical components for information processing. Reports dealing with communication between insects not only involve the field of zoology, but also attract electrical engineering as well [3]. Communication between insects is one of the most important aspects of insect life. There are many different ways of communicating, e.g., sound, vibration, chemical transportation [4]. One study has argued that two antennas on the head of the wasp may detect and radiate the radio wave energy from the piezoelectric or photoelectric source [5]. In previous studies, it has been suggested that both antennas behave like infrared antennas and radars [6–8].

It has already been reported that human body and body structures of different animals such as dolphins, wasps, bees, bats, snails have Fibonacci characteristics, which describe their very formation. Many researchers are interested to know the role of topology in information processing. Fibonacci numbers are straightforward to generate in such a way; the next digit is the sum of previous two successive digits like 0, 1, 2, 3, 5, 8 … [9–11]. One neat example is the sunflower structure, which has the maximum capability to absorb the sunlight energy due to orientation and distribution of seeds on its structure. The orientation of the seeds forms a spiral whose arrangement over the whole structure follows the Fibonacci sequence, which plays an important role in regard to their performance [12, 13].

In this section, we have studied various components of the wasp body, which are arranged following Fibonacci's sequence. By using the structural data file of the insect (wasp), we have created an artificial structure of wasp in the electromagnetic resonance software CST and analyzed the signal processing mechanism through wasp components. We have simulated electric and magnetic field energies, resonance frequency band and directivity. We detected the physical response of field energy, resonance band and directivity by varying the insect's body components according to Fibonacci numbers. We observed the resonance band from 1 to 30 MHz connecting the input energy supply source at different positions of the structure. Mainly we have identified only those resonance frequencies, which provide us significant results related to electric and magnetic field distribution in the MHz frequency range. The resonance characteristics hold essential information about which field energy dominates. In all figures, E depicts electric field, while H depicts magnetic field. We observed interesting results, which are discussed in the following three panels.

Panel 1 (i) We have studied different components of insect body as shown in Fig. 1(A). We have found interesting electric and magnetic energy profiles. At the initial stages B, C and D (Fig. 1), both energies are insignificant; but at (E) stage, both energies are equally dominating. The magnetic field is radiated in the particular direction, but the electric energy radiation is of isotropic nature. In this particular case putting the different components of insect body in Fibonacci order,

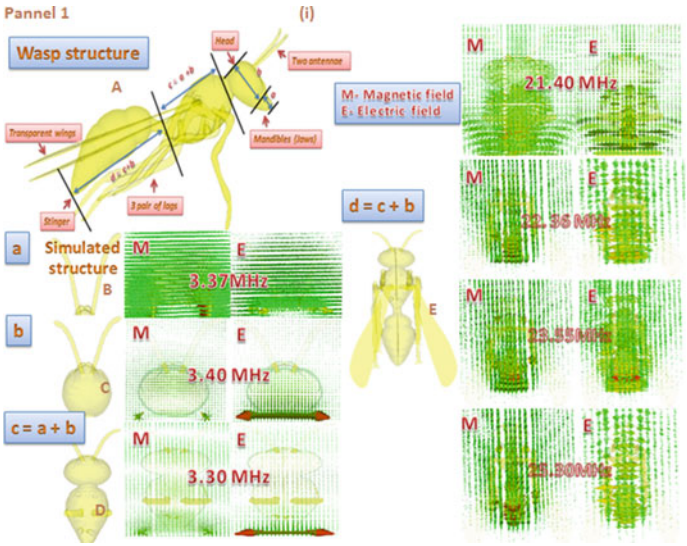

Fig. 1 Electric and magnetic field distributions over various components of the wasp's body (A): (a) wasp structure. Case (B) the energy source is modulated at frequency 3.37 MHz (resonance frequency); electric and magnetic field amplitudes are minimal at resonance frequency 3.40 MHz in case (C). E and H fields both are similar at 21.40 MHz (case D). In whole wasp structure, electric field dominates when compared to the magnetic field. Here the behavior of magnetic energy is straightforward, while electric energy is distributed in different directions around the insect body (see Fig. 1E)

we found improved results. **(ii)** In this panel, the absolute value profile of electric and magnetic field energies are represented in counter-form. The magnetic energy on component lengths represented at a, b and c dominates. The black rectangular box shows this. Both energies are radiating in the form of the pulse shown in section (E) of Fig. 2b.

Panel 2 In this panel (see Fig. 3), we have studied how directivity varies with frequency. Directivity may be defined as a parameter, which measures the degree of emitted radiation that is concentrated in a particular direction [14]. If we plot the curve between directivity and frequency, then the value of the directivity increases monotonically. It gained a higher value level [from (B), 5.45 dBi, to (E), 18.88 dBi] with increasing Fibonacci number through insects' components.

Panel 3 In this panel (see Fig. 4, we observed, by increasing the Fibonacci number over insects' components, that the single resonant band converts into multiple resonance bands. Since it has been shown that electromagnetic resonance is the key component for information processing and regulates biological processes [15, 16] the result in this panel demonstrates that Fibonacci's sequence increases the amount of information (one resonance band versus multiple bands).

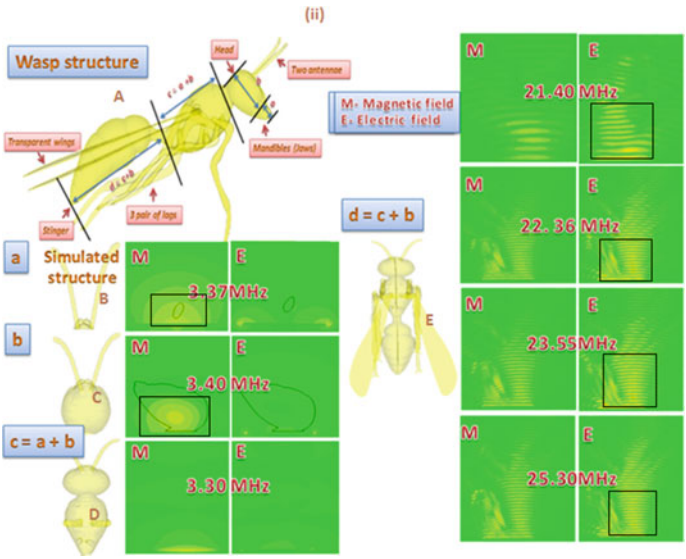

Fig. 2 Absolute value of the electric and magnetic field (in counter-form) distribution over different wasp insect components. Magnetic field dominates over the electric field in cases B and C, and the magnetic field is maximum around the head of the wasp, while electric field circulated the corner of the port. In D, at first resonance frequency, there is no field around the structure, but at the resonance frequency (21.40 MHz), both energy fields propagate along the structure in the form of a pulse. In E, the majority of the magnetic field is maximum at all resonance frequencies. Here, both fields' propagation nature is the same as described above. Simulation detail: used solver = time domain solver, boundary condition = open space, location of the port = bottom of the structure, (B) simulation frequency details = 1–20 MHz, port dimensional = 0.35e +003 × 0.35e+003 mm^2, (C) simulation frequency details = 1–7 MHz, port dimensional = 0.40e+003 × 0.40e+003 mm^2, (D) simulation frequency details = 17–30 MHz, port dimensional = 0.40e+003 × 0.40e+003 mm^2, (E) simulation frequency details = 22–26 MHz, port dimensional = 0.60e+003 × 0.60e+003 mm^2

In the next section, we will apply a similar methodology to study another fascinating biological system, the DNA.

3 Energy Propagation Through the DNA Structure

Fibonacci sequence applies to growth on every living thing in nature [17]. Previous studies have argued for a mathematical relation between nucleotide frequencies in human single-stranded DNA and the Fibonacci number [18], specifically that DNA holds the phi relation between major groove and minor groove. In the past, we have discussed that the electromagnetic behavior of DNA is an analog of an electromagnetic cavity as well as a fractal antenna in which we assumed the vibrational response of DNA molecules in the GHz frequency range [19]. The stored

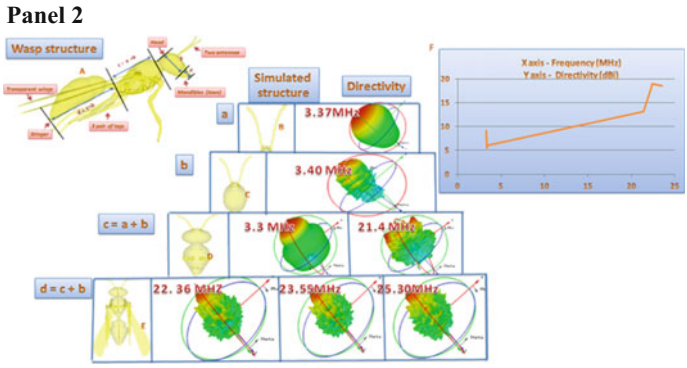

Fig. 3 (A) Wasp structure. From the above figure, the Fibonacci number based on insect body parts improved the performance in exhibiting their own function. The degree of the emitted radiation in a particular direction increases in the order shown from case B up to case E. Value levels of the directivity at their resonance frequencies: B = 5.45 dBi; C = 6.09 dBi; D = 9.14 and 13.14 dBi; E = 18.88 dBi, 18.54 dBi and 18.28 dBi. Directivity curve over the frequency increases monotonically. Simulation details: used solver = time domain solver, boundary condition = open space, location of the port = at the lower view of the structure. (B) Simulation frequency details = 1–20 MHz, port dimensional = 0.35e+003 × 0.35e +003 mm^2. (C) Simulation frequency details = 1–7 MHz, port dimensional = 0.40e +003 × 0.40e+003 mm^2. (D) Simulation frequency details = 17–30 MHz, port dimensional = 0.40e+003 × 0.40e+003 mm^2. (E) Simulation frequency details = 22–26 MHz, port dimensional = 0.60e+003 × 0.60e+003 mm^2

information in DNA is in the form of a code which is made up of four chemical molecules, namely guanine, cytosine, thymine and adenine. The whole human DNA contains approximately 3 million base pair molecules, and the information available for building and maintaining the cell relies upon the order and sequence of these base pair molecules [20–24]. Previous studies have argued that the DNA spiral presents the well-known golden section, which can be obtained from the Fibonacci sequence. The life formation program is based on the golden section 13 × 21 Å wide helix spiral cycle [25]. The essential DNA component of DNA structure is shown in Fig. 5.

In this section, we analyzed the electric and magnetic field distribution over the geometrical arrangement of DNA molecules. By using the structural database file, we have built the human DNA structure and simulated field distributions and resonance frequencies by using the same electromagnetic resonance simulation software as before (CST). We detected frequency responses from electric and magnetic fields over the variation of the source dimensions. The resonance frequency curves show the existence of the Fibonacci sequence over the DNA structure in such way that at specific frequencies the electric field dominates and in other frequencies the magnetic field dominates. We simulated the resonance band from GHz frequency range to THz frequency range. We took into account only peaks, which provide significant phase for electric and magnetic field distribution within that frequency range. Moreover, we analyzed only the energy transmission

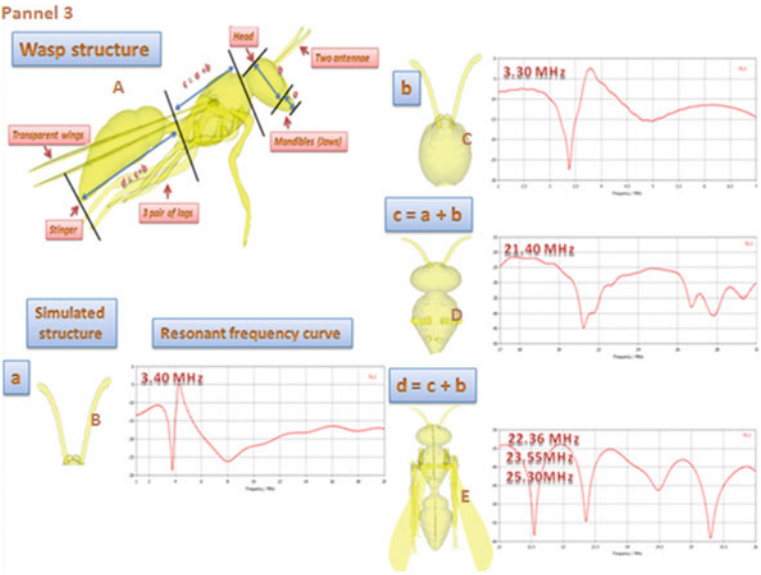

Fig. 4 (A) Wasp structure. From the above panel, we have observed that Fibonacci-based arrangement of the insect body suggests an important functional role related to insect communication. If we look carefully at the resonance frequency band, we can appreciate the importance of Fibonacci order arrangement over the insect body. From case A to case E, the resonance frequency curve converts from single band to multiple bands and such curves have the tendency to move toward the infrared frequency band. Simulation details: used solver = time domain solver, boundary condition = open space, location of the port = at the lower view of the structure. (B) Simulation frequency details = 1–20 MHz, port dimensional = 0.35e+003 × 0.35e +003 mm^2, (C) simulation frequency details = 1–7 MHz, port dimensional = 0.40e+003 × 0.40e +003 mm^2, (D) simulation frequency details = 17–30 MHz, port dimensional = 0.40e+003 × 0.40e+003 mm^2, (E) simulation frequency details = 22–26 MHz, port dimensional = 0.60e +003 × 0.60e+003 mm^2

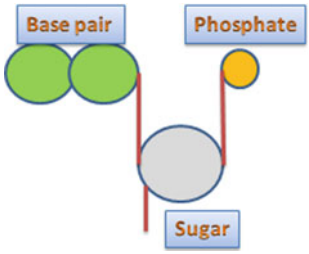

Fig. 5 Essential building component of DNA structure

through the DNA molecules at a particular frequency by placing at different locations the input energy supply port and by changing the dimensions of the input energy supply port.

The results are displayed in Figs. 6, 7, 8, 9, 10, 11 and 12.

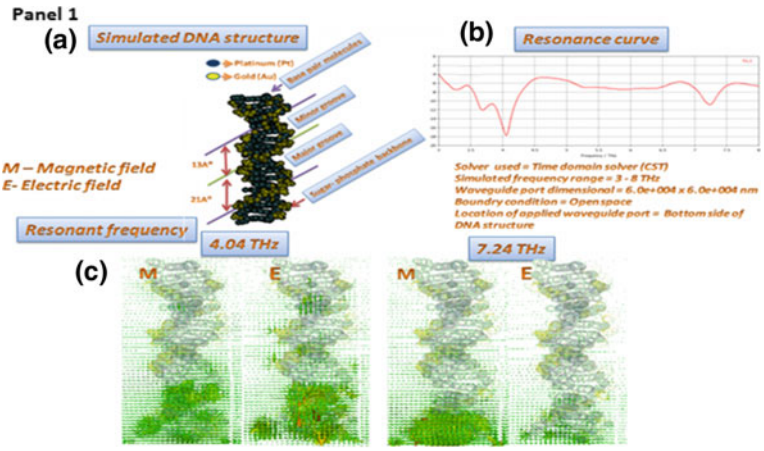

Fig. 6 **a** Simulated model of DNA structure; the energy source is applied at the bottom end. **b** The resonance curve with two resonance frequencies 4.04 and 7.24 THz. **c** Electric and magnetic field distribution profiles: At first resonance frequency, electric field dominates more, while at second resonance frequency magnetic field amplitude is higher. Also, the energy is not transmitted to the other end

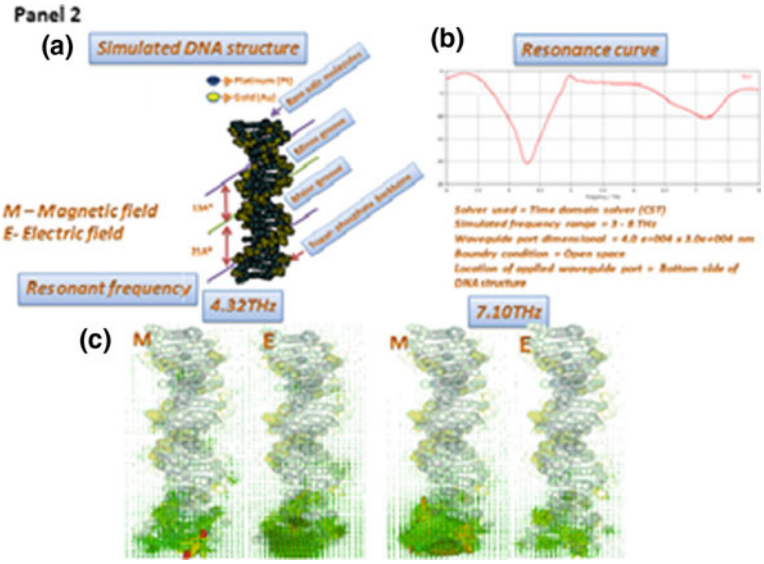

Fig. 7 By reducing the dimensions of the port, resonance frequencies are slightly shifted; the nature of the frequency curve became smooth. Simulation details: solver used = time domain solver (CST), simulated frequency range = 3–8 THz, port dimensional = 6.0e+004 × 6.0e +004 nm^2, boundary condition = open space, location of the port = bottom side of DNA structure

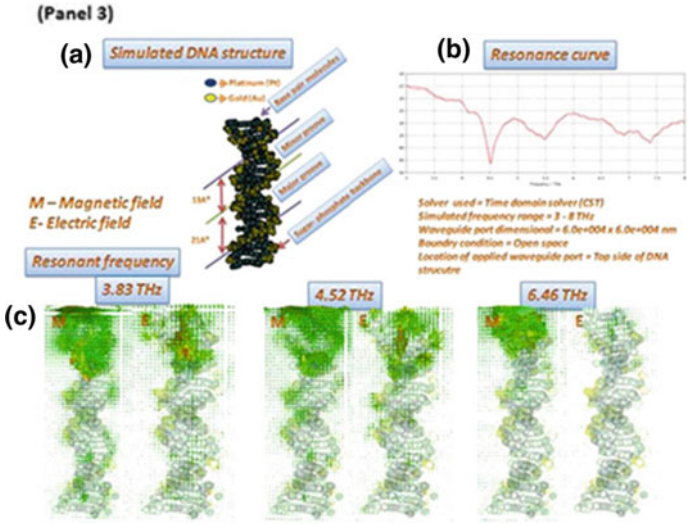

Fig. 8 **a** Simulated DNA structure: The port is located at the top of DNA structure, **b** simulated resonance curve. Here, the structure has three resonance frequencies: 3.83, 4.52 and 6.46 THz. **c** Magnetic field dominates more than the electric field, at the first resonance frequency; energy is transmitted partially through the whole structure. Electric field weakens by increasing the frequency within the studied range. Simulation details: solver used = time domain solver (CST), simulated frequency range = 3–8 THz, port location = top side of DNA structure

The First Case, When the Energy Source is Applied at the Bottom End of DNA Structure: (3–8 THz)

Panel 1—Fig. 6a shows the simulated structure of DNA model where the phi relationship is maintained between the major groove and minor groove. Panel 1—Fig. 6b shows the resonance curve. Panel 1—Fig. 6c shows, by increasing the energy source dimension, the structure gets the maximum time resonance. At the first resonance frequency, both fields are partially transmitted, but at the second resonance frequency, the electric field disappears, while the magnetic field dominates.

Panel 2—Fig. 7b shows the resonance behavior of the DNA structure that decreases by reducing the port dimensional. It shows sharp frequency resonance curve. Here, both fields appear around the energy source.

The Second Case, When the Energy Source is Applied at the Upper End of DNA Structure: (3–8 THz)

Panel 3—Fig. 8a–c shows DNA resonances at three different frequencies where magnetic field amplitudes are maxima in all cases. The magnetic energy and electric energy are not transmitted to the bottom end.

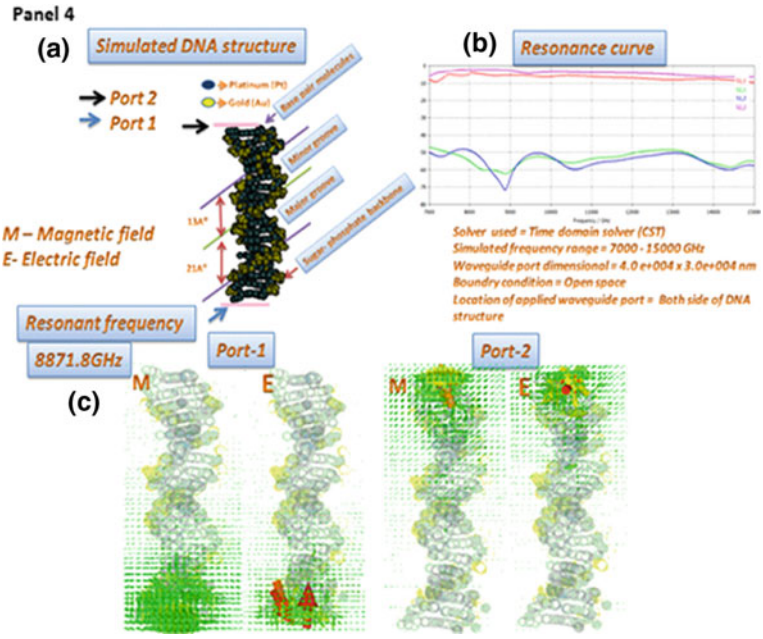

Fig. 9 **a** Simulated DNA structure: The energy port is located at both top and bottom sides of the DNA model. **b** Resonance frequency curve, the model design has the resonance at 8871.8 GHz. **c** Both fields oscillate, and the energy is not transmitted. Simulation details: solver used = time domain solver (CST), simulated frequency range = 3–8 THz, port dimensions = 4.0e+004 × 3.0e +004 nm^2, boundary condition = open space, location of the port = both sides of DNA structure

The Third Case, When the Energy Source is Applied at Both Ends of DNA Structure: (7–30 THz)

By supplying energy at both ends of the DNA structure, there are no improvements in the results. This is shown in Panel 4—Fig. 9a by keeping the energy source dimensions of 4.0e+0004 × 3.0e+0003 nm^2 and the simulation frequency range from 7 up to 15 THz. The transmission of both fields are very low near the energy source, but when the port dimensional is increased, both energy fields are partially transmitted from 7 THz up to 20 THz (see Panel 5—Fig. 10a). If we use the simulation range between 10 and 30 THz, the resonance frequency curve shows many resonance frequencies due to the combined effect of both ports. Both electric and magnetic energies oscillate around the applied energy source as shown in Panel 6—Fig. 11. In Panel 7—Fig. 12, we keep the same dimensions of the energy source in the simulated frequency range 6–20 THz. In this case, DNA structures have a deep resonance at 13.93 THz (see Fig. 12b), where again magnetic field dominates. At 23.39 THz, maximum energy transmits from one end to the other end of DNA structure (see Fig. 12c). Surface current flows through the superphosphate backbone chain are shown in Fig. 12d. The field energy oscillate around the applied energy

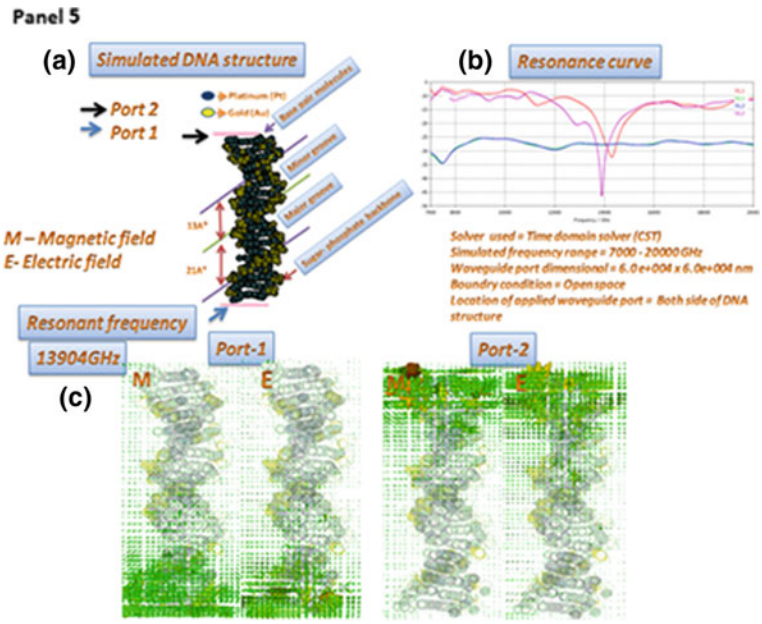

Fig. 10 **a** Simulated DNA structure: The energy source is placed at both top and bottom sides of the DNA model. **b** Simulated DNA model highly resonates at 13,904 GHz; both ports show the resonance at almost the same frequency. **c** By increasing the dimension of the waveguide ports, both electric and magnetic field energies are partially transmitted to the other end. Simulation details: solver used = time domain solver (CST), simulated frequency range = 7000–20,000 GHz, port dimensions = 6.0e+004 × 6.0e+004 nm^2, boundary condition = open space, location of the port = both sides of DNA structure

source which connected at one end of DNA structure. There is no energy transmission between both ends of DNA structure. By connecting the second energy source at other end, energy is successfully transmit across the DNA. This result is obtained at all resonance frequencies, and it is characteristic of a receiver.

Similar results can be found in an artificial architecture of retinal blood vessels in human eyes based on realistic geometry, but not with real dimensions. We observed that Fibonacci sequence also exists in human eye's blood vessel with a resonance peak in PHz frequency range. Moreover, the electric and magnetic field distributions at resonance (17 PHz) alternate their dominance at different spatial locations.

In this section, we have seen the effect of the Fibonacci sequence, which is intrinsic to DNA structure, on the electric and magnetic field behaviors within DNA. The fields showed different resonance peaks well defined inside the range of THz. Comparable results were found in an artificial architecture of retinal blood vessels in human eyes based on realistic geometry but not with real dimensions. In the next section, we will present another physiological system contained within our eyes where once again geometry can play a vital role. We will explore if translational symmetry displayed by photoreceptors causes the appearance of resonance bands.

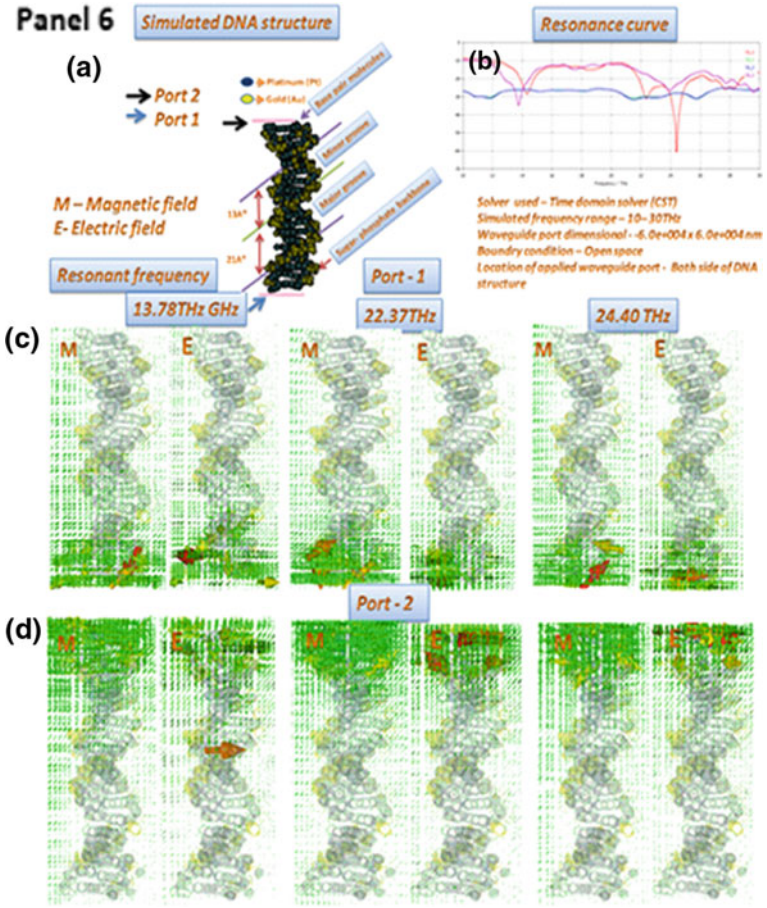

Fig. 11 **a** Simulated structure of DNA, where major and minor lobe lengths are 21 and 13 Å, respectively. The ratio of the major groove to minor groove is approximately 1.618, which is equivalent to the golden ratio (phi) [24]. **b** Simulated DNA structure shows resonances at 13,937, 14,507 and 23,398 GHz; maximum resonance appears at a frequency of 13,937 GHz. **c** Electric and magnetic field distribution profiles at their resonance frequencies; in this frequency range, magnetic field amplitude dominates over the electric field amplitude. At 13,937 GHz, the energy is not completely transmitted from one end to the other, but at 14,507 GHz, it is partially transmitted to the other end. At 23,398 GHz, whole energy is transmitted to the second end. Maximum energy passes through by sugar-phosphate backbone chain. **d** The electric field, magnetic field and surface current profile at 23,398 GHz frequency. Here, sugar-phosphate backbone chain plays an important role in the propagation of the surface current. Simulation details: solver used = time domain solver (CST), simulated frequency range = 6×10^3 to 2×10^4 GHz, port dimensions = 6.0e+004 $\times$ 6.0e+004 nm^2, boundary condition = open space, location of the port = bottom side of DNA structure

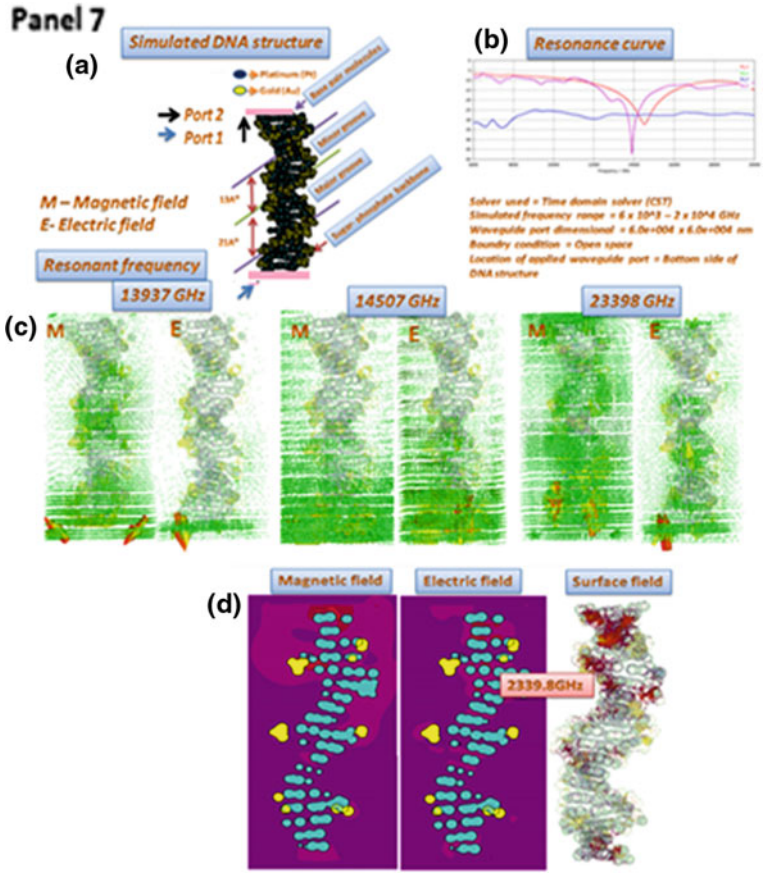

Fig. 12 **a** Simulated structure of DNA, where major and minor lobe lengths are 21 and 13 Å, respectively. The ratio of the major groove to minor groove is approximately 1.618, which is equivalent to the golden ratio (phi) [24]. **b** Simulated DNA structure shows resonances at 13,937, 14,507 and 23,398 GHz; maximum resonance appears at a frequency of 13,937 GHz. **c** Electric and magnetic field distribution profiles at their resonance frequencies; in this frequency range, magnetic field amplitude dominates over the electric field amplitude. At 13,937 GHz, the energy is not completely transmitted from one end to the other, but at 14,507 GHz, it is partially transmitted to the other end. At 23,398 GHz, whole energy is transmitted to the second end. Maximum energy passes through by sugar-phosphate backbone chain. **d** The electric field, magnetic field and surface current profile at 23,398 GHz frequency. Here, sugar-phosphate backbone chain plays an important role in the propagation of the surface current. Simulation details: solver used = time domain solver (CST), simulated frequency range = 6×10^3 to 2×10^4 GHz, port dimensions = 6.0e+004 × 6.0e+004 nm^2, boundary condition = open space, location of the port = bottom side of DNA structure

4 Delocalization of Electric and Magnetic Field Energies in Photoreceptor Cells

Human eye is often compared to a camera, which is self-focusing automatically adjustable for light intensity and provides the 3D colored image. Human eyes create visual world images, where the retina plays a vital role. Retina itself is a fantastic structure that translates the light into nerve signals under the condition of light wavelength so we can see color [26]. The retina is a thin, fragile meshwork, which lies below of a vitreous chamber. The thickness of retina is not homogenous; it has the minimum thickness at the fovea, which reduces light absorption and scattering before reaching photoreceptor cells such as rods and cones, while collector cells collect information from the photoreceptor cells and transfers to the brain [27–29]. Several millions of rods and cones exist in our retinal system and are responsible for light processing. Human eyes have three types of cones: long wavelength (∼red)-, short wavelength (∼blue)- and medium wavelength (∼green)-sensitive cones; these cones help us to detect broad kind of colors, while rods are not color sensitive and respond to intensity (black, white and gray). Many researchers are interested to understand the details about circuit mechanisms that underlie trichromatic color vision in human eyes. C. Canbay and I. Unal observed the spectral sensitivity of these three types of cones that are broadband in the visible light spectrum. The cones have a small significance peak near central peak due to their conical shape, while there was only one peak for rods due to their cylindrical geometry [30]. Gerald C. Huth provides current work on light interaction with the retina, which is based principally on nanostructure geometry. Photoreceptor cell structure (like space and phase difference between adjacent rods and cones) could in part control the light wavelength that we can detect.

Here, we have done a theoretical simulation study by creating an artificial architecture of photoreceptor cells “rods and cones” by using the original structure of photoreceptor cells in a computer simulation software (CST). For the purpose of simulation we consider that all photoreceptor cell structures are identical. We have studied two parameters, resonance frequency band and electric and magnetic field energies. We have compared the behavior of electric and magnetic fields over one complete phase cycle for the photoreceptor cell cross section (shown in Fig. 13). Resonance band shows a peak at a near-UV region for one single photoreceptor cell and within the visible region of the assembly of photoreceptor cells. We have found that by increasing the number of receptor cell units, both fields are delocalized in different functional domains (space and phase). At a particular resonance frequency, we have analyzed clocking phase phenomena in which both electric and magnetic energies are inhomogeneously distributed over the architecture. Results are displayed in Figs. 13 and 14.

In Fig. 13, we obtained exciting results related to field energy distribution over a photoreceptor cell cross section. For example, electric and magnetic field energies over one complete phase cycle almost presented the unique characteristic of clocking. Clocking is the fundamental property of resonance. Electric and magnetic

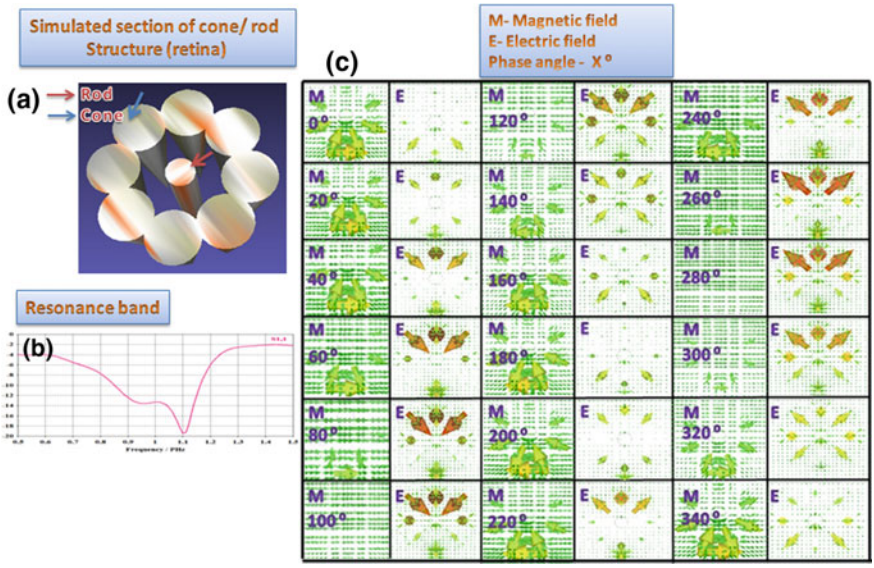

Fig. 13 **a** Small simulated section of retinal receptor system; here, several cones surround the central rod. **b** Resonance band graphic shows that this structure resonates in the NUV region at 1.1 PHz. **c** This section represents the clocking nature of the electric and magnetic energies at different phases (0°–340°) over the simulated structure. Over all the phases, magnetic field dominates more than the electric field. Here, we can easily analyze the behavioral mechanism of field energy. Magnetic energy comes at the phase duration 0°–60°, after that it became off for 80°–140°; it became on again for 160°–240°, while the electric energy runs just to the opposite phase of magnetic energy. Magnetic energy circulated on a particular cone, while electric field propagates inward or outward direction through the structure. Simulation details: solver used = time domain solver, boundary condition = open space, simulation frequency range = 0.4–1.2, port dimensions = $0.030 \times 0.15\ \mu m^2$, location of applied port = from side of cone

energies are distributed over the structure in a particular way during one phase cycle. In our previous work, the same kinds of energy characteristics have been observed in axons, microtubules and tubulin. Here, we have analyzed such type of features in the PHz frequency domain. Magnetic field concentrates at a particular region of the retinal cross section, while electric field distribution is inward or outward of the whole structure. Theoretical simulation studies based on such type of receptor system lead to good results matching with experimental results produced by Berkeley groups and Gerald Huth's theory [31]. Retinal cross section simulation shows the frequency band in NUV region.

In Fig. 14, we created an array of cones/rods by putting several small units of cones surrounding a rod (assembly of photoreceptors) that is shown in Fig. 14a. Our findings are shown in Fig. 14b, c. One result is based on electromagnetic energy. In Fig. 13, we have found the delocalization of electric energy at different functional domains on a receptor cell, while magnetic energy is concentrated on a particular area of a receptor cell. Resonance band has only one peak in the NUV

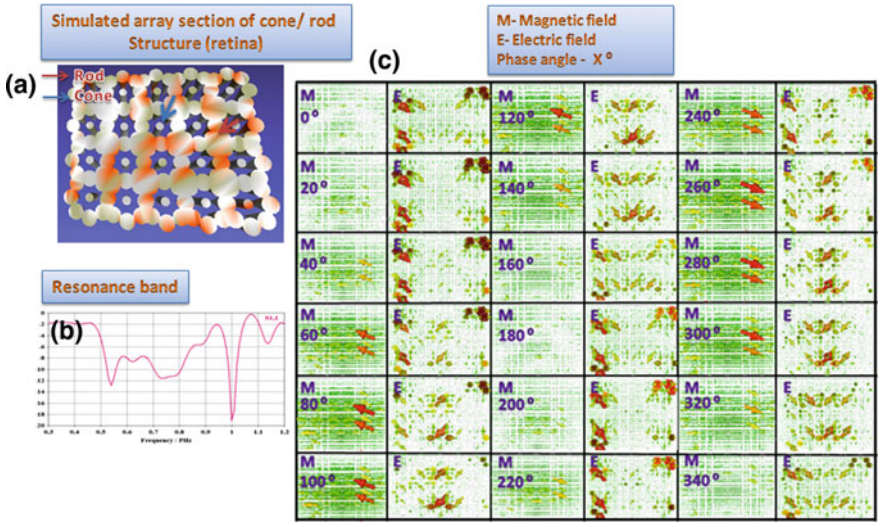

Fig. 14 **a** A simulated array structure of cones/rods receptor system of the retina. **b** The resonance frequency band of retinal array section, which has two electromagnetic resonance frequencies in the visible region and has one within NUV region at 0.54, 0.73 and 1 PHz frequency. **c** Magnetic and electric energy profiles at peak resonance frequency. Electric and magnetic fields are delocalized at different function domains in rods and cones structure over one complete cycle of the phase. Both fields are dominated at some particular phase duration. Initially, electric field dominates, while the magnetic field is silent, and after the next phase duration, magnetic field dominates and the electric field is silent. Such clocking nature repeats for the next phase cycle. Simulation details: solver used = time domain solver, boundary condition = open space, simulation frequency range = 0.5–1.5, port dimensions = 0.030×0.15 μm^2. Location of applied port = from the side of the cone

region. But in Fig. 14, both field energies are delocalized randomly at different areas. Electromagnetic resonance band shows three peaks: two peaks in the visible region and one peak within NUV region. For all three frequencies, electric and magnetic fields show the same amplitude maximization and minimization for complete phase duration, but we only depicted this process for the first frequency peak (0.54 PHz, is this correct?). This result shows that by changing the receptor cell scale, the mechanism of field delocalization is triggered. In general, any change in the receptor cell dimensional scale selects a particular energy delocalization domain.

5 Conclusions

We have shown the significance of Fibonacci numbers over living things and physiological organs in nature. We observed one major feature regarding wasp: Fibonacci numbers over the wasp body are essential to exhibit function because by

taking any parameter from electric and magnetic fields namely resonance band or directivity, we found that Fibonacci's sequence increases the information amount (one resonance band versus multiple bands).

Besides, here, we have also shown that electric and magnetic energies are functions of the Fibonacci sequence existing in the molecular arrangement of DNA structure. Electromagnetic energy propagates through the superphosphate backbone chain by applying an energy source on both DNA sides. One interesting finding is that, the current conduction occurs across the DNA structure at particular frequency (DNA conduction mode). We also found that DNA resonates at many different frequencies in the range from 3 up to 30 THz, but energy is transmitted at a particular rate. The second interesting result is the domination of the magnetic field energy over the electric field energy throughout the 3–30 THz frequency range. As regards the photoreceptor cells in our retina, we have also observed one major feature. Electric and magnetic field energies are the topological function of photoreceptor cell's structure. Here, we have compared both results obtained from a single unit and assembly of photoreceptor cells. The behavioral characteristic of magnetic field changes from localized to delocalized nature keeping clocking nature intact. Electric and magnetic fields go periodically in silent mode, always maintaining the opposite phase relation. Resonance peaks of rods and cones in retinal receptor system occur near PHz frequency range. The primary conclusion of our overall study can be explained in terms of result optimization. Mainly, the Fibonacci sequence-based structure or the periodical array of basic physiological units (such as photoreceptors within the retina) is responsible for optimizing the signal communication in biological living systems.

References

1. Klocke D., Schmitz A., Soltner H., Bousack H., and Schmitz H. (2011) Infrared receptors in pyrophilous ("fire loving") insects as model for new un-cooled infrared sensors Beilstein J Nanotechnol vol. 2: 186–197.
2. Persaud-Sharma D and O'Leary JP. (2015) Fibonacci Series, Golden Proportions, and the Human Biology. Austin J Surg. vol. 2(5): 1066.
3. Ali A., Hossein H., Mohammad M. S. (2013) The antenna analysis of insect antennae, World Journal of Modeling and Simulation Vol. 9(3): 235–240.
4. ZebTedford, "Communication between the insect" April 2011.
5. Gavan, J., Ishay, J.S. (2000)Hypothesis of natural radar tracking and communication direction finding systems affecting hornets flight, Journal of electromagnetic waves and applications 13(2):247–48
6. Singh P., Doti R., Lugo J.E., Faubert J., Rawat S., Ghosh S., Ray, K. and Bandyopadhyay A. (2016) Biological Infrared Antenna and Radar, ch-108; Soft Computing: Theories and Applications Proceedings of SoCTA vol. 2, Advanced Intelligent Systems and Computing, Springer.
7. Campbell, A.L., Rajesh, R., Laura, S., Morley, O.S.: Biological infrared imaging and sensing 206 micron. 33(2), 211–225 (2002)
8. Schmitz, H., Bleckmann, H.: The photomechanism infrared receptor for the detection of forest 2014 fires in the battle melanophila acuminate. J. Comp. Physiol. A 182, 647–657 (1997), 2054.

9. The golden ratio in nature, Web. link http://www.peacevalleynaturecenter.org/pdf/PVNCfall2014.pdf.
10. Y. Ramat- samii, J. M. Kovita, H. Rajagopalan: NatureInspired Optimization Technique in Communication Antenna Design. Proceeding of the IEEE, 100 (7), pp. 2132–2144, 2012.
11. H. Vogel. A better way to construction the sunflower head. Mathematical Bioscience, 44, pp. 179–189, 1997.
12. Singh P., Ray K., Rawat S. (2016) Nature Inspired Sunflower Shaped Microstrip Antenna for Wideband Performance IJCISIMA 8:364–371.
13. Singh P. Ray K., Rawat S. (2015) Design of Nature Inspired Broadband Microstrip Patch Antenna for Satellite Communication Advances in Nature and Biologically Inspired Computing pp 369–379 AISC, volume 419.
14. Stutsman W (1998) Estimating Directivity and Gain of Antennas. IEEE Antennas and Propagation Magazine, 40 (4): 7–11.
15. Sahu S., Ghosh S., Fujita D., Bandyopadhyay A. (2014) Live visualizations of single isolated tubulin protein self-assembly via tunneling current: effect of electromagnetic pumping during spontaneous growth of microtubule, Scientific Reports 4, 7303 http://dx.doi.org/10.1038/srep07303.
16. Sage C, Carpenter D (Eds.) A scientific perspective on health risk of electromagnetic fields. 244 Published online 31 August 2007 at: http://www.bioinitiative.org/report/index.htm
17. Aihua G., Yingying X. (2012) The Research of the Generalized Fibonacci Sequence-based Propagation. Physics Procedia, 24: 1737–1741.
18. Michel E. Yamagishi B., Shimabukura A. I., Nucleotide Frequencies in Human Genome and Fibonacci Number: 1–12.
19. P. Singh, R. Doti, J. E. Lugo, J. Faubert, S. Rawat, S. Ghosh, K. Ray and A. Bandyopadhyay, (2016) DNA as An Electromagnetic Fractal Cavity Resonator: Its Universal Sensing and Fractal Antenna Behavior, ch-98; Soft Computing: Theories and Applications Proceedings of SoCTA vol. 2, Advanced Intelligent Systems and Computing, Springer.
20. Web link https://ghr.nlm.nih.gov/primer/basics/dna.
21. Watson, J.D., Crick, F.C.H. (1993) Molecular structure of nucleic acids, a structure for deoxyribonucleic acids. Nature 171: 737–738.
22. Dewarrat, F. C.: Electric characterization of DNA thesis (2002). https://nanoelectronics.unibas.ch/…/theses/Dewarrat-PhD-Thesis.pdf
23. Sahu, S., Ghosh, S., Hirata, K., Fujita, D., Bandyopadhyay, A. (2013) Multi-level memory-switching properties of a single brain microtubule. Appl. Phys. Lett. 102, 123701.
24. Sahu, S., Ghosh, S., Ghosh, B., Aswani, K., Hirata, K., Fujita, D., Bandyopadhyay, A. (2013) Atomic water channel controlling remarkable properties of a single brain microtubule: correlating single protein to its supramolecular assembly. Biosens. Bioelectron. 47: 141–148.
25. Web link https://www.goldennumber.net/dna/.
26. Web. link http://hubel.med.harvard.edu/book/ch3.pdf.
27. Singh P., Doti R., Lugo J.E., Faubert J., Rawat S., Ghosh S., Ray K. and Bandyopadhyay A. (2016) Frequency Fractal Behavior in the Retina Nano-Center-Fed Dipole Antenna Network of a Human Eye, ASIC.
28. Rotanowska, M., Sarna, Y. (2005) Light-induced damage to the retina: role of rhodopsin chromophore revisited. Photochem. Photobiol. 81: 1305–1330. https://doi.org/10.1562/2004-11-13-1R3-371
29. The Interaction between Light and Matter. www.springer.com/cda/content/…/cda…/9783642322600-c1.pdf.
30. Canbay C. and Unal I. (2008) Electromagnetic Modeling of Retinal Photoreceptors, PIER, 83:353–374.
31. Gerald C. Huth, "A Modern Explanation for Light Interaction with the Retina of the Eye Based on Nanostructural Geometry: Rethinking the Vision Process, http://www.ghuth.com/.

Efficient Multiprocessor Scheduling Using Water Cycle Algorithm

Sasmita Kumari Nayak, Chandra Sekhar Panda and Sasmita Kumari Padhy

Abstract The multiprocessor scheduling problem consists of a set of tasks to be performed using a finite number of processors. This paper deals with the problem in a heterogeneous processing environment. A nature-inspired metaheuristic algorithm, water cycle algorithm (WCA), is being used for the purpose. For the purpose of comparison, contemporary strategies using genetic algorithm (GA), bacteria foraging optimization (BFO) and genetic-based bacteria foraging (GBF) found in the literature also reproduced in this paper. Because of close relationships between the matrixes formed by the problem with those of the WCA, proposed strategy of scheduling outperforms GA- and GBF-based strategies.

Keywords Water cycle algorithm · Multiprocessor processing Optimization

1 Introduction

From the issues of load balancing, the problem of multiprocessor scheduling is NP-hard [1–6]. The job of resource sharing is to allocate the set of task to a set of processors for deterministic execution [1]. Traditional method gives the global optimum value which is regularly prolonged yet does not influence for fathoming

S. K. Nayak
CUTM, Odisha, India
e-mail: sasmita.nayak@cutm.ac.in

C. S. Panda (✉)
Sambalpur University, Odisha, India
e-mail: dr.chandrasekharpanda@gmail.com

S. K. Padhy
VSSUT, Odisha, India
e-mail: chavisiba@rediffmail.com

K. Ray et al. (eds.), *Soft Computing Applications*, Studies in Computational Intelligence 761, https://doi.org/10.1007/978-981-10-8049-4_7

the present reality issues. The researchers have determined to minimize the execution time and communication costs using branch and bound method and simulation techniques, and they found the complexity of these methods [1, 7]. Traditional methods get stuck on local optima, and these are very fast, give accurate answers and deterministic [8]. A few focal points of element systems over the static strategies are, for example, the dynamic methods do not require any former data or knowledge, whereas the static techniques must oblige earlier information to execute every one of the assigned tasks [1].

Recent heuristics methods are [9] broadly useful optimization algorithms, and exactness or relevance or proficiency is most certainly not settled to any particular problem area. Works in [1, 10] frame the problem is a multi-objective optimization problem [1, 10] that is time-consuming. Hence, in this work, we study it as a single-objective function.

In heterogeneous systems, multiprocessor scheduling problem is a multi-objective optimization problem [1, 10]. Nonetheless, this paper formulates that the multiprocessor scheduling problem uses single-objective function in heterogeneous systems. A hybrid genetic-variable neighborhood search algorithm is a heuristic-based algorithm solved multiprocessor scheduling problem to minimize execution time [1, 11]. However, this paper does not use any genetic-variable neighborhoods search algorithm. The ACO (ant colony optimization) and SS (scatter search) algorithms are bonded together called as ACOSS algorithm (ACO-SS); a local search strategy is utilized to calculate the healthier result of resource-constrained project scheduling problems [1, 12]. Be that as it may, in this paper we utilize the proposed water cycle algorithm which is a strategy of global search to get the better solution in multiprocessor scheduling problem. This planned approach proves the higher performance of multiprocessor scheduling problem with experimental results by comparing with other evolutionary and nature-based algorithms.

Different algorithms have grown as of now to explain a different constrained engineering optimization problem in the most recent decade. On the other hand, these problems are very complex [13] and somewhat hard to solve. If a problem more than one local optimum value will have, then the results possibly depend on the choice according to the starting point and the optimum solution may not essentially be the global optimum value. Also when the objective (fitness) function and constraints have sharp and different peak values, the gradient search may transform into unbalanced. Depending on the efficiency and correctness, the disadvantages of existing numerical techniques, to answer engineering optimization problems using nature-inspired methods based on simulations, have urged specialists to put stock in metaheuristic algorithms [13].

Metaheuristic algorithms usually function by randomness and consolidating guidelines to reproduce natural phenomena [14]. This may include the animal activities, for example, Kennedy and Eberhart [15] developed PSO (particle swarm optimization) and Kirkpatrick et al. [16] developed the physical annealing also known as SA (simulated annealing), Holland [17] and Goldberg [18] developed genetic algorithms (GAs) based on biological evolutionary process.

From the various optimization algorithms, generally the EAs (evolutionary algorithms) are known as general purpose optimization algorithms [13]. It has the capacity to locate the close optimal solution from the numerical genuine esteemed test issues, and it utilized as a part of constrained optimization problems successfully [19].

GA depends on Darwin theory of evolution. It grew predominantly by imitating the nature and behavior of genetic chromosomes [13, 18]. Genetic algorithms are preferred for look issues which require the identification of a global optimal solution without stuck in local minima or maxima. All living organisms are made of cells. The cell is also called as gene. A chromosome is made from genes. Each chromosome represents a solution. The solution is also called as an individual [13, 18].

PSO, by Kennedy and Eberhart [15], is a metaheuristic technique propelled by social behavior of organisms, for example, bird gathering. It involves an individual called particle (or solution) changing its position (or state) gradually; each particle alters its position as per its own understanding on the base of the best location encountered by itself, its neighbors and the best position available globally.

In this paper uses the WCA a strategy of global search to get the better solution in multiprocessor scheduling problem. The fundamental goal of a WCA is to locate the best estimations of a predefined arrangement of free parameters connected with multiprocessor scheduling problem. The performance and the result of multiprocessor scheduling problems using WCA are compared in terms of number of iterations and the best function value with other optimizers. This planned approach proves the higher performance of multiprocessor scheduling problem with experimental results by comparing with other evolutionary and nature-based algorithms.

2 The Problem

The objective of the multiprocessor scheduling problem is to reduce the total execution time. This paper considers the multiprocessor scheduling problem which comprises of an arrangement of diverse processors (I) having distinctive processing resources including memory, which imply that tasks (J) executed on diverse processor experience distinctive execution time. Assume that the connected links are indistinguishable. The communication cost between two tasks is experienced, if they executed on diverse processors.

Consider fitness_function(I_i) is utilized to calculate the superiority of the task assignment processor I_i. Efficient processor utilization is expected to hold the idea of load balancing [20]. The fitness function is calculated using Eq. (1) [20].

$$\text{fitness\_function}(I_i) = (1 \,/\, \text{makespan}) \times \max(\text{utilization}) \tag{1}$$

Taking into account the individual execution of the processor, the average utilization is calculated. The operation of distinct processor can be calculated by using Eq. (2) [20].

$$\text{utilization}(I_x) = \text{completion\_time}(I_x)/\text{makespan} \tag{2}$$

The usage of optimized average processor is utilized to avoid those processors which are being unused for long period of time [1, 20].

The average of total execution time of all task assigned to the processors is called as the objective function of this problem which is calculated as shown in Eq. (3). In this case, m is considered as a number of processors. The purpose is to minimize Eq. (3). At this point, the balance between the processor utilization and the optimum schedule clearly indicated by this value.

$$\text{Objective function} = \min\left\{\frac{\sum_{i=1}^{m} \text{fitness\_function}(I_i)}{m}\right\} \tag{3}$$

The objective is to get the minimum value of total execution time of allocated task.

3 Methodology

The nature-inspired algorithm, WCA, introduced in [13, 21], is derived from the hydrologic cycle process as shown in Fig. 1, consisting of 5 stages such as (a) transpiration (the evaporation of water is from rivers and lakes at the same time as discharge of water by the plants during photosynthesis), (b) condensation (generation of cloud in atmosphere that condenses and makes it colder), (c) precipitation (release of water to earth like melting of ice), (d) percolation (reservation of water in field termed as groundwater) and (e) evaporation (water released from the underground converted into a stream through evaporation). For more detailed study on WCA, one can refer to [13, 21].

The proposed strategy starts from a primary population called the raindrops resulting from rain or precipitation. To start with, we expect that we have downpour or precipitation [13]. We know that the streams are made from the raindrops and connect one another to shape new rivers. A percentage of the streams might likewise stream straightforwardly to the ocean. All rivers and streams wind up in ocean which is a best optimal point. The outlook of flow of streams toward a particular river is presented in Fig. 2, where star denotes river and circle denotes stream, respectively.

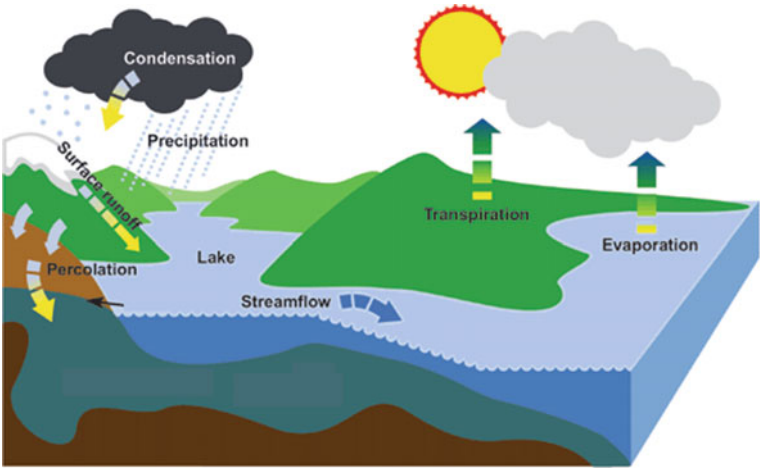

Fig. 1 Hydrologic cycle process

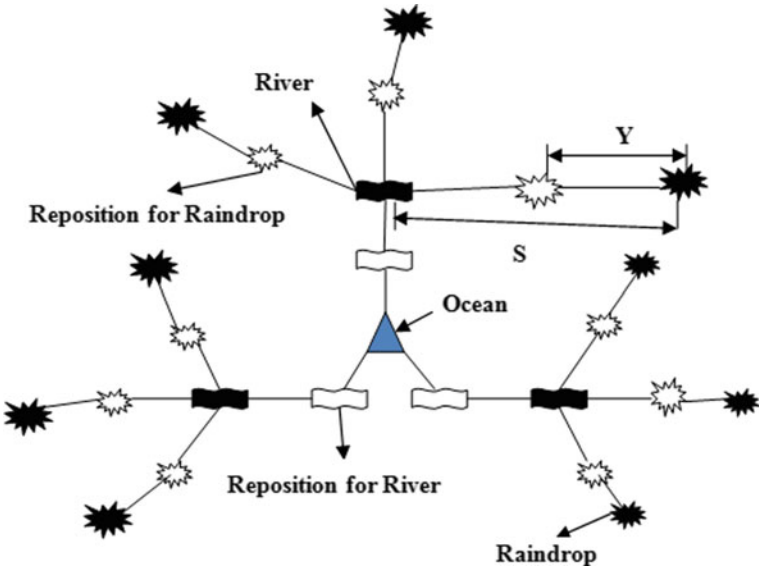

Fig. 2 Flow of stream (raindrop) to river and river to ocean

Initially, raindrops are created at arbitrary and the good raindrop is computed which chooses the integrity of the schedule. In the first place, we accept that we have downpour or precipitation [13]. The best individual that is best raindrop is picked as an ocean. At that point, various great raindrops are picked as a river and whatever is left of the raindrops is considered as streams which stream to the rivers

and ocean. A similar system is rehashed up to the maximum number of cycles determined, and then, an optimal solution is obtained. The proposed technique is delineated in Fig. 2, representing the raindrop, river and ocean. In the proposed method, Fig. 2 shows the "guidance points" are the rivers, various best picked points excluding the best one (ocean), utilized for managing other individuals in the population in the direction of better locations. Moreover, rivers are changeable points and move to the ocean. The unfilled white shapes describe relocation of streams (raindrop) and rivers. Steps of WCA are reproduced below for ease of reading.

Step 1 Select the initial parameters known as raindrops. In WCA, the raindrops play same role as "chromosome" in GA or "particle position" in PSO. The rain drop is defined as [21]:

$$\text{A stream or Raindrop} = [x_1, x_2, x_3, \cdots, x_N] \tag{4}$$

Step 2 Consider no. of raindrops is N_{pop} and *no*. of variables is defined as N_{var}. Generate the random initial population use Eq. (4) and.

$$\text{Population of Raindrops} = \begin{bmatrix} \text{Raindrops}_1 \\ \text{Raindrops}_2 \\ \text{Raindrops}_3 \\ \vdots \\ \text{Raindrops}_{N_{\text{pop}}} \end{bmatrix} = \begin{bmatrix} x_1^1 & x_2^1 & \cdots & x_{N_{\text{Var}}}^1 \\ x_1^2 & x_2^2 & \cdots & x_{N_{\text{Var}}}^2 \\ \cdots & \cdots & \cdots & \cdots \\ x_1^{N_{\text{pop}}} & x_2^{N_{\text{pop}}} & \cdots & x_{N_{\text{Var}}}^{N_{\text{pop}}} \end{bmatrix} \tag{5}$$

Step 3 Compute the fitness of raindrops using [13]:

$$\text{Cost}_i = f\left(x_1^i, x_2^i, \cdots, x_{N_{\text{Var}}}^i\right) \qquad i = 1, 2, 3, \cdots, N_{\text{pop}} \tag{6}$$

Step 4 Out of N_{pop} rain drops, N_{rs} best individuals are chosen as rivers and ocean. Find the number of rivers using as:

$$N_{\text{rs}} = \text{No. of Rivers} + 1 \tag{7}$$

Step 5 The best raindrop is selected as the ocean, and the remaining population is considered as streams or raindrops flows to the ocean and river using:

$$N_{\text{Raindrops}} = N_{\text{pop}} - N_{\text{rs}} \tag{8}$$

Step 6 Consider no. of streams as NS_n, streaming to a particular river or ocean. Determine the intensity of the flow of the ocean and rivers as:

$$NS_n = \text{round}\left\{\left|\frac{\text{Cost}_i}{\sum_{i=1}^{N_{\text{rs}}} \text{Cost}_i}\right| \times N_{\text{Raindrops}}\right\}, \qquad n = 1, 2, \ldots, N_{\text{rs}} \tag{9}$$

The separation of an individual stream flowing to a specific river is decided by

$$Y \in (0, L \times s), \qquad L > 1 \tag{10}$$

where L is a user defined somewhere around 1 and 2, i.e., $L = 2$ [13].
s is the current distance between stream and river.
Y is a number between 0 and $(L \times s)$ with any distribution.

Step 7 Flow of the streams into the rivers is calculated by using Eq. (11).
The new location for streams and rivers is computed as [13]

$$Y_{\text{Stream}}^{i+1} = Y_{\text{Stream}}^{i} + \text{rand} \times L \times \left(Y_{\text{River}}^{i} - Y_{\text{Stream}}^{i}\right) \tag{11}$$

Step 8 Flow of the rivers into the ocean (the most downhill location) is calculated using:

$$Y_{\text{River}}^{i+1} = Y_{\text{River}}^{i} + \text{rand} \times L \times \left(Y_{\text{Sea}}^{i} - Y_{\text{River}}^{i}\right) \tag{12}$$

where rand is an equally circulated random number somewhere around 0 and 1 [13, 21].

Step 9 Trade the position of the stream with the river in order to obtain the best solution.

Step 10 Like Step 7, the location of the river traded when a river discovers preferred solution over the ocean.

Step 11 Check the conditions of the evaporation using:

$$\text{if } \left|Y_{\text{Sea}}^{i} - Y_{\text{River}}^{i}\right| < s_{\max} \qquad i = 1, 2, \ldots, N_{\text{rs}} - 1 \tag{13}$$

where $s_{\max} \cong 0$ is a small value which controls the search depth, near the ocean.
Evaporation decreases till it rains; hence, the value of $s_{\max}$ decreases at each of the iterations as

$$s_{\max}^{i+1} = s_{\max}^{i} - \frac{s_{\max}^{i}}{\text{max iteration}} \tag{14}$$

Step 12 Consider *LB* as lower bound value.
UB is upper bound value characterized by the assumed problem.
New arbitrarily produced raindrops form new streams in distinctive areas that can be found by using Eqs. (15) and (16) [21].

$$Y_{\text{Stream}}^{\text{new}} = LB + \text{rand} \times (UB - LB) \tag{15}$$

Consider $\sqrt{\mu}$ as the standard deviation and μ (usually = 0.1 [21]) characterizes the idea of variance which illustrates the scope of seeking area close to the ocean. rand n is an ordinarily appropriated arbitrary number. The convergence rate [21] and computational execution of the algorithm optimum point are determined by

$$Y_{\text{Stream}}^{\text{new}} = Y_{\text{sea}} + \sqrt{\mu} \times randn(1, N_{\text{var}}) \tag{16}$$

Step 13 Use Eq. (14) to reduce the value of $s_{\max}$ [13].

Step 14 Check the criteria of convergence. On the off-chance that the halting criteria are met, the procedure will stop, else it will go back to Step 7

The technique for moving streams to the rivers and afterward moving rivers to the ocean leads to roundabout move to the best solution. Figure 3 shows the flowchart of proposed WCA. Consequently, the grouping continues changing with time taking into account the coming of new tasks.

Consider an illustration of Table 1 consists of [tasks, processors] alike [4, 5] where every row stands for the processors related to a task that doles out, and [I_1, J_1] = 0 implies that task J_1 is not allotted to processor I_1 that is 0. [I_3, J_1] = 1 implies that the task J_1 is allotted to processor I_3 that is 1.

4 Simulations

Keeping in mind the end goal to assess execution of the proposed strategy using WCA, we have reproduced the performance of GA-, BFO-, GBF-based strategies for the purpose of comparison. Simulations were carried out using MATLAB. Minimization of execution time was taken as the criteria.

Assume the no. of processor is 4 and the no. of task is 5. From this combination, we selected "S_1" number of task assigned to the processor. In WCA, S_1 is equal to N_{sr} (no. of rivers), i.e., $N_{\text{rs}} = S_1$. The parameters were situated at: $N_{\text{pop}} = 100, N_{\text{var}} = 10, s_{\max} = 1e-5, LB = -1, L = 2, s$ is any random value, "g" stands for the no. of streams, and the value is set to 20. Arbitrarily picked no. of stream hold in an array "c" framed utilizing [tasks, processors] form alike [4, 5]. c [I_1, J_1] = 0 implies that task J_1 is not allotted to processor I_1 that is 0. c [I_3, J_1] = 1 implies that the task J_1 is allotted to processor I_3 that is 1. S_1 is produced utilizing "c" that indicates total no. of tasks allocated. Maximum no. of iterations is 100.

The reproduction of GBF, BFO and GA calculations has taken up to 100 emphases. Compare this entire algorithm with our proposed WCA and get the feasible solution of multiprocessor scheduling problem. Here we have considered

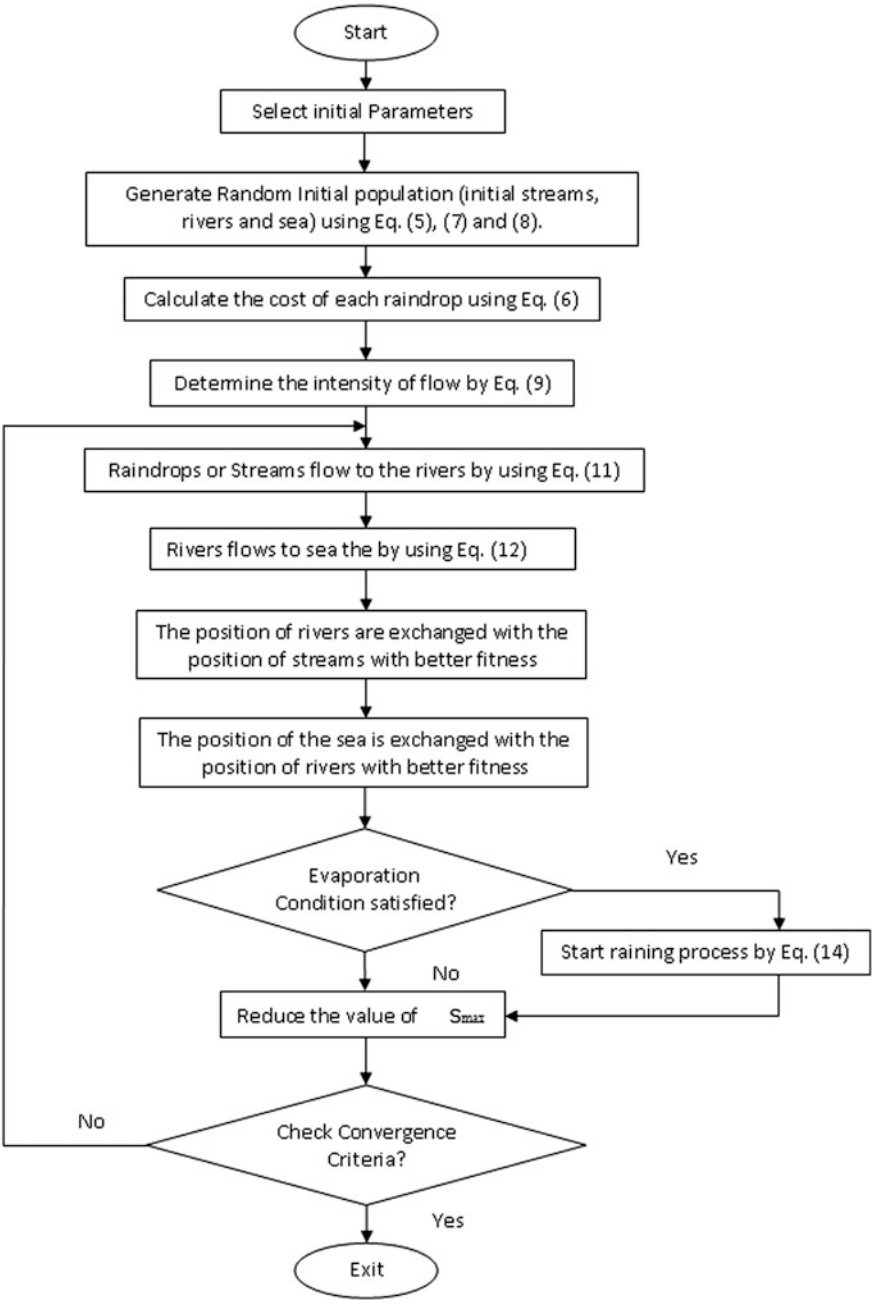

Fig. 3 Flowchart of proposed WCA

Table 1 Example of task assignment

Processor	J_1	J_2	J_3	J_4	J_5
I_1	0	1	1	0	0
I_2	0	0	1	0	1
I_3	1	0	1	1	1
I_4	0	0	1	1	0

four cases to prove our proposed algorithm, WCA, which finds the best solution according to the number of tasks and processors.

Case 1 Fixed no. of task and fixed no. of processors.
Case 2 Impact of the no. of processors.
Case 3 Impact of the no. of tasks.
Case 4 Impact of the no. of tasks and processors.

Case 1: Fixed no. of task and fixed no. of processors

Execution times are as shown in Figs. 4, 5, 6 and 7. Figures 4, 5, 6 and 7 demonstrate the performance result of GA, BFO, GBF and WCA algorithms, respectively, with the correlation among execution time, and no. of repetitions is 100. The execution consequences of all methods over fitness function are recorded in Table 2, examined that the proposed WCA finished in a general sense better execution on all esteems over the GBF, BFO and GA calculations.

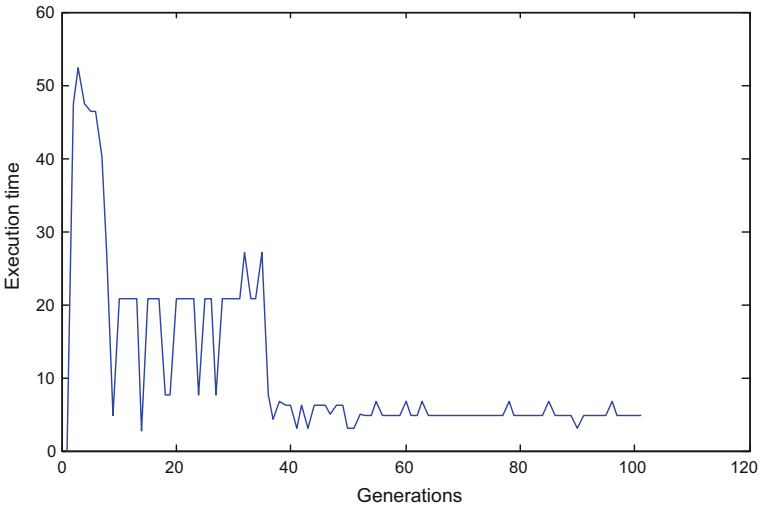

Fig. 4 Performance results of GA

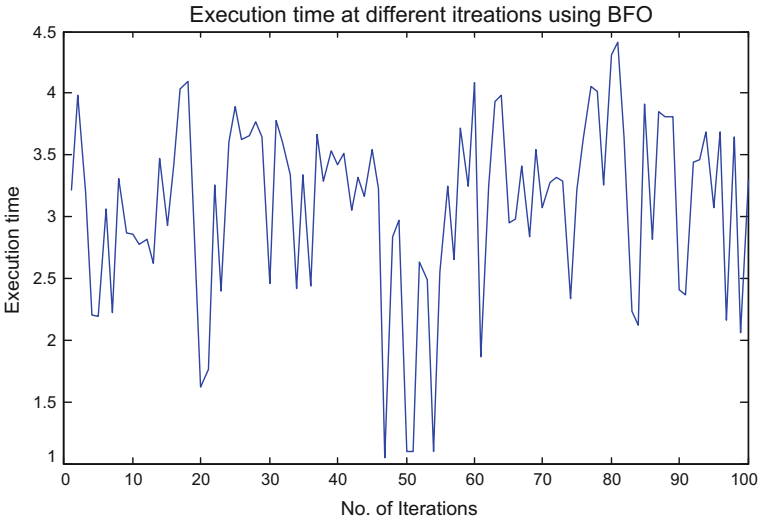

Fig. 5 Performance results of BFO

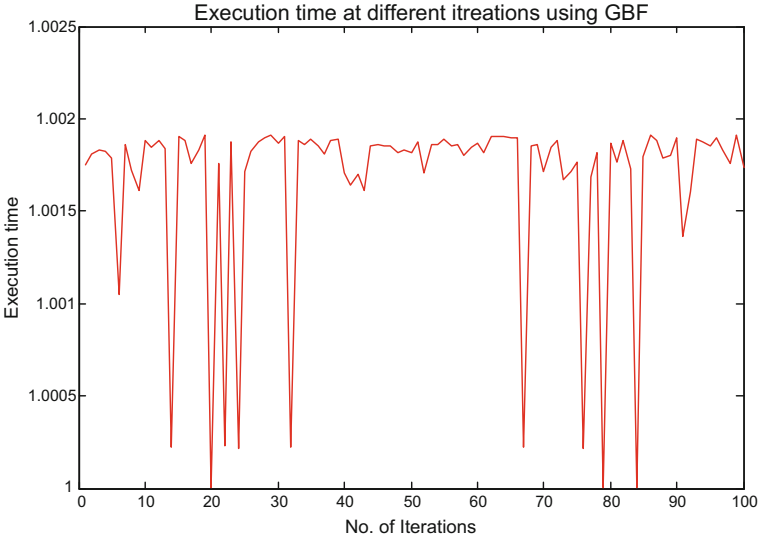

Fig. 6 Performance results of GBF

The parameters for this test result are shown below:

No. of task = 5
No. of processor = 4
No. of iteration = 100.

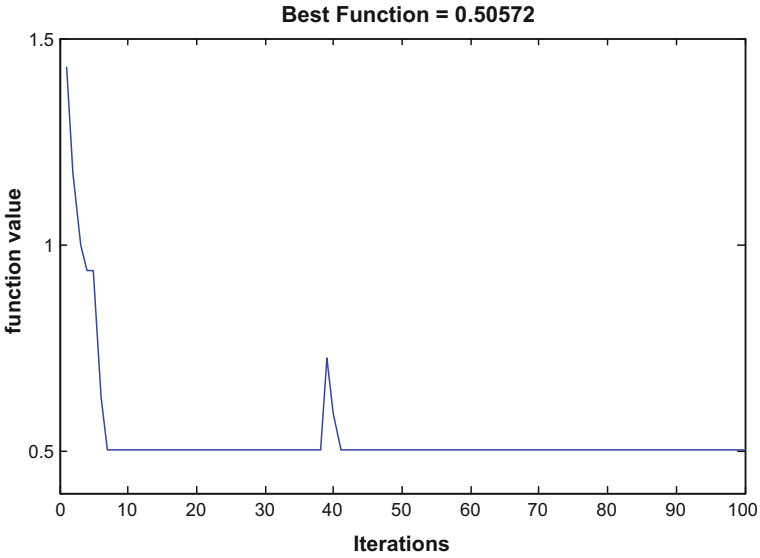

Fig. 7 Performance results of WCA

Table 2 Comparison between the performance of GA, BFO, GBF and WCA algorithms based on execution time and no. of repetitions with fixed number of task and processors

Iteration no.	GA	BFO	GBF	WCA
10	20.7714	2.8541	1.0019	0.50572
20	20.7714	1.6157	1.0000	0.50572
30	20.7714	2.4556	1.0019	0.50572
40	3.1269	3.4234	1.0017	0.59234
50	3.1269	1.0991	1.0018	0.50572
60	4.8984	4.0905	1.0019	0.50572
70	4.9010	3.0705	1.0017	0.50572
80	4.8984	4.3098	1.0019	0.50572
90	4.8984	2.4091	1.0019	0.50572
100	4.8984	3.2946	1.0017	0.50572

Case 2: Impact of the no. of processors

In this segment, we have presented simulation result for different processors with the same number of task of different execution time.

The parameters for this test result are shown below:

No. of task = 5
No. of processor = 7, 14, 21, 28, 35
No. of iteration = 100.

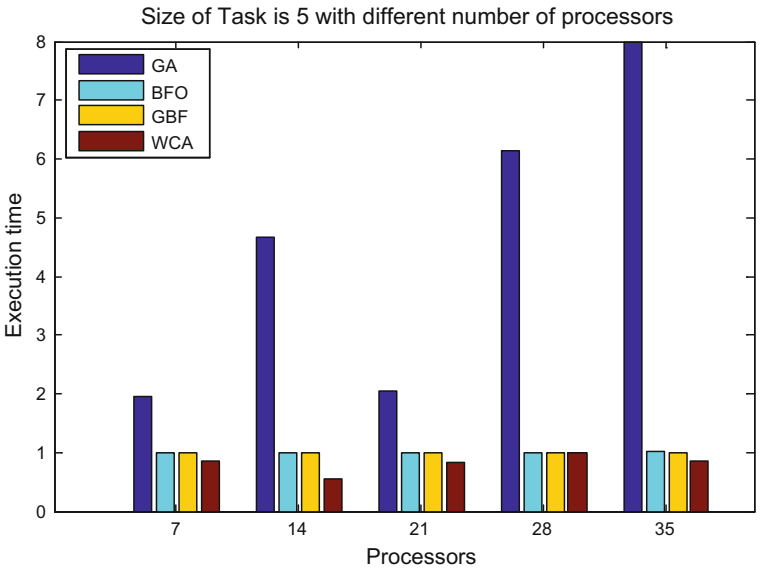

Fig. 8 Impact of number of processors on execution time

Table 3 Performance with variation in number of processors (fixed number of task = 5)

No. of processor	GA	BFO	GBF	WCA
7	1.9524	1.0000	1.0000	0.8527
14	4.6667	1.0000	1.0006	0.5564
21	2.0435	1.0000	1.0014	0.8200
28	6.1429	1.0007	1.0014	1.0000
35	8.0000	1.0218	1.0013	0.8462

The above-mentioned parameters are taken into different approaches, which result that our proposed algorithm, WCA, takes less execution time as depicted in Fig. 8.

The minimum execution time with the equal number of tasks assigned to various numbers of processors is shown in Table 3.

Here, execution time diminishes when quantity of processors expands, by using the proposed strategy. (WCA is compared to other mentioned algorithms.)

Case 3: Impact of the no. of tasks

In this segment, we have presented test result of different execution time for different no. of tasks with the same no. of processor as represented in Fig. 9 and the execution time is shown in Table 4. The parameters for this test result are shown below:

No. of task = 5, 10, 15, 20, 25
No. of processor = 4

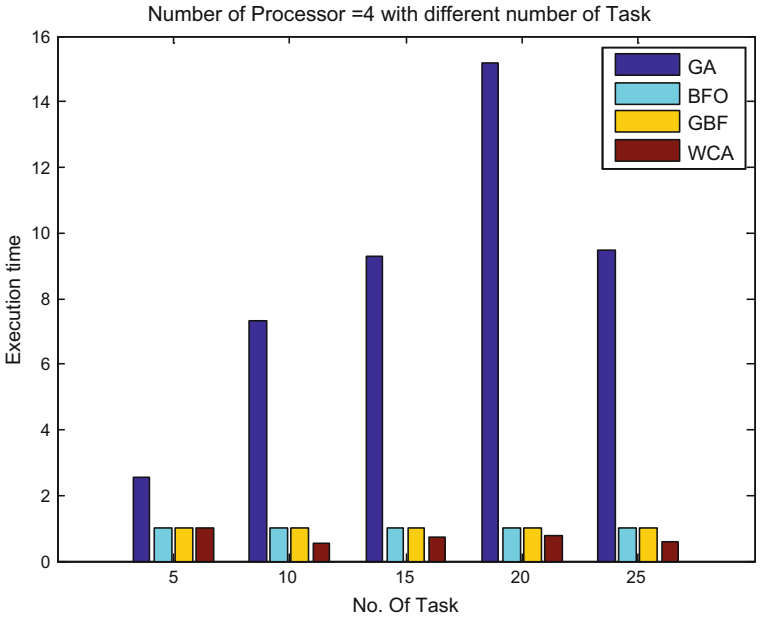

Fig. 9 Impact of number of tasks on execution time

Table 4 Performance with variation in number of tasks (fixed number of processor = 4)

No. of task	GA	BFO	GBF	WCA
7	2.5600	1.0054	1.0000	1.0000
14	7.3182	1.0000	1.0002	0.5259
21	9.2800	1.0000	1.0038	0.7351
28	15.1613	1.0000	1.0010	0.7949
35	9.4545	1.0000	1.0017	0.5720

No. of iteration = 100.

It is seen from the tests that when the no. of tasks expands, execution time diminishes by using the proposed strategy, WCA.

Case 4: Impact of the no. of tasks and processors.

In this section, we have presented the simulation of multiprocessor scheduling with different execution time from the different number of tasks and the different number of processors as represented in Fig. 10. The minimum execution time for different no. of task on different no. of processors is shown in Table 5. The parameters for this test result are shown below:

No. of task = 5, 11, 18, 26, 35
No. of processor = 6, 12, 18, 24, 30
No. of iteration = 100.

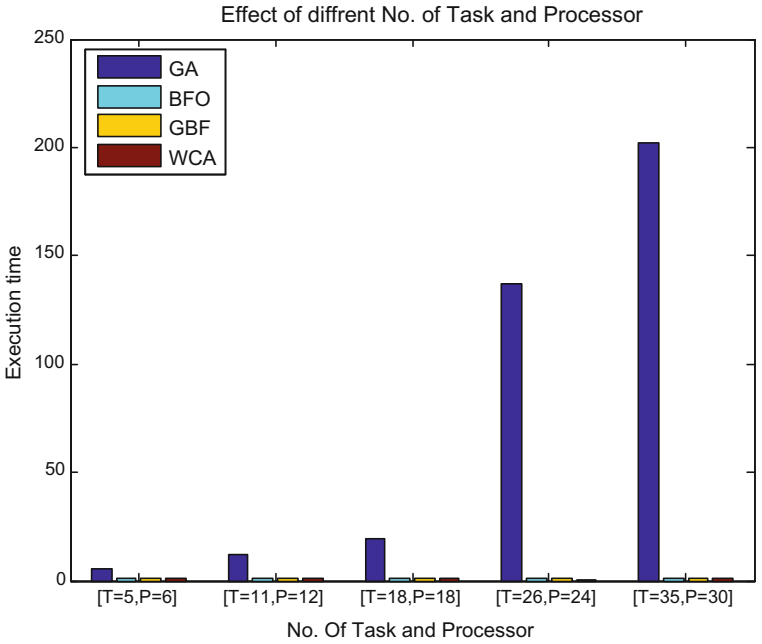

Fig. 10 Impact of change in number of processors and tasks

Table 5 Performance with variation in number of processors and tasks

No. of task	No. of processor	GA	BFO	GBF	WCA
5	6	5.4000	1.0071	1.0000	0.9278
11	12	12.3636	1.0224	1.0009	1.0000
18	18	19.4375	1.0785	1.0008	0.9114
26	24	137.0000	1.0000	1.0014	0.6478
35	30	202.0000	1.0000	1.0058	1.0000

It is seen from the tests that even if the number of task and processors increases, the proposed strategy, WCA, is getting the minimum execution time as compared with the other algorithms.

Except for the first case, in all the other cases we have taken 35 maximum numbers of tasks and processors but further it can increase or decrease the numbers to get the preferred execution time. From the outcomes, we study that the proposed WCA accomplished fundamentally better execution on all esteems over the GBF, BFO and GA methods.

5 Conclusion

This paper introduced a novel strategy for multiprocessor scheduling using water cycle algorithm. It has proved that proposed strategy gives a good result with lesser execution by simulation. The paper also shows a pointer for future work as the proposed strategy can be extended to other scheduling problems.

References

1. Sasmita Kumari Nayak, Sasmita Kumari Padhy, Siba Prasada Panigrahi, "A Novel algorithm for dynamic task scheduling", Future Generation Computer Systems, 2012, Volume 28, Issue 5, Pages 709–717.
2. Fatma A. Omara, Mona M. Arafa, Genetic algorithms for multiprocessor scheduling problem, Journal of Parallel and Distributed Computing 70 (1) (2010) 13–22.
3. Orhan Engin, Gülşad Ceran, Mustafa K. Yilmaz, An efficient genetic algorithm for hybrid flow shop scheduling with multiprocessor task problems, Applied Soft Computing 11 (3) (2011) 3056–3065.
4. Savaş Balin, Non-identical parallel machine scheduling using genetic algorithm, Expert Systems with Applications 38 (6) (2011) 6814–6821.
5. P. Brucker, Scheduling Algorithms, third ed., Springer, Berlin, 2001.
6. Hans-Ulrich Heiss, Michael Schmitz, Decentralized dynamic load balancing: the particles approach, Information Sciences 84 (2) (1995) 115–128.
7. Dar-Tzen Peng, Kang G. Shin, Tarek F. Abdelzaher, Assignment and scheduling communicating periodic tasks in distributed real-time systems, IEEE Transactions On Software Engineering 23 (12) (1997) 745–758.
8. Tzu-Chiang Chiang, Po-Yin Chang, Yueh-Min Huang, Multi-processor tasks with resource and timing constraints using particle swarm optimization, IJCSNS International Journal of Computer Science and Networking Security 6 (4) (2006) 71–77.
9. Elsadek A. Abdelmageed, Wells B. Earl, A heuristic model for task allocation in heterogeneous distributed computing systems, The International Journal of Computers and Their Applications 6 (1) (1999) 1–36.
10. P. Chitra, R. Rajaram, P. Venkatesh, Application and comparison of hybrid evolutionary multiobjective optimization algorithms for solving multiprocessor scheduling problem on heterogeneous systems, Applied Soft Computing 11 (2) (2011) 2725–2734.
11. Yun Wen, Hua Xu, Jiadong Yang, A heuristic-based hybrid genetic-variable neighborhood oceanrch algorithm for multiprocessor scheduling in heterogeneous multiprocessor system, Information Sciences 181 (3) (2011) 567–581.
12. Wang Chen, Yan-jun Shi, Hong-fei Teng, Xiao-ping Lan, Li-chen Hu, An efficient hybrid algorithm for resource-constrained project scheduling, Information Sciences 180 (6) (2010) 1031–1039.
13. Eskandar H, S.A., Bahreininejad A, Hamdi M, "Water cycle algorithm—A novel metaheuristic optimization method for solving constrained engineering optimization problems", Computers and Structure, 2012. 110–111: pp. 151–166.
14. Lee KS, Geem ZW. A new meta-heuristic algorithm for continuous engineering optimization: harmony oceanrch theory and practice. Comput Meth Appl Mech Eng 2005; 194: 3902–33.
15. Kennedy J, Eberhart R. Particle swarm optimization. In: Proceedings of the IEEE international conference on neural networks. Perth, Australia: 1995. p. 1942–8.
16. Kirkpatrick S, Gelatt C, Vecchi M. Optimization by simulated annealing. Science 1983; 220: 671–80.

17. Holland J. Adaptation in natural and artificial systems. Ann Arbor, MI: University of Michigan Press; 1975.
18. Goldberg D. Genetic algorithms in oceanrch, optimization and machine learning. Reading, MA: Addison-Wesley; 1989.
19. Coello CAC. Theoretical and numerical constraint-handling techniques used with evolutionary algorithms: a survey of the state of the art. Comput Meth Appl Mech Eng 2002; 191: 1245–87.
20. S.N. Sivanandam. "Dynamic task scheduling with load balancing using parallel orthogonal particle swarm optimisation", International Journal of Bio-Inspired Computation, 2009.
21. Mani Ashouri, Seyed Mehdi Hosseini, "Application of Krill herd and Water cycle algorithms on Dynamic Economic Load Dispatch Problem", IJIEEB, 2014, (4), pp: 12–19.

Estimating Software Reliability Growth Model Parameters Using Opposition-Based Shuffled Frog-Leaping Algorithm

Tarun Kumar Sharma

Abstract Software engineering (SE) is concerned with designing, developing and maintaining programs that behave reliably and efficiently. SE is composed of various phases which software goes through during and after its development. In today's prospects, predicting quality of software is a quite challenging task. This study focuses on a recent bio-inspired algorithm named shuffled frog-leaping algorithm (SFLA) for estimating parameters of software reliability growth models (SRGM). Most of the bio-inspired algorithms are inspired by some real-world phenomenon, generally a natural method of optimization. Over the last few decades, a number of bio-inspired algorithms have been introduced and applied on various problems of different domains. SFLA embeds features of particle swarm optimization (PSO) and shuffled complex evolution (SCE) algorithms. It is evident from the literature that SFLA can be efficiently applied to solve various engineering design problems. A variant of SFLA named O-SFLA that embeds opposition-based learning is also introduced in this study. This variant has been evaluated on a set of benchmark problems, which have been verified by performing nonparametric analysis. Later the application of O-SFLA has been carried out on estimating parameters of software reliability growth models (SRGM).

Keywords Shuffled frog-leaping algorithm · SFLA · Opposition-based learning OBL · Software reliability growth models · Global optimization

1 Introduction

Quality can be defined as conformance to predefined standards, whereas reliability is failure-free process in said conditions and defined time. Software reliability may be defined as failure-free operation in a defined time and environment [1–3]. This is why software developing is a challenging process in the competitive market, as the

T. K. Sharma (✉)
Amity University Rajasthan, Jaipur, India
e-mail: taruniitr1@gmail.com

K. Ray et al. (eds.), *Soft Computing Applications*, Studies in Computational Intelligence 761, https://doi.org/10.1007/978-981-10-8049-4_8

market desires quality product with the restriction of time. The demand of the market is highly unstable. This keeps changing with respect to time. That is why developing quality software becomes more challenging. Developed software must be capable enough of meeting changing requirements. The software development process is a layered process also named as software development life cycle (SDLC). There are various phases in SDLC that starts from problem identification followed by information gathering, analysis, designing, developing, testing and implementing. So change in any phase may result in poor quality of developed software. The development of software involves several issues and goals like reliability, overrun of costs, user requirements. The improvement in software process has important practical significance to defuse software crisis, as it influences the development and management of software.

This study focuses on the testing phase of the software development where SFLA and a variant have been applied in predicting the faults. This study uses the software historical data to perform the analysis.

SFLA, introduced in 2003 by Eusuff and Lansey [4, 5], is a recent member of memetic algorithms family. SFLA, like other memetic algorithms, is enthused by natural foraging behavior of species. In SFLA, these natural species are frogs. Since its introduction, SFLA and its variants have been successfully applied to solve many real-world optimization problems of versatile engineering and management domain. The same can be witnessed from the literature. SFLA embeds the features of both particle swarm optimization (PSO) and shuffled complex evolution (SCE) algorithms. PSO helps in performing local search, while SCE helps in global search. In SFLA, like other memetic algorithms, colony of frogs is initialized randomly and in second step, the colony is divided into subcolonies or memeplexes. SFLA performs both exploration by dividing the randomly initialized population of frogs into number of memeplexes and exploitation by performing evolution process in each of the memeplexes. Although SFLA emerges as successful optimizer, it also suffers in global convergence velocity. In this study, a modification in the memeplexes is introduced by embedding the concept of opposition-based learning. In general structure of SFLA, the frogs are divided into memeplexes based on their fitness values where they forage for food. In the proposed variant, the opposition-based learning concept is embedded into each memeplexes before the frog initiates foraging. After each iteration when information exchange process among memeplexes is performed, OBL is again introduced to improvise global search. The proposal is named as O-SFLA. This modification not only enhances local search mechanism of SFLA but also improves the diversity. The performance of the O-SFLA is evaluated on 6 well-known benchmark optimization functions referred from the literature and on estimating the parameters of SRGM.

The structure of the study is as follows: Sect. 2 discusses the SRGM. Section 3 describes SFLA in brief followed by the proposed scheme in Sect. 4. Test bed, experimental settings and computational results are presented and analyzed non-parametrically in Sect. 5. Section 6 presents the conclusions drawn and future work plan.

2 SRGM: Software Reliability Growth Models

Failure process modeling represents a challenge because of the various natures of faults discovered and the methodologies to be used in order to isolate the faults [3, 6]. Many software techniques were developed to assist in testing the software before its final release for public use. Most of these techniques are simply based on building prediction models that have the ability to predict future faults under different testing conditions [7]. These models are normally called *software reliability growth models*. Several reliability models of software have been introduced since last few decades and are a research subject to many researchers. In this work, three reliability models, namely exponential (EXP), power (POW) and delayed S-shaped (DSS) models, have been studied. The details of the models are as follows:

2.1 EXP Model

This model was initially introduced in [8, 9]. This model is known as a finite failure model. The relationship among various parameters is given as:

$$\begin{aligned} \mu(t;\beta) &= \beta_0(1 - e^{-\beta_1 t}) \\ \lambda(t;\beta) &= \beta_0\beta_1 e^{-\beta_1 t} \end{aligned} \tag{1}$$

$\mu(t;\ \beta)$ and $\lambda(t;\ \beta)$ represent the mean failure function and the failure intensity function, respectively. The parameter β_0 is the initial estimate of the total failure recovered at the end of the testing process (i.e., v_0). β_1 represents the ratio between the initial failure intensity λ_0 and total failure $v0$. Thus, $\beta_1 = \lambda_0/v_0$. It is important to realize that:

$$\lambda(t;\beta) = \frac{\partial \mu(t;\beta)}{\partial t} \tag{2}$$

2.2 POW

The model objective is to compute the reliability of a hardware system during testing process. It is based on the non-homogeneous Poisson process model and is provided in [10]. The equations which govern the relationship between the time t and $\mu(t;\ \beta)$ and $\lambda(t;\ \beta)$ are:

$$\begin{aligned} \mu(t;\beta) &= \beta_0 t^{\beta_1} \\ \lambda(t;\beta) &= \beta_0\beta_1 t e^{\beta_1 - 1} \end{aligned} \tag{3}$$

2.3 DSS

This model describes the software reliability process as a delayed S-shaped model [11]. It is also a finite failure model. The system equation for $\mu(t;\beta)$ and $\lambda(t;\beta)$ is:

$$\begin{aligned} \mu(t;\beta) &= \beta_0(1-(1+\beta_1 t)e^{-\beta_1 t}) \\ \lambda(t;\beta) &= \beta_0\beta_1^2 t^{-\beta_1 t} \end{aligned} \tag{4}$$

3 Brief Description of SFLA

SFLA, introduced by Eusuff and Lansey in 2003, has been successfully implemented in solving many real-world optimization problems. SFLA performed at par when compared to GA, PSO and ant colony optimization (ACO) algorithms [4, 5]. Researchers have proposed many improved variants of SFLA and applied them to many applications of science, engineering and management [4, 12–25].

SFLA is a memetic algorithm that is inspired from foraging behaviors of natural species called frogs. SFLA has the abilities to perform local search process as in PSO algorithm and at the later stage information sharing between memeplexes. The next paragraph details the working principle of SFLA.

Like in other memetic algorithms, a population of frogs (solutions) is randomly initialized in feasible search space. Then, frogs are distributed into small colonies called memeplexes. This is done by calculating fitness values using objective function. Now each memeplex contains frogs from different cultures, and each frog is supposed to perform local search process in order to modify worst's frog position (in terms of fitness value). This process, within each memeplex, is performed till some fixed criterion or generations. This process also helps in optimization. Later, the information or idea hold by the frogs in each memeplex is then exchanged among other memeplexes through shuffling process. Both local search process and information exchange process are performed till the fixed number of iterations. In general, there are 4 steps in basic SFLA and they are as follows.

3.1 Initialization of Frog Population

The population of frogs is randomly initialized between fixed upper and lower bounds, i.e., (ub_j) and (lb_j), using Eq. (5): Set of frogs is presented by F.

$$x_{ij} = lb_i + \text{rand}\,(0,1) \times (ub_i - lb_i) \tag{5}$$

where rand (0,1) is random number between zero and one which is uniformly distributed; i = 1, 2, …, F; j = 1, 2, …, D (dimension).

3.2 Sorting and Division of Frogs in Memeplexes

The fitness of each frog is calculated and then sorted in descending order. Then, division of sorted population is done into m memeplexes such that $F = m$ (memeplexes) × n (number of frogs in each memeplex). The division of frogs is done such that the frog with higher fitness value will be the part of first memeplex, accordingly the next frog into second memeplex, and following fashion frog m + 1 will again move to the 1st memeplex, and so on.

3.3 Local Searching Process

Global best (X_{global}), best (X_{best}) and worst (X_{worst}) frogs based on fitness values in each memeplex are noted. Now, an evolution process is implemented to update the position of worst frogs only using the following Eqs. (6) and (7):

Worst frog's updated position

$$\begin{aligned} X_{\text{new}} &= \text{current position}\,(X_{\text{worst}}) + \text{Mov}_t \\ &\quad - \text{Mov}_{\max} \le \text{Mov}_t \le \text{Mov}_{\max} \end{aligned} \tag{6}$$

where

$$\text{Mov}_t = \text{rand}\,(0,1) \times (X_{\text{best}} - X_{\text{worst}}) \tag{7}$$

where t and Mov_t represent the generations (1, 2, …, N_{gen}) and movement of a frog, respectively. $\text{Mov}_{\max}$ is the maximum acceptable frog movement in the feasible region. When using above equations, the worst frog's position shows significant improvement and then the position of worst frog is updated; otherwise, the same process using Eqs. (6) and (7) is repeated with respect to the global best frog (i.e., X_{global} replaces X_{best}). If the process shows no improvements, then a new solution is

randomly generated using Eq. (5) to update the position of worst frog. This is an iterative process which continued till the maximum number of generations (N_{gen}).

3.4 Information Exchange or Shuffling Process

Information exchange is performed among memeplexes, or the frogs are sorted and shuffled again to perform the evolution process. This process again continues till the fixed number of iterations.

The searching process and basic SFLA algorithm are depicted in Figs. 1 and 2, respectively.

4 Proposed O-SFLA

SFLA has three phases, initialization of frog positions, local search process in each memeplex and information exchange, i.e., shuffling process. SFLA performs both exploration and exploitation. However, because of poor exploration capabilities SFLA sometimes gets trapped in local optima, which results in poor convergence. In this study, OBL is introduced in the structure of basic SFLA to eliminate its limitations.

OBL

This concept was introduced by Tizhoosh [26]. The opposite positions of frogs can be calculated using Eq. (8):

$$x_{ijOpp} = \alpha_j - \beta_j - x_{ij} \tag{8}$$

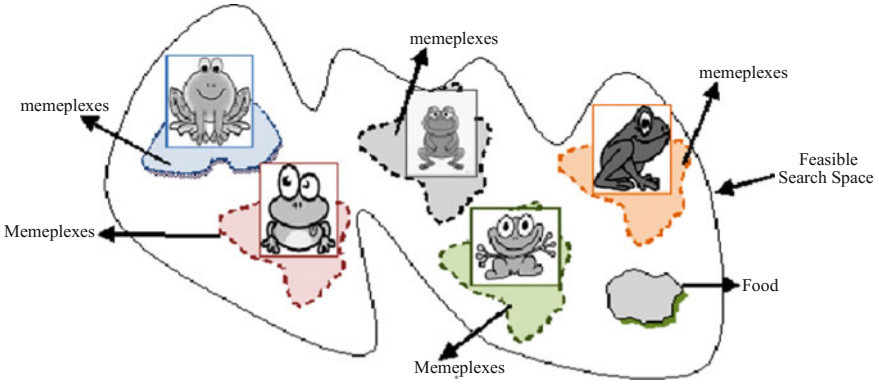

Fig. 1 Frogs performing local search initially and then exchanging information with other memeplexes

Algorithm – Basic SFLA

Step 1: Initial population of frog size F is generated and evaluated (fitness value)
Step 2: Distribute the population of frog in m memeplexes where each memeplex contains n fog members such that $F = m$ x n.
Step 3: Start Evolutionary process
Step 4: Set $i = 1$
Step 5: while $i \leq i_{max}$
Step 6: Identify the global best (x_g) position of frog in the population.
Step 7: Identify the worst (x_{worst}) and best (x_{best}) frog in each memeplex.
Step 8: Apply eq. (2) & (3) to generate new frog position and evaluate.
Step 9: **If** $f(x_{new}) < f(x_{worst})$
Step10: Set $x_{worst} = x_{new}$ and go to Step 13.
Step 11: $x_{best} = x_{global}$. Repeat Step 8 & Step 9.
Step 12: Random position is generated and replaced with x_{worst}.
Step 13: $i = i + 1$
Step 14: End While
Step 15: Population of frog is shuffled.
Step 16: If fixed termination criterion (N_{gen}) is achieved then exit else go to Step 2.

Fig. 2 SFL algorithm

where the upper range and lower range of search process are represented by α and β; Frogs by $i = 1, 2, \ldots, F$; and problem's dimension by $j = 1, 2, \ldots, D$.

Embedded OBL in O-SFLA

In the present study, OBL has been employed in local search process of SFLA to improve positions of frogs within memeplex. In each memeplex, opposite positions are generated using OBL (shown in Fig. 3) and then, elite n positions are selected based on fitness values $(f(n_{pop}) \cup f(n_{\mathrm{OBL-pop}}))$. Further, in order to enhance diversity and convergence, one extra step to improve the performance of memeplex is included in the structure of basic SFLA (STEP14) in Fig. 4.

The proposed algorithm is discussed in Fig. 4.

5 Test Bed, Experimental Settings and Results

To validate efficacy of the proposal, ten unimodal and multimodal benchmark functions are referred from the literature [16, 27]. These functions are Sphere (F1), Rosenbrock (F2), Step (F3), Rastrigin (F4), Ackley (F5) and Griekwank (F6). The search space taken for Sphere is [−100, 100], Rosenbrock [−30, 30], Step [−100, 100], Ackley [−32, 32], Rastrigin [−5.12, 5.12] and Griekwank [−600, 600] with the dimension of 30. The optimum value in each case is 0. The population of frog is fixed to 200 with 20 memeplexes. There will be 10 frogs in each memeplexes performing local search. Ten generations are performed in each memeplexes to explore the local region. The maximum movement step is fixed to 0.5 times of the

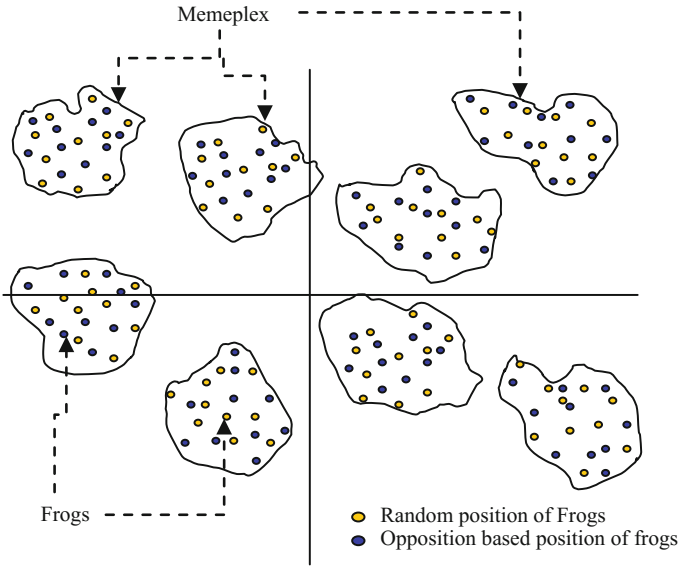

Fig. 3 Generation of opposite position of frogs in each memeplex

search area. Twenty-five runs are performed to evaluate mean function value and standard deviation. The simulations are performed on Dev C++ following machine configurations: Intel(R) CPU T1350@1.86 GHz with 1 GB of RAM.

6 Simulated Results

6.1 Benchmark Problems

The results of O-SFLA are compared with that of PSO, ABC, SFLA and a recent variant of SFLA, i.e., EOLSFLA [27]. In order to perform unbiased comparison of O-SFLA with the performance of the other evolutionary algorithms, the population size is kept same with their standard parameter values. The comparative results [mean fitness values (mean) and standard deviation (std. dev)] are given in Tables 1 and 2, respectively, where F_{un} is function.

It can be analyzed from the simulated results presented in Table 2 that the O-SFLA outperforms or at par with the results of most of the algorithms for all functions, except F_4 where EOLSFLA outperforms all the algorithms. Results

Proposed Algorithm: O – SFLA

Step 1: Initial population of frog size N is generated and evaluated (fitness value)

Step 2: Distribute the population of frog in m memeplexes where each memeplex contains n_{pop} fog members such that $F = m$ x n.

Step 3: Start Evolutionary process

Step 4: Set $i = 1$

Step 5: while $i \leq i_{max}$

Step 6: Identify the global best (x_g) position of frog in the population.

Step 7: Apply OBL to generate opposition positions of frogs ($n_{OBL\text{-}pop}$) in each memeplex.

Step 8: Select the elite n frogs positions from a set of $n_{pop} \cup n_{OBL\text{-}pop}$ based on fitness values.

Step 9: Identify the worst (x_{worst}) and best (x_{best}) frog in each memeplex.

Step10: Apply eq. (2) & (3) to generate new frog position and evaluate.

Step11: **If** $f(x_{new}) < f(x_{worst})$

Step12: Set $x_{worst} = x_{new}$ and go to Step 16 .

Step13: $x_{best} = x_{global}$. Repeat Step 11 & Step 12.

Step14: Apply OBL to generate opposite point of x_{worst} i.e. $x_{OBL\text{-}worst.}$ If $f(x_{OBL\text{-}worst}) < f(x_{worst})$ go to Step 16.

Step15: Random position is generated and replaced with x_{worst}.

Step16: $i = i + 1$

Step17: End While

Step18: Population of frog is shuffled.

Step19: If fixed termination criterion (N_{gen}) is achieved then exit else go to Step 2.

Fig. 4 O-SFL algorithm

Table 1 Comparative simulated results in terms of mean of PSO, ABC, SFLA, EOLSFLA and the proposal O-SFLA

F_{un}	PSO	SFLA	ABC	EOLSFLA	O-SFLA
F_1	9.6E−07	6.5E+00	1.2E−12	0.0E+00	**0.0E+00**
F_2	2.6E−04	3.0E+01	3.0E+01	2.4E+01	**1.9E+01**
F_3	0.0E−00	1.6E+01	0.0E+00	0.0E+00	**0.0E+00**
F_4	7.9E−00	5.1E+00	2.4E+07	**0.0E+00**	4.7E+01
F_5	6.8E−01	7.8E−01	4.0E−06	5.9E−16	**2.2E−19**
F_6	1.8E−02	1.5E−01	1.0E−09	1.2E−14	**1.1E−16**

Best results are highlighted in bold

Table 2 Comparative simulated results in terms of standard deviation of PSO, ABC, SFLA, EOLSFLA and the proposal O-SFLA

F_{un}	PSO	SFLA	ABC	EOLSFLA	O-SFLA
F_1	±7.2E−06	±8.3E+01	±5.1E−12	±0.0E+00	±0.0E+00
F_2	±2.6E+05	±0.0E+00	±1.3E+00	±7.5E+01	±3.6E+01
F_3	±0.0E+00	±1.9E+02	±0.0E+00	±0.0E+00	±0.0E+00
F_4	±1.9E+02	±1.3E+12	±2.9E+06	**±0.0E+00**	±7.0E+01
F_5	±9.2E+00	±3.8E+00	±9.9E−06	±0.0E+00	±3.0E−17
F_6	±1.0E−01	±5.7E−01	±1.0E−08	±1.6E−13	±5.2E−15

Best results are highlighted in bold

Table 3 Friedman's rank

Algorithm	Rank
PSO	3.01
ABC	2.80
SFLA	2.67
EOLSFLA	2.1
O-SFLA	1.98
Critical difference (CD) $\alpha = 0.05$	2.280
Critical difference (CD) $\alpha = 0.10$	2.045

Analysis In order to perform in-depth analysis of results, a statistical analysis [28, 29] is done for testing the algorithms' efficiency. Bonferroni–Dunn [30] test is also done to calculate the significant difference. Critical difference for Bonferroni–Dunn's graph is calculated as (Eq. 9):

$$CD = Q_\alpha \sqrt{\frac{k(k+1)}{6N}} \tag{9}$$

Q_α is critical value for a multiple nonparametric comparison with control [30], and k and N represent the total number of algorithms and number of problems considered for comparison, respectively. To show two levels of significance at $\alpha = 0.05$ and 0.10, horizontal lines are drawn. *Ranks calculated using Friedman's test are* presented in Table 3 and presented as graph in Fig. 5.

Bonferroni–Dunn's test states subsequent significant differences with:

- **O-SFLA as a control algorithm:**

  O-SFLA is better than PSO, ABC and SFLA at $\alpha = 0.05$.
  O-SFLA is better than PSO, ABC, SFLA and EOLSFLA at $\alpha = 0.10$.

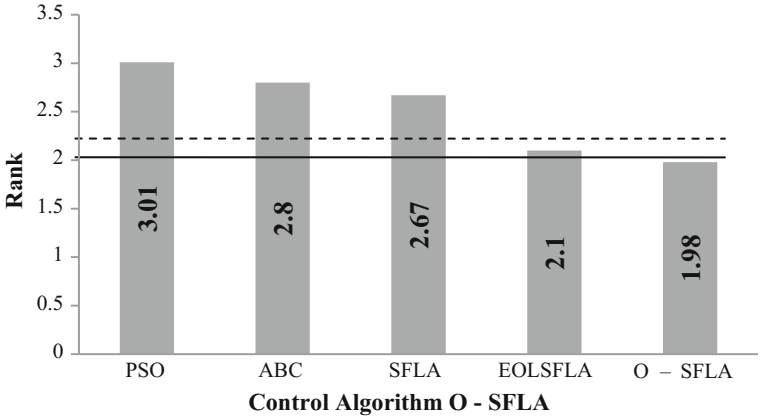

Fig. 5 Bonferroni–Dunn's graph

6.2 Local Searching Process

Test/debug data for estimating the parameters of software reliability growth models

SFLA and O-SFLA are used to find the best parameters to tune the EXP, POW and DSS models. A test/debug data set of 111 measurements (Table 4a and b) presented in [31] was used for the experiments.

RMSE criterion is used to measure the performance of the proposed O-SFLA. RMSE is frequently used to measure differences between values predicted by a model or estimator and the values actually observed from the thing being modeled or estimated. It is just the square root of the mean square error as shown in Eq. (10) given below:

$$\text{RMSE} = \sqrt{\frac{1}{N}\sum_{i=1}^{N}(y_i - \hat{y}_i)^2} \tag{10}$$

where y_i represents the ith value of the effort, $\hat{y}_i$ is the estimated effort, and N is the number of measurements used in parameter estimation of growth models. The convergence graph of the three growth models is shown in Fig. 6. The computed parameters and RMSE (training and testing) of all the three software reliability growth models using SFLA and proposed O-SFLA algorithms are given in Tables 5 and 6, respectively. It can clearly be analyzed that delayed S-shaped model provided the minimum RMSE in comparison with other models.

Table 4 **a** Test data (1–52); those marked with * are interpolated data. **b** Test data (53–111); those marked with * are interpolated data

Days	Faults	Cumulative faults	Number of test workers tester(i)	Days	Faults	Cumulative faults	Number of test workers tester(i)
a							
1	5*	5*	4*	27	3	243	5
2	5*	10*	4*	28	9	252	6
3	5*	15*	4*	29	2	254	6
4	5*	20*	4*	30	5	259	6
5	6*	26*	4*	31	4	263	6
6	8	34	5	32	1	264	6
7	2	36	5	33	4	268	6
8	7	43	5	34	3	271	6
9	4	47	5	35	6	277	6
10	2	49	5	36	13	290	6
11	31	80	5	37	19	309	8
12	4	84	5	38	15	324	8
13	24	108	5	39	7	331	8
14	49	157	5	40	15	346	8
15	14	171	5	41	21	367	8
16	12	183	5	42	8	375	8
17	8	191	5	43	6	381	8
18	9	200	5	44	20	401	8
19	4	204	5	45	10	411	8
20	7	211	5	46	3	414	8
21	6	217	5	47	3	417	8
22	9	226	5	48	8	425	4
23	4	230	5	49	5	430	4
24	4	234	5	50	1	431	4
25	2	236	5	51	2	433	4
26	4	240	5	52	2	435	4
b							
53	2	437	4	83	0	473	2*
54	7	444	4	84	0	473	2*
55	2	446	4	85	0	473	2*
56	0	446	4*	86	0	473	2*
57	2	448	4*	87	2	475	2*
58	3	451	4	88	0	475	2*
59	2	453	4	89	0	475	2*
60	7	460	4	90	0	475	2*
61	3	463	4	91	0	475	2*

(continued)

Table 4 (continued)

62	0	463	4*	92	0	475	2*
63	1	464	4*	93	0	475	2*
64	0	464	4*	94	0	475	2*
65	1	465	4*	95	0	475	2*
66	0	465	3*	96	1	476	2*
67	0	465	3*	97	0	476	2*
68	1	466	3*	98	0	476	2*
69	1	467	3	99	0	476	2*
70	0	467	3*	100	1	477	2*
71	0	467	3*	101	0	477	1*
72	1	468	3*	102	0	477	1*
73	1	469	4	103	1	478	1*
74	0	469	4*	104	0	478	1*
75	0	469	4*	105	0	478	1*
76	0	469	4*	106	1	479	1*
77	1	470	4*	107	0	479	1*
78	2	472	2	108	0	479	1*
79	0	472	2*	109	1	480	1*
80	1	473	2*	110	0	480	1*
81	0	473	2*	111	1	481	1*
82	0	473	2*				

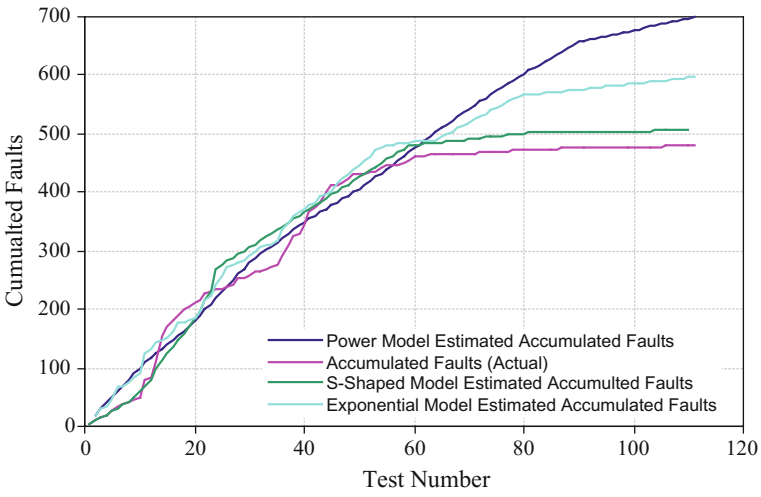

Fig. 6 Actual and accumulated failures for the three growth models using test/debug data (111 measurements)

Table 5 Estimated reliability growth model parameters using SFLA and O-SFLA

EXP	SFLA	$\mu(t;\beta) = 681.0961\,(1 - \mathrm{e}^{-0.158176})$
	O-SFLA	$\mu(t;\beta) = 317.171\,(1 - e^{-0.188818})$
POW	SFLA	$\mu(t;\beta) = 28.8964\,t^{0.0134280}$
	O-SFLA	$\mu(t;\beta) = 22.3988\,t^{0.234023}$
DSS	SFLA	$\mu(t;\beta) = 779.723\,(1 - (1 + 0.01144\,t)\mathrm{e}^{-0.011434})$
	O-SFLA	$\mu(t;\beta) = 659.011(1 - (1 + 0.02176\,t)\,\mathrm{e}^{-0.05177})$

Table 6 Computed RMSE for test/debug data

Model	Algorithm	RMSE training	RMSE testing (validation)
EXP	SFLA	27.0915	87.0932
	O-SFLA	19.7197	32.0490
POW	SFLA	41.0481	98.9531
	O-SFLA	34.3900	60.8044
DSS	SFLA	21.0831	22.7125
	O-SFLA	18.9214	16.9345

7 Conclusions of the Study and the Future Scope

In this study, a novel variant of SFLA that embeds OBL is proposed and named as O-SFLA. The concept is embedded into the memeplexes before the frog initiates foraging, and if the position of the worst frog does not improve, then again OBL comes into picture to generate opposite point of worst frog's position. The proposal is investigated on 6 benchmark functions, and its performance is tested by comparing it with other algorithms. The efficiency of the proposal is validated using nonparametric test analysis. The results prove the efficiency of the proposal. In future, the proposal will be implemented on a real-world problem of paper and pulp industry.

References

1. J. Musa, A. Iannino, and K. Okumoto. *Software Reliability: Measurement, Prediction, Applications*. McGraw Hill, 1987.
2. H. Pham. Software Reliability. Springer-Verlag, 2000.
3. P. G. Bishop and R. Bloomfield. Worst case reliability prediction on a prior estimate of residual defects. In Proceedings of the 13th IEEE International Symposium on Software Reliability Engineering (ISSRE-2002), pages 295–303, 2002.
4. M.M. Eusuff, K.E. Lansey, Optimization of water distribution network design using the shuffled frog leaping algorithm, J. Water Resour. Plan. Manage 129 (2003) 210–225.
5. M. Eusuff, K. Lansey, F. Pasha, Shuffled frog-leaping algorithm: a memetic meta-heuristic for discrete optimization, Eng. Optim. 38 (2006) 129–154.

6. M. Xie. Software reliability models - past, present and future. In N. Limnios and M. Nikulin (Eds). Recent Advances in Reliability Theory: Methodology, Practice and Inference, pages 323–340, 2002.
7. S. Yamada. Software reliability models and their applications: A survey. In International Seminar on Software Reliability of Man Machine Systems—Theories Methods and Information Systems Applications - August 17–18, Kyoto University, Kyoto, Japan, 2000.
8. P. B. Moranda. Predictions of software reliability during debugging. In Proceedings of Annual Reliability and Maintainability Symposium, pages 327–332, 1975.
9. J. Musa. A theory of software reliability and its application. IEEE Trans. Software Engineering, 1:312–327, 1975.
10. L. H. Crow. Reliability for complex repairable systems. Reliability and Biometry, SIAM, pages 379–410, 1974.
11. S. Yamada, M. Ohba, and Osaki S. S-Shaped software reliability growth models and their applications. IEEE Trans. Reliability, pages 289–292, 1984.
12. M.A. Ahandani, H. Alavi-Rad, Opposition-based learning in the shuffled differential evolution algorithm, Soft Comput. 16 (2012) 1303–1337.
13. J. Li, Q. Pan, S. Xie, An effective shuffled frog-leaping algorithm for multi-objective flexible job shop scheduling problems, Appl. Math. Comput. 218 (2012) 9353–9371.
14. F. Tang-Huai, L. Li, Z. Jia, Improved shuffled frog leaping algorithm and its application in node localization of wireless sensor network, Intell. Autom. Soft Comput. 18 (2012) 807–818.
15. M.A. Ahandani, H. Alavi-Rad, Opposition-based learning in shuffled frog leaping: An application for parameter identification, Information Sciences 291 (2015) 19–42.
16. Tarun Kumar Sharma, Millie Pant, Shuffled Artificial Bee Colony Algorithm. Soft Computing, 21 (2017) 6085–6104.
17. Tarun Kumar Sharma, Millie Pant, Identification of noise in multi noise plant using enhanced version of shuffled frog leaping algorithm, International Journal of Systems Assurance Engineering and Management, Springer (https://doi.org/10.1007/s13198-016-0466-7), 2016.
18. Tarun Kumar Sharma, Millie Pant, Opposition based learning ingrained shuffled frog-leaping algorithm, Journal of Computational Science 21 (2017) 307–315.
19. Tarun Kumar Sharma and Millie Pant, Opposition Based Learning Embedded Shuffled Frog-Leaping Algorithm. In Proceedings of International Conference on Soft Computing: Theories and Applications Volume 2 of the series Advances in Intelligent Systems and Computing, 2016.
20. Chao Liu, Peifeng Niu, Guoqiang Li, Yunpeng Ma, Weiping Zhang, Ke Chen. Enhanced shuffled frog-leaping algorithm for solving numerical function optimization problems. Journal of Intelligent Manufacturing, 1–21, 2015.
21. Pasura Aungkulanon, Pongchanun Luangpaiboon. Vertical transportation systems embedded on shuffled frog leaping algorithm for manufacturing optimisation problems in industries. Springer Plus, https://doi.org/10.1186/s40064-016-2449-1, 2016.
22. Haorui Liu, Fengyan Yi, Heli Yang. Adaptive Grouping Cloud Model Shuffled Frog Leaping Algorithm for Solving Continuous Optimization Problems. Computational Intelligence and Neuroscience, Volume 2016 (2016), Article ID 5675349.
23. Amol M. Dalavi, Padmakar J. Pawar, Tejinder Paul Singh. Tool path planning of hole-making operations in ejector plate of injection mould using modified shuffled frog leaping algorithm. Journal of Computational Design and Engineering, Volume 3, Issue 3, July 2016, Pages 266–273.
24. Deming Lei, Xiuping Guo. A shuffled frog-leaping algorithm for hybrid flow shop scheduling with two agents. Expert Systems with Applications, Volume 42, Issue 23, 15 December 2015, Pages 9333–9339.
25. Morteza Jadidoleslam, Akbar Ebrahimi. Reliability constrained generation expansion planning by a modified shuffled frog leaping algorithm. International Journal of Electrical Power & Energy Systems, Volume 64, January 2015, Pages 743–751.

26. H.R. Tizhoosh, Opposition-based learning: a new scheme for machine intelligence, in: Proc. Int. Conf. Comput. Intell. Modeling, Control and Autom., Vienna, Austria, 2005, pp. 695–701.
27. Jia Zhao; Li Lv. Shuffled frog-leaping algorithm using elite opposition-based learning. Int. J. of Sensor Networks, 2014 Vol. 16, No. 4, pp. 244–251.
28. Demšar J. Statistical comparisons of classifiers over multiple data sets. J Mach Learn Res, (2006), 7:1–30.
29. García S., Herrera F. An extension on statistical comparisons of classifiers over multiple data sets for all pairwise comparisons, J Mach Learn Res, (2008), 9:2677–2694.
30. Dunn OJ. Multiple comparisons among means, J Am Stat Assoc,(1961),56(293):52–64.
31. A. Sheta. Estimation of the COCOMO model parameters using genetic algorithms for NASA software projects. Journal of Computer Science, USA, 2(2):118–123, 2006.

Author Index

K. Ray et al. (eds.), *Soft Computing Applications*, Studies in Computational Intelligence 761, https://doi.org/10.1007/978-981-10-8049-4